

MODELING SPANWISE NONUNIFORMITY IN THE CROSS-SECTIONAL ANALYSIS OF COMPOSITE BEAMS

A Thesis
Presented to
The Academic Faculty

by

Jimmy Cheng-Chung Ho

In Partial Fulfillment
of the Requirements for the Degree
Doctor of Philosophy in
Aerospace Engineering

School of Aerospace Engineering
Georgia Institute of Technology
August 2009

MODELING SPANWISE NONUNIFORMITY IN THE CROSS-SECTIONAL ANALYSIS OF COMPOSITE BEAMS

Approved by:

Professor Dewey H. Hodges, Advisor
School of Aerospace Engineering
Georgia Institute of Technology

Professor Donald W. White
School of Civil and Environmental
Engineering
Georgia Institute of Technology

Professor Olivier A. Bauchau
School of Aerospace Engineering
Georgia Institute of Technology

Professor Vitali V. Volovoi
School of Aerospace Engineering
Georgia Institute of Technology

Professor Wenbin Yu
Department of Mechanical and
Aerospace Engineering
Utah State University

Date Approved: 27 June 2009

*To the increasingly diminishing breed of students, who upholds the
Honor Code and whose main motivation for attending school is for the
sake of scholarly pursuits.*

ACKNOWLEDGEMENTS

All things are from God and all are part of His plan. I thank the Father, the Son, and the Spirit for permitting the completion of this degree. Not that the contents of this thesis is perfect by any means, but I praise the Lord for granting me the immense satisfaction that I reaped in performing all labors associated with the generation of this thesis.

I could not hope for a better academic advisor than Professor Dewey Hodges. Not only does he try to instill his vast technical knowledge in me, but he does so in a way that forces me to think and fosters my intellect. Despite often seemingly overwhelmed by his responsibilities, he is never lax in devoting his attention to me. By his overall conduct regarding his job, he is one of the most professional men I know. In addition, he is also a kind man. These are just some of the ways that truly makes him my teacher and friend.

We should all be grateful for those who paved the path before us. The research presented in this thesis focuses on certain aspects of the cross-sectional analysis of beam theory. My theoretical approach for addressing these aspects is based on a framework, which is established by Professor Hodges and his co-workers and has been under development since the late 1980s. Their work on cross-sectional analysis is embodied in a software. As part of my work, I used and modified this software. Therefore, I am grateful for all involved in the development of the theory and the software. In particular, Professor Hodges and Professor Wenbin Yu both helped me tremendously in understanding the theory.

A requirement for the PhD degree in Aerospace Engineering at Georgia Tech is that the work of the student must be evaluated and approved by a thesis committee,

so I am thankful to all five members of my committee for serving this duty that is important to me. Professor Hodges, Professor Olivier Bauchau, and Professor Yu have been on my committee since my proposal. Professor Vitali Volovoi and Professor Donald White joined the committee to evaluate this thesis and my defense presentation. Each member provided me with valuable feedback that has improved this thesis.

I am fortunate to have been financially supported for the entirety of my studies at Georgia Tech, so I am grateful to my sponsors. The funding for my first two semesters came from the DARPA Heliplane program. The funding for my final seven semesters came from the U. S. Army Vertical Lift Research Center of Excellence (VLRCE) at Georgia Institute of Technology. All of the research performed in the generation of this thesis may be viewed as part of my funded task from VLRCE.

The number of individuals, who deserve to be acknowledged, are too numerous to list, so I will provide only a short list. From my family, I thank my father Dr. Lawrence Ho, my mother Mrs. Alice Ho, my brother Mr. Eric Ho, my uncle Mr. David Chang, and my aunt Mrs. Helen Chang. From Georgia Tech, I thank Dr. Chang-Yong Lee, Dr. Chongseok Chang, Mr. Wei-En Li, Dr. Samer Tawfik, Mrs. Zahra Sotoudeh, Mr. Pei Yoong Koh, and Mr. Benjamin Jonen. From Ames Research Center, I thank Dr. Chee Tung, Dr. Ben Sim, Dr. Hyeonsoo Yeo, Dr. Bob Ormiston, Mr. Tom Maier, Mr. José Navarrete, and Dr. Bill Warmbrodt.

TABLE OF CONTENTS

DEDICATION	iii
ACKNOWLEDGEMENTS	iv
LIST OF TABLES	ix
LIST OF FIGURES	x
SUMMARY	xiii
I INTRODUCTION	1
1.1 Motivation	1
1.1.1 Beam Theory	1
1.1.2 Spanwise Nonuniformity	2
1.1.3 Modeling Transverse Shear	3
1.2 Previous Work	6
1.3 Present Work and Outline	10
II NONUNIFORM BEAMS OF ARBITRARY CROSS-SECTIONS	13
2.1 3D Formulation	14
2.2 Dimensional Reduction	18
2.2.1 Classical Beam Theory	19
2.2.2 Asymptotically-Correct Refined Theory	21
2.3 Generalized Timoshenko Beam Theory	23
2.4 Reduced Classical Beam Stiffness Matrix	28
2.5 Recovery Relations	29
2.6 Calculating Derivatives by Finite Differences	31
2.7 Numerical Solution Procedure	35
III TRANSFORMATION TO GENERALIZED TIMOSHENKO FORM FOR UNIFORM BEAMS	41
3.1 Prismatic Beams	43
3.2 Initially Twisted and Curved Beams	51

3.3	Solution by Iterative Method	70
3.4	Implications on Global Analysis	71
3.4.1	Static Analysis	72
3.4.2	Dynamic Analysis	75
3.5	Latest Implementation to VABS	76
3.6	Validation of Initially Twisted Beams	76
IV	LINEARLY TAPERED ISOTROPIC STRIP	84
4.1	Analytical Beam Solution	85
4.1.1	Asymptotically-Correct Refined Theory	85
4.1.2	Generalized Timoshenko Beam Theory	90
4.2	Classical Loading Cases	93
4.2.1	Analytical Beam Solutions	94
4.2.2	Exact Elasticity Solutions	98
4.2.3	Validation of Analytical Beam Solutions: Stiffness	102
4.2.4	Validation of Analytical Beam Solutions: Recovery Relations	106
4.3	Correlation with Numerical Beam Solutions	112
4.3.1	Asymptotically-Correct Refined Theory	114
4.3.2	Generalized Timoshenko Beam Theory	121
V	CONCLUSIONS AND RECOMMENDATIONS	126
5.1	Accomplishments	126
5.1.1	Nonuniform Beams of Arbitrary Cross-Sections	126
5.1.2	Modeling Transverse Shear	127
5.1.3	Linearly Tapered Isotropic Strip	128
5.2	Unresolved Issues	129
5.2.1	Nonuniform Beams of Arbitrary Cross-Sections	129
5.2.2	Modeling Transverse Shear	130
5.3	Recommendations for Future Work	131
5.3.1	Nonuniform Beams of Arbitrary Cross-Sections	131

5.3.2	Solutions to Linearly Tapered Beams	132
5.3.3	Modeling Transverse Shear	132
5.3.4	Transition Elements	134
5.3.5	Recovery Relations	134
5.3.6	Validation Needs	134
5.3.7	Nonuniform Plates and Shells	135
APPENDIX A	3D STRAIN FIELD FORMULATION	136
APPENDIX B	CONSTRAINTS ON WARPING	139
APPENDIX C	SOLVING CLASSICAL BEAM THEORY	140
APPENDIX D	TRANSFORMATION TO FIND THE REDUCED CLASSICAL STIFFNESS MATRIX	142
REFERENCES	147
VITA	152

LIST OF TABLES

1	Stiffness for the prismatic CUS cross-section, neglecting underlined terms	47
2	Stiffness for the prismatic CUS cross-section, including underlined terms	48
3	Comparison of stiffness for the prismatic CUS cross-section between Matlab solver, VABS, and NABSA	49
4	Stiffness for the prismatic CAS1 cross-section	50
5	Stiffness for initially twisted isotropic square cross-sections from VABS	68
6	Stiffness for initially twisted isotropic square cross-sections from Matlab	69
7	Dimensions and material properties for the tapered strip evaluated for ABAQUS calculations	101

LIST OF FIGURES

1	Contrasting a prismatic beam with a tapered beam	4
2	Schematics of beam deformation (courtesy of Dewey H. Hodges) . . .	15
3	Planar view of coordinate system used for transverse shear formulation with $2\gamma_{13}$ exaggerated in magnitude (courtesy of Dewey H. Hodges) .	24
4	Example of approximating derivatives by finite differences with three sections	33
5	Example of spanwise nonuniformity from material boundary	36
6	Solution procedure	37
7	CUS and CAS1 cross-sectional geometry (courtesy of Dewey H. Hodges)	45
8	Generalized Timoshenko extension stiffness, X_{11} , for the CUS section featuring initial twist	53
9	Generalized Timoshenko torsional stiffness, X_{22} , for the CUS section featuring initial twist	54
10	Generalized Timoshenko bending stiffness, X_{33} , for the CUS section featuring initial twist	55
11	Generalized Timoshenko bending stiffness, X_{44} , for the CUS section featuring initial twist	56
12	Generalized Timoshenko extension-twist coupling, X_{21} , for the CUS section featuring initial twist	57
13	Generalized Timoshenko bending-shear coupling, Y_{31} , for the CUS sec- tion featuring initial twist	58
14	Generalized Timoshenko bending-shear coupling, Y_{42} , for the CUS sec- tion featuring initial twist	59
15	Generalized Timoshenko shear stiffness, G_{11} , for the CUS section fea- turing initial twist	60
16	Generalized Timoshenko shear stiffness, G_{22} , for the CUS section fea- turing initial twist	61
17	Reduced classical extension stiffness, $A_{cl}(1,1)$, for the CUS section featuring initial twist	62
18	Reduced classical torsional stiffness, $A_{cl}(2,2)$, for the CUS section fea- turing initial twist	63

19	Reduced classical bending stiffness, $A_{cl}(3, 3)$, for the CUS section featuring initial twist	64
20	Reduced classical bending stiffness, $A_{cl}(4, 4)$, for the CUS section featuring initial twist	65
21	Reduced classical extension-twist coupling, $A_{cl}(2, 1)$, for the CUS section featuring initial twist	66
22	Lateral displacement at the tip, $u_2(L)$, for the CUS section featuring initial twist	73
23	Vertical displacement at the tip, $u_3(L)$, for the CUS section featuring initial twist	74
24	Natural frequencies for the CUS section featuring initial twist	77
25	Lateral displacement at the tip, $u_2(L)$, for the isotropic rectangular section featuring initial twist	81
26	Vertical displacement at the tip, $u_3(L)$, for the isotropic rectangular section featuring initial twist	82
27	Natural frequencies for the isotropic rectangular section featuring initial twist	83
28	Schematic of beam loaded for either pure extension or pure bending	94
29	Schematic of beam loaded for flexure	97
30	Deformed shape of the tapered strip loaded under a constant bending moment	101
31	Effective extension stiffness under loading for constant axial force	104
32	Effective bending stiffness under loading for constant bending moment, $\nu = 0.3$	105
33	Effective bending-shear coupling under loading for constant shear force, $x_1 = L$	107
34	Normalized extension stiffness A_{11} , from the 2 nd -order asymptotically-correct refined theory, $\nu = 0.3$	117
35	Normalized bending stiffness A_{44} , from the 2 nd -order asymptotically-correct refined theory, $\nu = 0.3$	118
36	Normalized coupling B_{11} , between γ_{11} and γ_{11}' from the 2 nd -order asymptotically-correct refined theory	119
37	Normalized coupling B_{44} , between κ_3 and κ_3' from the 2 nd -order asymptotically-correct refined theory	120

38	Generalized Timoshenko extension stiffness, isotropic tapered strip . .	123
39	Generalized Timoshenko bending stiffness about the x_3 -axis, isotropic tapered strip, $\nu=0.3$	124
40	Generalized Timoshenko bending-shear coupling, Y_{41} , isotropic tapered strip, $\nu=0.3$	125

SUMMARY

Spanwise nonuniformity effects are modeled in the cross-sectional analysis of beam theory. This modeling adheres to an established numerical framework on cross-sectional analysis of uniform beams with arbitrary cross-sections. This framework is based on two concepts: decomposition of the rotation tensor and the variational-asymptotic method. Allowance of arbitrary materials and geometries in the cross-section is from discretization of the warping field by finite elements. By this approach, dimensional reduction from three-dimensional elasticity is performed rigorously and the sectional strain energy is derived to be asymptotically-correct. Elastic stiffness matrices are derived for inputs into the global beam analysis. Recovery relations for the displacement, stress, and strain fields are also derived with care to be consistent with the energy. Spanwise nonuniformity effects appear in the form of pointwise and sectionwise derivatives, which are approximated by finite differences. The formulation also accounts for the effects of spanwise variations in initial twist and/or curvature.

A linearly tapered isotropic strip is analyzed to demonstrate spanwise nonuniformity effects on the cross-sectional analysis. The analysis is performed analytically by the variational-asymptotic method. Results from beam theory are validated against solutions from plane stress elasticity. These results demonstrate that spanwise nonuniformity effects become significant as the rate at which the cross-sections vary increases.

The modeling of transverse shear modes of deformation is accomplished by transforming the strain energy into generalized Timoshenko form. Approximations in this transformation procedure from previous works, when applied to uniform beams, are identified. The approximations are not used in the present work so as to retain more

accuracy. Comparison of present results with those previously published shows that these approximations sometimes change the results measurably and thus are inappropriate. Static and dynamic results, from the global beam analysis, are calculated to show the differences between using stiffness constants from previous works and the present work. As a form of validation of the transformation procedure, calculations from the global beam analysis of initially twisted isotropic beams from using curvilinear coordinate axes featuring twist are shown to be equivalent to calculations using Cartesian coordinates.

CHAPTER I

INTRODUCTION

1.1 Motivation

1.1.1 Beam Theory

Structural analysis is an everyday practice in numerous engineering disciplines. Structural members, in which at least one of the dimensions is dominant in comparison with another, are usually analyzed using simplified theories to reduce the computational costs associated with analysis. Beam theory is applied to 1D structures, which possess the quality that its length is much greater than its other two dimensions. Examples of beam-like structures in aeronautics include propellor blades, helicopter rotor blades, and high aspect-ratio aircraft wings. These lift-producing wings are often twisted and the twist distribution is a primary variable in maximizing aerodynamic efficiency by reducing downwash, so beams may be initially twisted prior to deformation from loading. Beams may also feature initial curvature. Coiled springs and DNA molecules both feature components that may be modeled as curved beams. The Gateway Arch of St. Louis is a beam with a varying distribution of curvature along its length. Structural analysis based on beam theory is typically several orders of magnitude less in computational costs in comparison with full 3D analysis. This saving in costs is vital to researchers performing analysis for basic research as well as to designers with numerous designs to analyze.

For a comprehensive structural analysis, 1D beam theory requires a complementary 2D cross-sectional analysis. This complementary analysis must be performed to attain elastic constants prior to the 1D global beam analysis. Elastic constants are synonymous with the term “stiffnesses.” Three of the better-known stiffnesses are

bending, torsion, and extension stiffness, which are typically denoted by the symbols EI , GJ , and EA , respectively. Upon performing the initial complementary analysis to attain the elastic constants, one may then perform the global analysis. Results from the global analysis include displacements, rotations, generalized strains, and internal stress resultants for each section of the beam. Stress resultants are meant as the forces and moments that result from stresses acting at the section. Generalized strains may be thought of as measures of displacements and rotations of the section that result from the stress resultants. In the case of a helicopter rotor blade that is modeled as a beam, results from the global analysis are needed as inputs for further analysis in diverse areas such as aerodynamics, vibrations, handling qualities, and aeroacoustics. To make decisions on aspects such as internal blade design and blade life expectancy, one would need to perform another cross-sectional analysis to recover the 3D stress and strain fields. The cross-sectional analysis may also yield the deformed shape of the cross-section and a conclusion from Ref. [38] is that this warped shape may alter aerodynamic predictions significantly.

1.1.2 Spanwise Nonuniformity

Spanwise nonuniformity is meant to describe a beam whose cross-sections are varying geometrically along its span. A common example of this is the tapering of rotary and fixed wings. Taper is a spanwise nonuniformity in which, say, the chord varies along its span. Much like the twist distribution, the chord distribution is also a primary variable in optimizing the aerodynamic efficiency of lift-producing wings. Another example of a nonuniform beam is a wing whose airfoil section and chord are constant along its span, but whose internal structural components may be varying geometrically. It is not unusual for this case to be realized considering that the thicknesses of individual plies, which constitute the skin, are sometimes designed to vary along the span.

The significance of spanwise nonuniformity is that it introduces 3D effects that are neglected in current cross-sectional analysis. This statement is easily justified by noting that stresses at physical boundaries, which are varying geometrically along the span, are in violation of the traction-stress relationships from Cauchy's formula unless nonuniformity effects are properly modeled. In the analysis of nonuniform beams, the bending stiffness may be regarded as $EI(x_1)$ with x_1 being the beam axial coordinate. If the beam is isotropic with rectangular cross-sections of width $2b$ and thickness t , then the familiar bending stiffness formula of

$$EI = \frac{Et(2b)^3}{12} = \frac{2Etb^3}{3} \quad (1)$$

would be correct only if it is a uniform beam. In Fig. 1, a prismatic beam is shown alongside a linearly tapered beam. Let us introduce the x_2 -axis as perpendicular to x_1 along with unit vectors, \mathbf{a}_1 and \mathbf{a}_2 , parallel to x_1 and x_2 , respectively. For the tapered beam such that $b = b(x_1)$, current cross-sectional analysis would find $EI(x_1)$ by simply replacing b with $b(x_1)$; the local taper of the beam $b'(x_1) = -\tau(x_1)$ does not further influence the local bending stiffness. In the figure, \mathbf{n} represents the outward-directed unit normal vector to the surface. One can there easily see that neglecting the local taper parameter τ is equivalent to regarding the local normal vector as being parallel to \mathbf{a}_2 , which is only true for beams with no taper. Instead, the true outward-directed normal vector features a component parallel to \mathbf{a}_1 , omission of which means that the surface boundary conditions are erroneous. Calculated elastic stiffnesses of tapered beams, performed without consideration of taper, would then be incorrect and thereby degrade results to the 1D beam analysis. Furthermore, the recovery relations for the 3D displacement, stress, and strain fields must also incorporate taper.

1.1.3 Modeling Transverse Shear

Beams are especially susceptible to transverse shear deformations if the ratio of the cross-sectional characteristic length to wavelength of deformation along the beam is

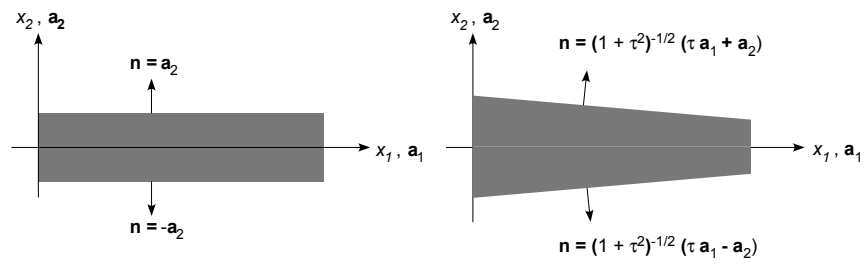


Figure 1: Contrasting a prismatic beam with a tapered beam

large enough. The length of the dominant cross-sectional dimension may serve as a measure of its characteristic length. This implies that it is important to model transverse shear for stubby beams, which are cases in which the limits of the original assumptions regarding dimensions of the structure are being approached.

Typical attempts at modeling transverse shear result in adding modes of deformation that are not included in classical theory. In the 1D analysis of beams, classical beam theory allows for extension, torsion, and bending in two directions. Timoshenko beam theory accounts for transverse shear by allowing for shear deformations in two directions in addition to the four modes from classical beam theory.

The increasing usage of composite structures means that the capability to accurately model transverse shear is also increasing in importance, because beams composed of composite materials tend to be more susceptible to transverse shear effects than beams composed of isotropic materials. Composite structures can exhibit the property that its shear deformations are coupled with the classical modes of deformation, so the importance of modeling transverse shear can be even more pronounced. Engineers still view predictions of composite structures with skepticism, because the predictions are often inaccurate. The source of inaccurate predictions may often be attributed to factors outside of structural analysis such as the inability of material scientists to provide accurate material behaviors, but it is nevertheless true that the accuracy of structural analysis predictions worsens with greater transverse shear deformations. Hypersonic scramjet engines and the much-anticipated Boeing 787 Dreamliner are recent examples that rely heavily on composite materials to achieve its mission specifications. Therefore, they underscore the need for structural analysis tools to accurately model transverse shear.

1.2 *Previous Work*

The widespread usage of beam theory has resulted in an abundance of research on the topic, but it seems that most structural analysts are either unaware or simply ignore the significance of spanwise nonuniformity. Due to the overwhelming amount of work on beams, this section will only attempt to mention those with most influence and relevance with respect to the present work.

A recent book [18] on beam theory includes a summary of the major developments in its field up to the present day, so much more details may be found there for interested readers. Formulated in the 18th-century by Swiss mathematicians Léonhard Euler and Jean Bernoulli, Euler-Bernoulli beam theory, also known as classical beam theory, allows for extension, torsion, and bending in two directions in its 1D analysis. It is the most widely taught and used beam theory for its simplicity. For extension and bending modes, its primary assumptions are that normal cross-sectional planes, which are normal to the beam reference line, of the undeformed configuration remain both plane and normal to the deformed reference line upon loading. Torsion of the beam is allowed by applying the torsion theory of A. J. C. Barré de Saint-Venant [13], which means that a normal cross-section may warp out of its own plane. In the first half of the 20th-century, Stephen Timoshenko (see Refs. [43] and [44]) allowed for the possibility that normal cross-sectional planes from the undeformed configuration could become oblique to the deformed reference line by introducing two transverse shear modes of deformation in its 1D analysis. The theory by Timoshenko is a type of refined beam theory in the sense that it is a refinement to classical beam theory. New theories may be derived by adding new modes of deformation as done in Ref. [31], but the six modes of deformation introduced thus far are usually considered sufficient and the vast majority of beam theories to date do not contain other modes. One notable exception is Vlasov beam theory, which accounts for the possibility that end constraints may restrain interior sections of the beam from warping freely and hence

violate Saint-Venant’s free warping assumption. The solution by Vasilii Zakharovich Vlasov [47] is to introduce an additional mode of deformation. The Vlasov effect is important to thin-walled beams with open sections, but will not be considered in the present work.

As mentioned before, a 2D cross-sectional analysis is required to attain stiffness values and 3D recovery results. A common source of error in analysis is that the 1D and 2D analyses are in violation of each other, such as assuming that the cross-section is rigid in the 1D analysis [11]. Another common source of error is that the 2D analysis is based upon an assumed displacement or assumed stress field, which is not correct in general. Stiffness values are often simply calculated using integral formulae from elementary strength of materials books such as Ref. [16], but the underlying assumptions of those formulae are only applicable to prismatic isotropic beams. Furthermore, the analytical formula for torsional stiffness is limited to prismatic isotropic beams with elliptical or rectangular cross-sections [45], and there is not even a consensus regarding the shear stiffness formula [40] for this simplest of cases. A cross-sectional analysis tool that could circumvent the need for unnecessary assumptions while also accommodating arbitrary materials and geometries would inevitably involve a numerical approach. Variational Asymptotic Beam Sectional Analysis (VABS) [6] and Nonhomogeneous Anisotropic Beam Section Analysis (NABSA) are two finite element based cross-sectional analysis tools that have shown much success. NABSA is based on the theory of Ref. [15].

Regardless of which modes of deformation are included in the theory, Hodges [18] categorizes modern beam theories into three main categories. The three categories are (1) theories with 1D global equations derived based on *ad hoc* assumptions of the cross-sectional deformations, (2) theories based on equations for the beam as a 1D continuum while cross-sectional properties are obtained independently, and (3)

“theories in which the equations governing cross-sectional deformation and the one-dimensional equations governing behavior of the blade as an equivalent beam are rigorously reduced from the common framework of three-dimensional elasticity theory.”

Efforts since 1985 by Hodges and his co-workers belong to category (3) of the modern theories. This set of works are both general and accurate for allowing all possible forms of deformation, while also being practical for its results are easily interpreted. The only assumption in the 1D global analysis is the 1D constitutive relationships. Details to the 1D global analysis, which is nonlinear and geometrically-exact, can be found in Refs. [17] and [18]. Meanwhile, the 2D cross-sectional analysis is simplified by systematically ignoring quantities that are small enough in comparison with unity. (An exception to this occurs in modeling of the trapeze effect, which is discussed in Refs. [18] and [34]. To capture the nonlinear phenomenon from the trapeze effect, the cross-sectional analysis retains terms of a higher order.) The resulting cross-sectional analysis is then solved by the variational-asymptotic method (VAM), which Berdichevsky [3] originated. By this method, the solutions are asymptotically-correct with respect to a set of pre-determined small parameters. Theoretical derivations of the 2D analysis are embodied in VABS. Having already stated that VABS may model cross-sections with arbitrary materials and geometries, it should also be stated that it accounts for effects due to initial twist and curvatures. The VABS solution to classical beam theory is asymptotically-correct, but there is no known way [35] to attain an asymptotically-correct solution if transverse shear effects are modeled except in special cases. The current procedure in VABS, to attain solutions to a generalized Timoshenko model, is to transform the classical beam strain energy into the form of the Timoshenko beam strain energy by using 1D static equilibrium equations [57]. Reference [48] provides details on the solution to a Vlasov model.

Exact solutions to the 2D plane stress equations, which are applicable to strip

beams with negligible thickness, exist for linearly tapered isotropic beams with the geometry as shown in Fig. 1 under specific loading conditions. Solutions to the two cases, where loading is applied such that either the internal axial force or bending moment is constant along the span, are found in Ref. [45]. Solutions to the flexure case, where loading is applied such that the internal shear force is constant along the span, is found in Ref. [26]. These exact elasticity solutions provide a standard from which the accuracy of beam theory solutions may be determined. In 1963, Boley [4] showed that the accuracy of predictions by beam theory worsened as τ increased for the constant bending moment case. Reference [26] appeared in 1975 and concluded likewise for the flexure case. Beam theory solutions by these two references were performed while ignoring the influence of spanwise nonuniformity on the cross-sectional analysis as well as transverse shear modes of deformation.

The significance of spanwise nonuniformity on cross-sectional analysis has been considered by some researchers, albeit all with limiting assumptions which preclude generality. In analyzing lateral-torsional buckling of tapered I-beams, Andrade and Camotim [1] reported that the taper effects on stiffnesses is not negligible in general; however, their analysis is restricted to the case in which $\nu \approx 0$. For finite element analysis of linearly tapered I-beams, Vu-Quoc and Léger [49] derived a flexibility matrix showing a dependence on τ ; however, the basis of their derivation is at best only an approximation in that they assumed that the bending stiffness equation for a prismatic beam, $\sigma_{11} = Mx_2/I$, remains valid in the presence of taper. Kitipornchai and Trahair [25] analyzed tapered monosymmetric I-beams and seem to account for the taper effects partially based on physical reasoning, but their derivations may not be applied to arbitrary sections. There is relatively little other research regarding the effects of nonuniformity on the local cross-sectional analysis in either stiffness properties or recovery relations. On the other hand, beam analyses with stiffness (or flexibility) matrices formulated for numerical computations in Refs. [2], [8], [24], [30],

[33], [39], [42], and [46] are only selected examples of the immense body of research performed on the analysis of tapered beams that ignore the effects of nonuniformity.

1.3 Present Work and Outline

The ultimate goal of this thesis is to present a theory for a general cross-sectional analysis which properly models spanwise nonuniformity. This theory allows for the possibility of nonlinear spanwise variations in geometry including nonlinear twist and curvatures prior to loading. VABS has been validated extensively for prismatic beams, so the theory adheres to implicit assumptions that currently exist in VABS and may be implemented as an enhancement to VABS. Theoretical derivations with the new implementations begin with an introduction to the 3D kinematics and its governing equations from elasticity. The VAM is then applied to rigorously split the 3D elasticity problem into a 1D global analysis and a 2D cross-sectional analysis. A result of this “dimensional reduction” is the derivation of the classical sectional strain energy. This sectional strain energy is then repackaged into a generalized Timoshenko framework to model transverse shear. Recovery relations for the 3D displacement, stress, and strain fields are found from expressions that are consistent with the described procedure to attain the energy. Allowance for the possibility of nonuniformity results in additional terms that appear in the classical strain energy, in the transformation to generalized Timoshenko form, and also in the recovery relations.

The solution procedure for the transformation to generalized Timoshenko form, that is presented in this thesis, represents a departure from the procedure currently embedded in VABS (see Refs. [18] and [57]). The current solution to the Timoshenko stiffness matrices in VABS is given by analytical formulae that may simply be found from substitution operations. Unfortunately, the derivation to the current VABS solution contains inappropriate approximations and it does not appear that

simple analytical formulae may be derived in general. The solution procedure advocated in this thesis is rather to iteratively solve a system of nonlinear algebraic equations. Additionally, a mistake in derivation to the current VABS solution, in the case of beams featuring initial twist and/or curvature (and would also be true for nonuniform beams), is identified as stemming from a misunderstanding that a simple relationship exists between certain stiffness matrices from a “condensation” of shear strain measures. Results from a 1D global analysis illustrate the implications of these approximations and mistakes from the 2D cross-sectional analysis. Of relation to this illustration for initially twisted beams, calculations based on coordinates where cross-sections have an initial twist are shown (possibly for the first time) to be equivalent to calculations based on coordinates where cross-sections have no initial twist.

As a demonstration of spanwise nonuniformity effects, the linearly tapered isotropic strip beam, with the geometry as shown in Fig. 1, is analyzed as a 2D plane stress problem undergoing in-plane deformations. This example is chosen, because (1) it is simple enough that an analytical beam theory solution based on the VAM may be derived without resorting to the finite element method, and (2) exact elasticity solutions exist for the three loading conditions mentioned in Sec. 1.2 and may be used to validate the beam theory solution. Upon successful validations, the analytical beam theory solution is further used as a standard from which correlation studies with the general, numerical VAM beam theory solution are formed.

The remaining chapters consist of theoretical formulations, results, and discussions related to the cross-sectional analysis of beams with an emphasis on modeling spanwise nonuniformity. Chapter 2 presents derivations, based on the VAM, to the general cross-sectional analysis of a nonuniform beam. Chapter 3 documents problems with the solution procedure regarding the transformation to generalized Timoshenko form that is currently embedded in VABS. Chapter 4 presents an analytical solution, also based on the VAM, to the specific case of a linearly tapered isotropic strip beam. The

analytical solution demonstrates the effects of taper. Correlations between the analytical and numerical beam theory solutions are also presented in Chapter 4. Lastly, Chapter 5 summarizes the conclusions and offers recommendations for future works on this topic.

CHAPTER II

NONUNIFORM BEAMS OF ARBITRARY CROSS-SECTIONS

For the purpose of analyzing nonuniform beam-like structures by beam theory, a general theory which properly models the effects brought on by spanwise nonuniformity to the cross-sectional analysis is presented. The variational-asymptotic method and the finite element method are combined to obtain an asymptotically-correct expression to the sectional strain energy based on a discretized warping field. This asymptotically-correct strain energy is then transformed into the form of a generalized Timoshenko beam theory for ease of use. The energy expressions identify the stiffness matrices. Recovery relations for 3D displacement, stress, and strain fields are obtained with consistency to the energy. The effects of spanwise nonuniformity appear in the theory through derivatives of both pointwise and sectionwise quantities, so the derivatives are approximated by finite differences.

The following conventions apply to this chapter. Greek indices assume values 2 and 3 while Latin indices assume values 1, 2, and 3. Conventions associated with indice notations, such as summation over the range in cases of repeated indices, are in use except where explicitly indicated. The operator $(\cdot)'$ implies taking the derivative with respect to x_1 so that $(\cdot)' = \partial(\cdot)/\partial x_1$. The tilde symbol transforms a vector into a skew-symmetric matrix such that components of the matrix are $\tilde{(\cdot)}_{ij} = -e_{ijk}(\cdot)_k$ with e_{ijk} as the permutation symbol. The notations $\langle(\cdot)\rangle = \int_S (\cdot) dx_2 dx_3$ and $\langle\langle(\cdot)\rangle\rangle = \int_S (\cdot) \sqrt{g} dx_2 dx_3$ are also used.

2.1 3D Formulation

This section serves to formulate the 2D cross-sectional analysis prior to making assumptions associated with dimensional reduction. The formulations are entirely based on kinematics and the theory of elasticity. The goal here is to write the 3D strain field, constraints, and sectional energy in terms of quantities that are amenable to the 2D analysis. The problem is first formulated analytically, and then restated in a numerical sense for finite element analysis. The formulation presented in this section has been applied to the cross-sectional analysis by Hodges and his co-workers as early as 1994 [5], and is heavily influenced by the work of Danielson and Hodges [12].

Figure 2 displays the coordinate axes, position vectors, displacement vectors, and base vectors which are used in defining the beam kinematics. The reference line of the beam and a cross-section are shown in both its undeformed and deformed states. The cross-section is restricted to be normal to the reference line prior to deformation (Ref. [53] gives a full explanation of how this restriction may be removed for classical Euler-Bernoulli beam theory). The undeformed reference line is allowed to be initially twisted and curved. The lines \mathbf{r} and \mathbf{R} are the reference lines in its undeformed and deformed states, respectively. Symbols x_1 and s denote arc-lengths along \mathbf{r} and \mathbf{R} , respectively. At each point along \mathbf{r} , coordinates axes x_i exist with the origin set at the point on \mathbf{r} . Coordinates x_α may be arbitrarily chosen so as long as it forms a local right-handed coordinate system with x_1 . At each point along both \mathbf{r} and \mathbf{R} , there exist frames \mathbf{b} and \mathbf{B} , respectively. The frame \mathbf{b} contains orthogonal unit vectors \mathbf{b}_i , such that \mathbf{b}_α is tangent to x_α and \mathbf{b}_1 is tangent to \mathbf{r} . By the definition of \mathbf{b}_1 , it is apparent that $\mathbf{r}' = \mathbf{b}_1$. The frame \mathbf{B} contains orthogonal unit vectors \mathbf{B}_i , such that $\mathbf{B}_1 = \mathbf{B}_2 \times \mathbf{B}_3$ with \mathbf{B}_1 being normal to the cross-sectional plane in the deformed state.

Position and displacement vectors are defined in a common absolute reference frame. The position vectors of a point on the undeformed and deformed reference

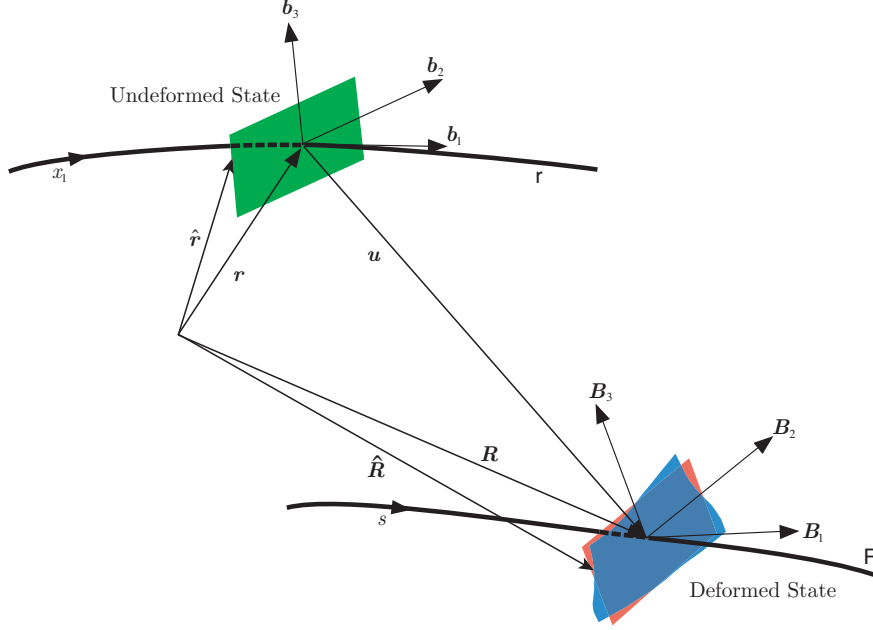


Figure 2: Schematics of beam deformation (courtesy of Dewey H. Hodges)

lines are denoted by \mathbf{r} and \mathbf{R} , respectively. The position vectors of an arbitrary point in the undeformed and deformed states are denoted by $\hat{\mathbf{r}}$ and $\hat{\mathbf{R}}$, respectively. The displacement vector of the reference line is denoted by \mathbf{u} .

In addition to displacements due to translations and rotations of the reference line, there are also warping displacements. Let $\mathbf{w} = w_i \mathbf{b}_i$ represent the warping displacement field, which defines the small local deformations of the cross-sections and is a function of x_i . In other words, superimposing the warping field, along with translations and rotations of the reference line, on the undeformed state will result in the deformed state. With these definitions, position vectors $\hat{\mathbf{r}}$ and $\hat{\mathbf{R}}$ are written as

$$\hat{\mathbf{r}} = \mathbf{r} + x_\alpha \mathbf{b}_\alpha \quad (2)$$

$$\hat{\mathbf{R}} = \mathbf{r} + \mathbf{u} + x_2 \mathbf{B}_2 + x_3 \mathbf{B}_3 + w_i \mathbf{B}_i \quad (3)$$

Now that the concept of warping is explained, frame B can be more clearly defined. Using a combination of citing and paraphrasing words from Hodges [18], “The frame B is chosen so that the portion of the displacement relegated to the warping is small,

so that the deformed beam reference cross-sectional plane is the plane that is closest to those material points of the deformed beam that make up the reference cross-section of the undeformed beam at” a particular section “of the undeformed beam.”

The 3D strain field is now given in terms of the warping field and 1D strain measures. The 1D strain measures of classical beam theory are denoted by

$$\bar{\epsilon} = [\bar{\gamma}_{11} \quad \bar{\kappa}_1 \quad \bar{\kappa}_2 \quad \bar{\kappa}_3]^T \quad (4)$$

where $\bar{\gamma}_{11}$ is the extensional strain measure, $\bar{\kappa}_1$ is the torsional strain measure, and $\bar{\kappa}_\alpha$ are bending strain measures. Upon reading the steps outlined in Appendix A, one may derive the linearized 3D strain field as

$$\Gamma = \Gamma_a w + \Gamma_\epsilon \bar{\epsilon} + \Gamma_R w + \Gamma_\ell w' \quad (5)$$

where

$$\Gamma = [\Gamma_{11} \quad 2\Gamma_{12} \quad 2\Gamma_{13} \quad \Gamma_{22} \quad 2\Gamma_{23} \quad \Gamma_{33}]^T \quad (6)$$

$$w = [w_1 \quad w_2 \quad w_3]^T \quad (7)$$

$$\Gamma_a = \begin{bmatrix} 0 & 0 & 0 \\ \frac{\partial}{\partial x_2} & 0 & 0 \\ \frac{\partial}{\partial x_3} & 0 & 0 \\ 0 & \frac{\partial}{\partial x_2} & 0 \\ 0 & \frac{\partial}{\partial x_3} & \frac{\partial}{\partial x_2} \\ 0 & 0 & \frac{\partial}{\partial x_3} \end{bmatrix}; \quad \Gamma_\epsilon = \frac{1}{\sqrt{g}} \begin{bmatrix} 1 & 0 & x_3 & -x_2 \\ 0 & -x_3 & 0 & 0 \\ 0 & x_2 & 0 & 0 \\ 0 & 0 & 0 & 0 \\ 0 & 0 & 0 & 0 \\ 0 & 0 & 0 & 0 \end{bmatrix} \quad (8)$$

$$\Gamma_R = \frac{1}{\sqrt{g}} \begin{bmatrix} \tilde{k} + \Delta_3 k_1 (x_3 \frac{\partial}{\partial x_2} - x_2 \frac{\partial}{\partial x_3}) \\ O_3 \end{bmatrix}; \quad \Gamma_\ell = \frac{1}{\sqrt{g}} \begin{bmatrix} \Delta_3 \\ O_3 \end{bmatrix}$$

$$k = [k_1 \quad k_2 \quad k_3]^T \quad (9)$$

$$\sqrt{g} = 1 - x_2 k_3 + x_3 k_2 \quad (10)$$

and Δ_3 and O_3 are the identity and zero matrices, respectively, of order three. Components of the column matrix k are k_1 , the initial twist, and k_α , the initial curvature components of the reference line about x_α .

In order for the warping field to be unique, constraints on the warping field are needed. Following Appendix B, the chosen constraints are

$$\langle \Gamma_c w \rangle = 0 \quad (11)$$

where Γ_c is given as

$$\Gamma_c = \begin{bmatrix} 1 & 0 & 0 \\ 0 & 1 & 0 \\ 0 & 0 & 1 \\ 0 & \frac{\partial}{\partial x_3} & -\frac{\partial}{\partial x_2} \end{bmatrix} \quad (12)$$

The 2D cross-sectional analysis is now posed as a constrained minimization problem. By the principle of minimum potential, the equilibrium state of the cross-section may be found by minimizing the sectional strain energy. The potential of the applied loads are neglected, because internal stresses are typically several orders of magnitude greater than external aerodynamic pressures of lifting surfaces in aeronautics. Twice the sectional strain energy is

$$2U = \langle \langle \Gamma^T \overline{D} \Gamma \rangle \rangle \quad (13)$$

where \overline{D} is the 6×6 symmetric material matrix from Hooke's law. The warping field adequately describes the state of the cross-section, so the 2D analysis problem is essentially finding w_i that minimizes Eq. (13) subject to Eq. (11).

In order to allow for a cross-sectional analysis that may accommodate arbitrary materials and geometries, the finite element method is applied to solve the minimization problem. Without making any unnecessary assumptions, let the warping field be discretized as

$$w(x_i) = S(x_i)V(x_1) \quad (14)$$

with $S(x_i)$ representing the matrix of finite element shape functions, and V as a column matrix of nodal value of the warping displacement over the cross-section. Substituting Eq. (14) into Eq. (5) results in twice the strain energy as

$$\begin{aligned}
2U = & V^T E V + 2V^T (D_{a\epsilon} \bar{\epsilon} + D_{aR} V + D_{aS'} V + D_{a\ell} V') + \bar{\epsilon}^T D_{\epsilon\epsilon} \bar{\epsilon} + V^T D_{RR} V \\
& + V'^T D_{\ell\ell} V' + V^T D_{S'S'} V + 2V^T (D_{R\epsilon} + D_{S'\epsilon}) \bar{\epsilon} + 2V'^T D_{\ell\epsilon} \bar{\epsilon} \\
& + 2V^T (D_{R\ell} + D_{S'\ell}) V' + 2V^T D_{RS'} V
\end{aligned} \tag{15}$$

where

$$\begin{aligned}
E &= \langle \langle [\Gamma_a S]^T \bar{D} [\Gamma_a S] \rangle \rangle; & D_{a\epsilon} &= \langle \langle [\Gamma_a S]^T \bar{D} [\Gamma_\epsilon] \rangle \rangle \\
D_{aR} &= \langle \langle [\Gamma_a S]^T \bar{D} [\Gamma_R S] \rangle \rangle; & D_{a\ell} &= \langle \langle [\Gamma_a S]^T \bar{D} [\Gamma_\ell S] \rangle \rangle \\
D_{aS'} &= \langle \langle [\Gamma_a S]^T \bar{D} [\Gamma_\ell S'] \rangle \rangle; & D_{\epsilon\epsilon} &= \langle \langle [\Gamma_\epsilon]^T \bar{D} [\Gamma_\epsilon] \rangle \rangle \\
D_{RR} &= \langle \langle [\Gamma_R S]^T \bar{D} [\Gamma_R S] \rangle \rangle; & D_{\ell\ell} &= \langle \langle [\Gamma_\ell S]^T \bar{D} [\Gamma_\ell S] \rangle \rangle \\
D_{S'S'} &= \langle \langle [\Gamma_\ell S']^T \bar{D} [\Gamma_\ell S'] \rangle \rangle; & D_{R\epsilon} &= \langle \langle [\Gamma_R S]^T \bar{D} [\Gamma_\epsilon] \rangle \rangle \\
D_{\ell\epsilon} &= \langle \langle [\Gamma_\ell S]^T \bar{D} [\Gamma_\epsilon] \rangle \rangle; & D_{S'\epsilon} &= \langle \langle [\Gamma_\ell S']^T \bar{D} [\Gamma_\epsilon] \rangle \rangle \\
D_{R\ell} &= \langle \langle [\Gamma_R S]^T \bar{D} [\Gamma_\ell S] \rangle \rangle; & D_{RS'} &= \langle \langle [\Gamma_R S]^T \bar{D} [\Gamma_\ell S'] \rangle \rangle \\
D_{S'\ell} &= \langle \langle [\Gamma_\ell S']^T \bar{D} [\Gamma_\ell S] \rangle \rangle
\end{aligned} \tag{16}$$

In discretized form, the constraints are now

$$V^T D_c = 0 \tag{17}$$

where $D_c^T = \langle \Gamma_c S \rangle$. The constrained minimization problem is now transformed into finding V that minimizes Eq. (15) subject to Eq. (17).

Unlike uniform beams, there is the possibility that S' is nonzero for nonuniform beams. The explanation for this is given later in Sec. 2.6.

2.2 Dimensional Reduction

In this section, the VAM is applied to solve the 2D cross-sectional analysis. The problem is first solved for classical Euler-Bernoulli beam theory, which is regarded

as a 0th-order theory, and then for a higher-order refined theory. The method starts with the identification of small parameters. The solution to classical beam theory is attained by applying the calculus of variations, along with Lagrange multipliers, to the constrained minimization problem while discarding all terms higher than 0th-order. One attains the higher-order solution by perturbing the 0th-order solution by one order, and then repeating the same procedure as before while keeping all terms that are needed for calculations of the 1st-order warping. The energy functional is in quadratic form with respect to the unknown warping field, so a 0th- and a 1st-order asymptotically-correct warping result in energies that are asymptotically-correct up to 0th- and 2nd-order in terms of the small parameters, respectively.

The ordering, which is influenced by Starosel'skii [41], is now given. Two small parameters are identified as a/ℓ and a/R . a is the characteristic length of the cross-section dimension. ℓ is the characteristic wavelength of deformation along the beam axial coordinate. R is the characteristic radius of initial twist/curvature of the beam. The two small parameters are assumed to be of the same order, which is one order less than unity. For convenience, we will denote a as simply a small parameter that represents $O(a/\ell)$ and $O(a/R)$. Despite the abuse in notations, the context should easily dictate what is meant. The order of \bar{D} , the matrix containing the material moduli, will simply be denoted $O(\mu)$. The order of $\bar{\epsilon}$ is denoted by $\hat{\epsilon}$.

2.2.1 Classical Beam Theory

The discussion leading up to this point implies that the 0th-order theory is obtained by minimizing Eq. (15) subject to Eq. (17) while discarding all terms higher than 0th-order. Denoting the 0th-order sectional energy as U_0 and keeping only leading order terms to Eq. (15), then twice the 0th-order energy is

$$2U_0 = V^T E V + 2V^T D_{a\epsilon} \bar{\epsilon} + \bar{\epsilon}^T D_{\epsilon\epsilon} \bar{\epsilon} \quad (18)$$

Appendix C gives the solution, i.e. the 0th-order warping field which minimizes Eq. (18) subject to Eq. (17), as

$$V = [\Delta_3 - \Psi(\Psi^T D_c)^{-T} D_c^T] V^* = V_0 = \hat{V}_0 \epsilon \quad (19)$$

As explained in Appendix C, Ψ represents nodal values of the kernel matrix of E .

Having solved the unknown warping field, any remaining cross-sectional quantities that are desired can be found. By plugging Eq. (19) into Eq. (18), the asymptotically-correct energy up to $O(\mu\hat{\epsilon}^2)$ is found as

$$2U_0 = \bar{\epsilon}^T (\hat{V}_0^T D_{a\epsilon} + D_{\epsilon\epsilon}) \bar{\epsilon} \quad (20)$$

The above equation is the energy per unit length for classical theory. The coefficient $(\hat{V}_0^T D_{a\epsilon} + D_{\epsilon\epsilon})$ is the stiffness matrix. Explicitly expanding the matrices, the energy can be written as

$$2U = \begin{Bmatrix} \bar{\gamma}_{11} \\ \bar{\kappa}_1 \\ \bar{\kappa}_2 \\ \bar{\kappa}_3 \end{Bmatrix}^T \begin{bmatrix} \bar{S}_{11} & \bar{S}_{12} & \bar{S}_{13} & \bar{S}_{14} \\ \bar{S}_{12} & \bar{S}_{22} & \bar{S}_{23} & \bar{S}_{24} \\ \bar{S}_{13} & \bar{S}_{23} & \bar{S}_{33} & \bar{S}_{34} \\ \bar{S}_{14} & \bar{S}_{24} & \bar{S}_{34} & \bar{S}_{44} \end{bmatrix} \begin{Bmatrix} \bar{\gamma}_{11} \\ \bar{\kappa}_1 \\ \bar{\kappa}_2 \\ \bar{\kappa}_3 \end{Bmatrix} \quad (21)$$

This implies a 1D constitutive law of the form

$$\begin{Bmatrix} \bar{F}_1 \\ \bar{M}_1 \\ \bar{M}_2 \\ \bar{M}_3 \end{Bmatrix} = \begin{bmatrix} \bar{S}_{11} & \bar{S}_{12} & \bar{S}_{13} & \bar{S}_{14} \\ \bar{S}_{12} & \bar{S}_{22} & \bar{S}_{23} & \bar{S}_{24} \\ \bar{S}_{13} & \bar{S}_{23} & \bar{S}_{33} & \bar{S}_{34} \\ \bar{S}_{14} & \bar{S}_{24} & \bar{S}_{34} & \bar{S}_{44} \end{bmatrix} \begin{Bmatrix} \bar{\gamma}_{11} \\ \bar{\kappa}_1 \\ \bar{\kappa}_2 \\ \bar{\kappa}_3 \end{Bmatrix} \quad (22)$$

where \bar{F}_1 is the axial force, \bar{M}_1 is the torque, and \bar{M}_α are the bending moments as a result of the internal stresses. It is apparent that neither spanwise nonuniformity nor initial twist and curvatures have any impact up to this point due to being higher-order effects. However, for simplicity of programming, this energy captures part of the initial twist and curvature effects by the \sqrt{g} term that implicitly appears within both $D_{a\epsilon}$ and $D_{\epsilon\epsilon}$.

2.2.2 Asymptotically-Correct Refined Theory

A higher-order refined theory, which would result in a 2nd-order asymptotically-correct sectional energy, is now sought. Now the unknown warping field must be more accurate than 0th-order, so it is perturbed as a series in the small parameter a as

$$V = V_0 + aV_1 + a^2V_2 + O(a^3) \quad (23)$$

V_0 is the solution from classical theory. Upon inspecting the result from substituting Eq. (23) into Eq. (15), it is realized that the sectional energy is asymptotically-correct up to $O(\mu a^2 \hat{\epsilon}^2)$ even without including a^2V_2 and higher-order terms from Eq. (23). Without considering the terms of higher order than $O(\mu a^2 \hat{\epsilon}^2)$, twice the sectional energy is

$$\begin{aligned} 2U_1 = & \bar{\epsilon}^T (\hat{V}_0^T D_{a\epsilon} + D_{\epsilon\epsilon}) \bar{\epsilon} + 2(V_0^T D_{aR} V_0 + V_0^T D_{a\ell} V'_0 + V_0^T D_{R\epsilon} \bar{\epsilon} + V_0^T D_{\ell\epsilon} \bar{\epsilon} \\ & + V_0^T D_{aS'} V_0 + V_0^T D_{RS'} V_0 + V_0^T D_{S'\ell} V'_0 + V_0^T D_{S'\epsilon} \bar{\epsilon}) + \underline{V_1^T E V_1} \\ & + \underline{2V_1^T (D_{aR} V_0 + D_{aR}^T V_0 + D_{R\epsilon} \bar{\epsilon} + D_{aS'} V_0)} + \underline{2V_1^T (D_{aS'}^T V_0 + D_{S'\epsilon} \bar{\epsilon})} \\ & + \underline{2V_1^T D_{a\ell} V'_0} + \underline{2V_0^T D_{a\ell} V'_1} + \underline{2V_1^T D_{\ell\epsilon} \bar{\epsilon}} + V_0^T D_{RR} V_0 + 2V_0^T D_{R\ell} V'_0 \\ & + V_0^T D_{\ell\ell} V'_0 + V_0^T D_{S'S'} V_0 \end{aligned} \quad (24)$$

The underlined terms, from Eq. (24), represent the 2nd-order leading terms. The terms involving V'_1 may be rearranged using the technique of integration by parts with respect to x_1 . An implicit assumption here is that the 2D cross-sectional analysis is performed at a location far from the beam ends. Therefore, end effects are negligible, and the constants of integration are dropped. Note that unlike uniform beams, the warping influence coefficients are now functions of x_1 . The 2nd-order leading terms are now rearranged as

$$2U_2 = V_1^T E V_1 + 2V_1^T D_{Rr} \bar{\epsilon} + 2V_1^T D_{S\epsilon} \bar{\epsilon}' \quad (25)$$

where

$$\begin{aligned} D_{R\tau} &= D_{aR}\hat{V}_0 + D_{aR}^T\hat{V}_0 + D_{R\epsilon} + D_{a\ell}\hat{V}'_0 - (D_{a\ell}^T\hat{V}_0)' - D'_{\ell\epsilon} + D_{aS'}\hat{V}_0 + D_{aS'}^T\hat{V}_0 + D_{S'\epsilon} \\ D_S &= D_{a\ell}\hat{V}_0 - D_{a\ell}^T\hat{V}_0 - D_{\ell\epsilon} \end{aligned} \quad (26)$$

Now one may go through the minimization of $2U_2$ subject to the constraints once more. The result is that the 1st-order approximation of warping is obtained as

$$V_1 = V_{1R\tau}\bar{\epsilon} + V_{1S}\bar{\epsilon}' \quad (27)$$

where $V_{1R\tau}$ and V_{1S} are new warping influence coefficients. Substituting Eqs. (25), (26) and (27) into Eq. (24) will now yield the 2nd-order asymptotically-correct sectional energy. It is explicitly written as

$$2U = \bar{\epsilon}^T A \bar{\epsilon} + 2\bar{\epsilon}^T B \bar{\epsilon}' + \bar{\epsilon}'^T C \bar{\epsilon}' + 2\bar{\epsilon}^T D \bar{\epsilon}'' \quad (28)$$

where

$$\begin{aligned} A &= \hat{V}_0^T D_{a\epsilon} + D_{\epsilon\epsilon} + \hat{V}_0^T (D_{aR} + D_{aR}^T + D_{RR} + D_{aS'} + D_{aS'}^T + D_{RS'} + D_{RS'}^T \\ &\quad + D_{S'\ell} + D_{S'\ell}^T + D_{S'S'}) \hat{V}_0 + \hat{V}_0^T (D_{R\epsilon} + D_{S'\epsilon}) + (D_{R\epsilon} + D_{S'\epsilon})^T \hat{V}_0 + D_{R\tau}^T V_{1R\tau} \\ &\quad + 2[(\hat{V}_0^T D_{a\ell})' + (D'_{\ell\epsilon})^T] V_{1R\tau} + 2\hat{V}_0^T (D_{a\ell} + D_{R\ell}) \hat{V}'_0 + 2D_{\ell\epsilon}^T \hat{V}'_0 + 2\hat{V}_0^T D_{a\ell} V'_{1R\tau} \\ &\quad + 2D_{\ell\epsilon}^T V'_{1R\tau} + (\hat{V}'_0)^T D_{\ell\ell} \hat{V}'_0 \\ B &= \hat{V}_0^T D_{a\ell} \hat{V}_0 + D_{\ell\epsilon}^T \hat{V}_0 + \hat{V}_0^T D_{a\ell} V_{1R\tau} + D_{\ell\epsilon}^T V_{1R\tau} + \hat{V}_0^T D_{R\ell} \hat{V}_0 \\ &\quad + [(\hat{V}_0^T D_{a\ell})' + (D'_{\ell\epsilon})^T] V_{1S} + \frac{1}{2} (D_{R\tau}^T V_{1S} + V_{1R\tau}^T D_{a\ell} \hat{V}_0 + V_{1R\tau}^T D_{a\ell}^T \hat{V}_0 + V_{1R\tau}^T D_{\ell\epsilon}) \\ &\quad + D_{\ell\epsilon}^T V'_{1S} + \hat{V}_0^T D_{a\ell} V'_{1S} + \frac{1}{2} (\hat{V}'_0)^T (D_{\ell\ell} + D_{\ell\ell}^T) \hat{V}'_0 \end{aligned} \quad (29)$$

(30)

$$C = \hat{V}_0^T D_{a\ell}^T V_{1S} + V_{1S}^T D_{a\ell}^T \hat{V}_0 + V_{1S}^T D_{\ell\epsilon} + \hat{V}_0^T D_{\ell\ell} \hat{V}_0 \quad (31)$$

$$D = (D_{\ell\epsilon}^T + \hat{V}_0^T D_{a\ell}) V_{1S} \quad (32)$$

Contribution by spanwise nonuniformity is seen through the derivative terms within matrices A and B . One approach to calculating these derivative terms is by finite differences, which is discussed later in Sec. 2.6.

2.3 Generalized Timoshenko Beam Theory

The 2nd-order asymptotically-correct sectional strain energy from Eq. (28) is sufficiently high in its order of accuracy such that one may transform it into that for a generalized Timoshenko theory. One motivation for performing the transformation is that the theory from Eq. (28) is difficult to use in practice, because of the presence of derivatives of the classical strain measures. Another motivation is that the generalized Timoshenko theory accounts for transverse shear, the importance of which is discussed in Sec. 1.1.3.

Transverse shear modes of deformation cause additional rotations to the cross-section in its deformed state. Therefore, a new coordinate system is introduced to ensure that the \mathbf{B}_1 basis vector remains normal to the cross-section during deformation. To account for the additional rotations due to shear forces, shear angles $2\gamma_{12}$ and $2\gamma_{13}$ are introduced. Figure 3 depicts the situation in the x_1 - x_3 plane. Derivations from Sec. 2.2, which neglected transverse shear, employed the symbol \mathbf{B}_i to denote the basis vectors in the deformed state, but basis vectors neglecting transverse shear are now denoted as \mathbf{T}_i from this point forward. Vectors \mathbf{T}_i and \mathbf{B}_i are now the basis vectors when transverse shear effects are neglected and included, respectively. The classical 1D strain measures, which neglects transverse shear, are still given by Eq. (4) while the 1D strain measures in a generalized Timoshenko model are

$$\epsilon = [\gamma_{11} \ \kappa_1 \ \kappa_2 \ \kappa_3]^T; \quad \gamma_s = [2\gamma_{12} \ 2\gamma_{13}]^T \quad (33)$$

The transformation is accomplished by combining kinematics, the 1D constitutive law, and the 1D static equilibrium equations. Reference [57] shows that the kinematic relationships, assuming small values of γ_{12} and γ_{13} , between the strain measures to be given by

$$\begin{aligned} \bar{\gamma}_{11} &= \gamma_{11} \\ \bar{\epsilon} &= \epsilon + Q \ \gamma'_s + P \ \gamma_s \end{aligned} \quad (34)$$

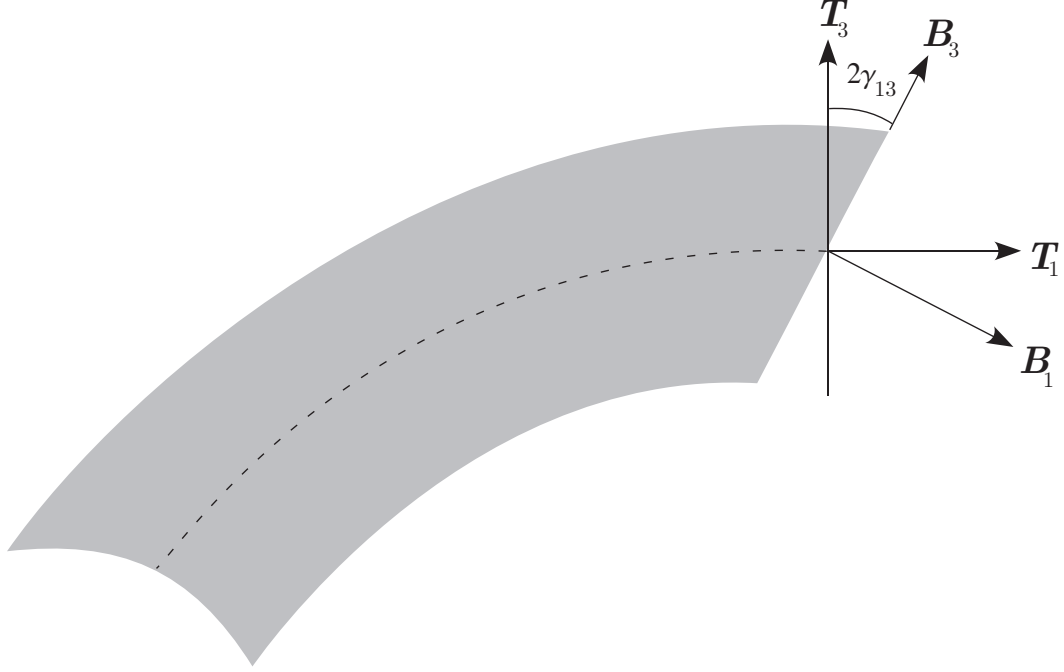


Figure 3: Planar view of coordinate system used for transverse shear formulation with $2\gamma_{13}$ exaggerated in magnitude (courtesy of Dewey H. Hodges)

where

$$Q = \begin{bmatrix} 0 & 0 \\ 0 & 0 \\ 0 & -1 \\ 1 & 0 \end{bmatrix}; \quad P = \begin{bmatrix} 0 & 0 \\ k_2 & k_3 \\ -k_1 & 0 \\ 0 & -k_1 \end{bmatrix} \quad (35)$$

The form of the sectional strain energy in a generalized Timoshenko theory is

$$2U = \epsilon^T X \epsilon + 2\epsilon^T Y \gamma_s + \gamma_s^T G \gamma_s \quad (36)$$

The 1D constitutive law is then

$$\begin{Bmatrix} F_1 \\ M_1 \\ M_2 \\ M_3 \\ F_2 \\ F_3 \end{Bmatrix} = \begin{bmatrix} X & Y \\ Y^T & G \end{bmatrix} \begin{Bmatrix} \epsilon \\ \gamma_s \end{Bmatrix} \quad (37)$$

It is helpful to introduce matrices \overline{R} , \overline{S} , and \overline{T} as submatrices to the flexibility matrix so that

$$\begin{bmatrix} \overline{R} & \overline{S} \\ \overline{S}^T & \overline{T} \end{bmatrix} \begin{bmatrix} X & Y \\ Y^T & G \end{bmatrix} = \Delta_6 \quad (38)$$

where Δ_6 is the identity matrix of order six. From this definition of the flexibility matrix, one may derive

$$\begin{aligned} \overline{R} &= (X - YG^{-1}Y^T)^{-1} \\ \overline{S} &= -\overline{R}YG^{-1} \\ \overline{T} &= (\Delta_2 - \overline{S}^TY)G^{-1} \end{aligned} \quad (39)$$

where Δ_2 is the identity matrix of order two. The linearized 1D static equilibrium equations, with applied loads set to zero, is taken from page 79 of Ref. [18] and rearranged to read

$$\begin{Bmatrix} F_1 \\ M_1 \\ M_2 \\ M_3 \\ F_2 \\ F_3 \end{Bmatrix}' + \begin{bmatrix} D_3 & D_4 \\ D_2 & D_1 \end{bmatrix} \begin{Bmatrix} F_1 \\ M_1 \\ M_2 \\ M_3 \\ F_2 \\ F_3 \end{Bmatrix} = 0 \quad (40)$$

where

$$D_1 = \begin{bmatrix} 0 & -k_1 \\ k_1 & 0 \end{bmatrix}; \quad D_2 = \begin{bmatrix} k_3 & 0 & 0 & 0 \\ -k_2 & 0 & 0 & 0 \end{bmatrix}; \quad D_3 = \begin{bmatrix} 0 & 0 & 0 & 0 \\ 0 & 0 & -k_3 & k_2 \\ 0 & k_3 & 0 & -k_1 \\ 0 & -k_2 & k_1 & 0 \end{bmatrix} \quad (41)$$

and $D_4 = Q - D_2^T$. Upon substituting Eq. (37) into Eq. (40) and taking the derivatives, one may express the derivatives of the strain measures as

$$\begin{Bmatrix} \epsilon \\ \gamma_s \end{Bmatrix}' = -[Z] \begin{Bmatrix} \epsilon \\ \gamma_s \end{Bmatrix} \quad (42)$$

where

$$\begin{bmatrix} Z \end{bmatrix} = \begin{bmatrix} \bar{R} & \bar{S} \\ \bar{S}^T & \bar{T} \end{bmatrix} \left[\begin{bmatrix} X & Y \\ Y^T & G \end{bmatrix}' + \begin{bmatrix} D_3 & D_4 \\ D_2 & D_1 \end{bmatrix} \begin{bmatrix} X & Y \\ Y^T & G \end{bmatrix} \right] \quad (43)$$

By taking derivatives of the above equation, along with recursive substitutions, the second and third derivatives of the strain measures are found as

$$\begin{Bmatrix} \epsilon \\ \gamma_s \end{Bmatrix}'' = [Z_2] \begin{Bmatrix} \epsilon \\ \gamma_s \end{Bmatrix}; \quad \begin{Bmatrix} \epsilon \\ \gamma_s \end{Bmatrix}''' = -[Z_3] \begin{Bmatrix} \epsilon \\ \gamma_s \end{Bmatrix} \quad (44)$$

where

$$\begin{aligned} [Z_2] &= [Z]^2 - [Z]' \\ [Z_3] &= [Z]'' - 2[Z]'[Z] - [Z][Z]' + [Z]^3 \end{aligned} \quad (45)$$

Now one may find expressions for matrices X , Y , and G by substituting Eqs. (34), (42), (43), (44), and (45) into Eq. (28), and then equating the resulting equation with Eq. (36). The resulting equations involve the unknown stiffness matrices, its derivatives, and known matrices A , B , C , and D . Note that if derivatives of k_1 , k_2 , and k_3 , which implicitly appear in these equations, are nonzero, then it implies the presence of nonlinear variations of twist and curvatures.

The resulting equations may be written as

$$\begin{aligned} X &= X_A + X_B + X_C + X_D \\ Y &= Y_A + Y_B + Y_C + Y_D \\ G &= G_A + G_B + G_C + G_D \end{aligned} \quad (46)$$

where the subscript indicates the source of the contribution. For example, Y_A represents the contribution to Y from stiffness matrix A whereas G_D represents the contribution to G from stiffness matrix D . If only terms up to 2nd-order in the small

parameters are kept, then these individual contributions may be written as

$$\begin{aligned}
X_A &= (\Delta_4 - Q[Z]_{21})^T A (\Delta_4 - Q[Z]_{21}) \\
X_B &= 2 (\Delta_4 - Q[Z]_{21})^T B (Q[Z_2]_{21} - [Z]_{11} - P[Z]_{21}) \\
X_C &= (Q[Z_2]_{21} - [Z]_{11} - P[Z]_{21})^T C (Q[Z_2]_{21} - [Z]_{11} - P[Z]_{21}) \\
X_D &= 2 (\Delta_4 - Q[Z]_{21})^T D ([Z_2]_{11} - Q[Z_3]_{21} + P[Z_2]_{21} - 2P'[Z]_{21})
\end{aligned} \tag{47}$$

$$\begin{aligned}
Y_A &= (\Delta_4 - Q[Z]_{21})^T A (P - Q[Z]_{22}) \\
Y_B &= (\Delta_4 - Q[Z]_{21})^T B (Q[Z_2]_{22} - [Z]_{12} - P[Z]_{22} + P') \\
&\quad + ([Z]_{11} - Q[Z_2]_{21} + P[Z]_{21})^T B^T (Q[Z]_{22} - P) \\
Y_C &= (Q[Z_2]_{21} - [Z]_{11} - P[Z]_{21})^T C (Q[Z_2]_{22} - [Z]_{12} - P[Z]_{22} + P') \\
Y_D &= (\Delta_4 - Q[Z]_{21})^T D ([Z_2]_{12} - Q[Z_3]_{22} + P[Z_2]_{22} - 2P'[Z]_{22}) \\
&\quad + (Q[Z_3]_{21} - [Z_2]_{11} - P[Z_2]_{21} + 2P'[Z]_{21})^T D^T (Q[Z]_{22} - P)
\end{aligned} \tag{48}$$

and

$$\begin{aligned}
G_A &= (P - Q[Z]_{22})^T A (P - Q[Z]_{22}) \\
G_B &= 2 (P - Q[Z]_{22})^T B (Q[Z_2]_{22} - [Z]_{12} - P[Z]_{22} + P') \\
G_C &= (Q[Z_2]_{22} - [Z]_{12} - P[Z]_{22} + P')^T C (Q[Z_2]_{22} - [Z]_{12} - P[Z]_{22} + P') \\
G_D &= 2 (P - Q[Z]_{22})^T D ([Z_2]_{12} - Q[Z_3]_{22} + P[Z_2]_{22} - 2P'[Z]_{22})
\end{aligned} \tag{49}$$

The matrices are partitioned such that subscript 11 refers to the partition occupying rows 1–4 and columns 1–4, subscript 12 refers to the partition occupying rows 1–4 and columns 5–6, subscript 21 refers to the partition occupying rows 5–6 and columns 1–4, and subscript 22 refers to the partition occupying rows 5–6 and columns 5–6. For clarity,

$$[Z] = \begin{bmatrix} [Z]_{11} & [Z]_{12} \\ [Z]_{21} & [Z]_{22} \end{bmatrix}; \quad [Z_2] = \begin{bmatrix} [Z_2]_{11} & [Z_2]_{12} \\ [Z_2]_{21} & [Z_2]_{22} \end{bmatrix}; \quad [Z_3] = \begin{bmatrix} [Z_3]_{11} & [Z_3]_{12} \\ [Z_3]_{21} & [Z_3]_{22} \end{bmatrix} \tag{50}$$

Explicit expressions for matrices $[Z]'$ and $[Z]''$ are found by simply taking derivatives

of $[Z]$. Matrix $[Z]'$ is found to be

$$\begin{aligned}
[Z]' = & \begin{bmatrix} \bar{R} & \bar{S} \\ \bar{S}^T & \bar{T} \end{bmatrix}' \begin{bmatrix} X & Y \\ Y^T & G \end{bmatrix}' + \begin{bmatrix} D_3 & D_4 \\ D_2 & D_1 \end{bmatrix} \begin{bmatrix} X & Y \\ Y^T & G \end{bmatrix} \\
& + \begin{bmatrix} \bar{R} & \bar{S} \\ \bar{S}^T & \bar{T} \end{bmatrix} \begin{bmatrix} X & Y \\ Y^T & G \end{bmatrix}'' + \begin{bmatrix} D_3 & D_4 \\ D_2 & D_1 \end{bmatrix}' \begin{bmatrix} X & Y \\ Y^T & G \end{bmatrix} \\
& + \begin{bmatrix} \bar{R} & \bar{S} \\ \bar{S}^T & \bar{T} \end{bmatrix} \begin{bmatrix} D_3 & D_4 \\ D_2 & D_1 \end{bmatrix} \begin{bmatrix} X & Y \\ Y^T & G \end{bmatrix}'
\end{aligned} \tag{51}$$

$[Z]''$ may be simplified by discarding terms that are higher than 2nd-order in terms of the small parameters. The submatrices of $[Z]''$, after discarding most higher-order terms, are then

$$\begin{aligned}
[Z]''_{11} &= \bar{R}'' Q Y^T + 2\bar{R}' Q (Y^T)' + \bar{R} Q (Y^T)'' \\
[Z]''_{12} &= \bar{R}'' Q G + 2\bar{R}' Q G' + \bar{R} Q G'' \\
[Z]''_{21} &= (\bar{S}^T)'' Q Y^T + 2(\bar{S}^T)' Q (Y^T)' + \bar{S}^T Q (Y^T)'' \\
[Z]''_{22} &= (\bar{S}^T)'' Q G + 2(\bar{S}^T)' Q G' + \bar{S}^T Q G''
\end{aligned} \tag{52}$$

This particular problem is then restated as finding X , Y , and G to satisfy Eq. (46).

Due to modeling spanwise nonuniformity, the system of nonlinear equations are 2nd-order ordinary differential equations (ODEs) in X , Y , and G . Submatrices of the flexibility matrix \bar{R} , \bar{S} , and \bar{T} are fully defined by X , Y , and G , so the presence of derivatives of these flexibility submatrices does not change the system from being a system of nonlinear 2nd-order ODEs in any quantities other than X , Y , and G . Section 2.7 discusses one approach to solving these equations.

2.4 Reduced Classical Beam Stiffness Matrix

In addition to transforming the 2nd-order asymptotically-correct energy into generalized Timoshenko form, it is also desirable to be able to transform it into the form from classical beam theory. The stiffness matrix from such a transformation is referred to

as the reduced classical stiffness matrix A_{cl} . This matrix would be compatible with 1D global analysis based on classical beam theory, which is still widely used. This matrix is more accurate than simply using the classical stiffness matrix from Eq. (20), because it is derived from a higher-order theory and includes geometric corrections from spanwise nonuniformity, initial twist, and initial curvatures.

The transformation is performed in a similar manner as the transformation to generalized Timoshenko form. The main idea is to eliminate derivatives of the classical strain measures, which is accomplished using the 1D constitutive law and the 1D static equilibrium equations. Unfortunately, the transformation does not work in practice. First, the described transformation is not valid for prismatic beams. Regarding beams that are not prismatic, an issue arises due to a need to take the inverse of a matrix that is either singular or nearly singular. The derivation and the issue are both documented in Appendix D.

The reduced classical stiffness matrix A_{cl} may still be found. One can recover A_{cl} from the 6×6 generalized Timoshenko stiffness matrix by a “condensation” of shear strain measures. The strain energy from generalized Timoshenko theory is derived from the 2nd-order asymptotically-correct energy along with kinematics. Therefore, both energies must be identical in cases where the shear strain measures are zero. Stiffness matrix A_{cl} could then be recovered by minimizing the generalized Timoshenko energy with respect to shear strain measures, which results in the following relationship:

$$A_{cl} = X - YG^{-1}Y^T \quad (53)$$

2.5 *Recovery Relations*

A complete 2D cross-sectional analysis would provide relations for the 3D stress, strain, and displacement fields. These quantities became lost to the 1D global analysis due to dimensional reduction, so relations which use results from the 1D global

analysis are needed to recover these quantities. The 1D strain measures are more abstract, so derivations here are based on 1D stress resultants and displacements as inputs to the recovery relations. Recovery relations are shown for the generalized Timoshenko theory and not for classical theory, because classical theory does not account for nonuniformity effects.

From the 2nd-order asymptotically-correct theory, the warping field that is correct up to $O(a/R)$ and $O(a/\ell)$ is expressed as

$$w(x_1, x_2, x_3) = S(x_1, x_2, x_3) \left[(\hat{V}_0 + V_{1R\tau})\bar{\epsilon} + V_{1S}\bar{\epsilon}' \right] \quad (54)$$

The 3D strain field, in terms of 1D generalized Timoshenko strain measures and its derivatives, is derived by substituting Eqs. (54) and (34) into Eq. (5). The result explicitly reads

$$\begin{aligned} \Gamma = & \Gamma_\ell S V_{1S} \epsilon'' + \Gamma_\ell S V_{1S} Q \gamma_s''' + \Gamma_\ell S V_{1S} P \gamma_s'' + \Gamma_\ell S V_{1S} P'' \gamma_s + 2\Gamma_\ell S V_{1S} P' \gamma_s' + \\ & \left[(\Gamma_a + \Gamma_R) S V_{1S} + \Gamma_\ell S (\hat{V}_0 + V_{1R\tau} + V_{1S}') + \Gamma_\ell S' V_{1S} \right] (\epsilon' + Q \gamma_s'' + P \gamma_s' + P' \gamma_s) + \\ & \left[(\Gamma_a + \Gamma_R) S (\hat{V}_0 + V_{1R\tau}) + \Gamma_\epsilon + \Gamma_\ell S (\hat{V}_0' + V_{1R\tau}') + \Gamma_\ell S' (\hat{V}_0 + V_{1R\tau}) \right] (\epsilon + Q \gamma_s' + P \gamma_s) \end{aligned} \quad (55)$$

Derivatives of the generalized Timoshenko strain measures are needed, so they are derived from the 1D constitutive law. Let S_R be the stiffness matrix of a rearranged form of Eq. (37) so that

$$\epsilon_R = S_R^{-1} F_R \quad (56)$$

where $\epsilon_R = [\gamma_{11} \ 2\gamma_{12} \ 2\gamma_{13} \ \kappa_1 \ \kappa_2 \ \kappa_3]^T$ and $F_R = [F_1 \ F_2 \ F_3 \ M_1 \ M_2 \ M_3]^T$. Unlike the derivation of the strain energy, calculations of strains need to include distributed applied and inertial loads to be sufficiently accurate. The first derivative of F_R is found from the 1D nonlinear equilibrium equations (Eq. (5.39) of Ref. [18]) and given here as

$$F_R' = -R_R F_R - \phi = - \begin{bmatrix} \tilde{K} & O_3 \\ \tilde{e}_1 + \tilde{\gamma} & \tilde{K} \end{bmatrix} F_R - \phi \quad (57)$$

where $\phi = [f_1 \ f_2 \ f_3 \ m_1 \ m_2 \ m_3]^T$ is the distributed 1D applied and inertial loads in the \mathbf{B}_i basis. Differentiating Eq. (57), while applying recursive relationships, results in

$$\begin{aligned} F_R'' &= (R_R^2 - R_R')F_R + R_R\phi - \phi' \\ F_R''' &= (-R_R^3 + R_R R_R' + 2R_R' R_R - R_R'')F_R + (-R_R^2 + 2R_R')\phi + R_R\phi' - \phi'' \end{aligned} \quad (58)$$

Differentiating Eq. (56) results in

$$\begin{aligned} \epsilon_R' &= S_R^{-1} F_R' + (S_R^{-1})' F_R \\ \epsilon_R'' &= S_R^{-1} F_R'' + 2(S_R^{-1})' F_R' + (S_R^{-1})'' F_R \\ \epsilon_R''' &= S_R^{-1} F_R''' + 3(S_R^{-1})' F_R'' + 3(S_R^{-1})'' F_R' + (S_R^{-1})''' F_R \end{aligned} \quad (59)$$

Finally, Eqs. (57) and (58) may be substituted into Eq. (59) to obtain derivatives of the generalized Timoshenko strain measures, which are then substituted into Eq. (55) for the 3D strain field. The stress field is calculated using Hooke's law.

The 3D displacement field is found using the following expression

$$U_i(x_1, x_2, x_3) = u_i(x_1) + x_\alpha [C_{\alpha i}(x_1) - \delta_{\alpha i}] + C_{ji}(x_1) w_j(x_1, x_2, x_3) \quad (60)$$

where C_{ij} are components of the direction cosine matrix representing finite rotations of the cross-sectional frame of the deformed beam. Both u_i and C_{ij} are outputs from the 1D global analysis, which are inputs to the recovery relations.

2.6 Calculating Derivatives by Finite Differences

The formulations thus far show that effects of spanwise nonuniformity originate from the appearance of derivative terms, so this section discusses one way of approximating the derivatives. One type of derivatives are pointwise derivatives, such as $D_{\ell\epsilon}'$ and \hat{V}_0' , which are functions of all three spatial variables. The calculations of $D_{R\tau}$, $V_{1R\tau}$, A , and B are influenced by pointwise derivatives as shown in Eqs. (26), (29), and (30). Another type of derivatives are sectionwise derivatives, such as X' and \overline{R}' , which are

only defined for sections. The sectionwise derivatives appear in Eqs. (51) and (52), so they influence calculations of the generalized Timoshenko stiffness matrices X , Y and G . Both pointwise and sectionwise derivatives appear in the recovery relations.

Analytical formulae to both pointwise and sectionwise derivatives may be impossible to derive. Therefore they are approximated by finite differences. The main idea of derivative approximation by finite differences is that derivatives of a locally-smooth function $f(x_1)$ may be approximated at location $x_1 = m$ by Taylor series expansions about location $x_1 = m$, which implies that $f(x_1)$ is needed at certain locations within a small radius from $x_1 = m$. These formulae are easily derived for derivatives of any order up to any order of accuracy (in terms of a parameter that represents a small distance from $x_1 = m$). Note that the order of accuracy from derivative approximations correspond in meaning to the order of accuracy from cross-sectional analysis quantities, e.g. 2nd-order energy; but the experience of this author in performing these computations leads to a recommendation of using derivative approximation formulae that are at least 2nd-order accurate.

Figure 4 illustrates an example of applying finite differences. Let the decision be made that 1st-order derivatives at location $x_1 = m$ are to be approximated by the 2nd-order accurate central-difference approximation of

$$f'(m) \approx \frac{f(m+h) - f(m-h)}{2h} \quad (61)$$

where $x_1 = (m+h)$ and $(m-h)$ are both considered to be near enough to $x_1 = m$. Finite element meshes at locations $x_1 = (m-h)$, m , and $(m+h)$ are drawn so that $f(x_1)$ may be computed at these three locations. Computations of sectionwise derivatives are straightforward. Pointwise derivatives are computed between points having the same values of x_2 and x_3 . An implication of employing the finite element method is that pointwise functions are computed only at x_2 and x_3 locations where a node is placed in the mesh.

The sections of realistic rotary and fixed wings are complicated enough that it

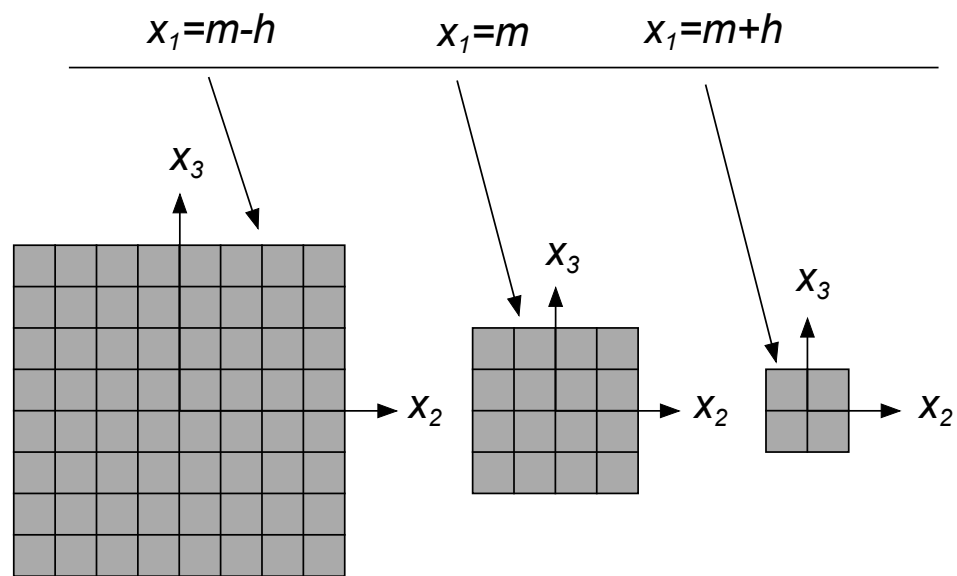


Figure 4: Example of approximating derivatives by finite differences with three sections

is rarely practical to generate meshes, such that corresponding nodes exist for each mesh at all points where pointwise derivatives are desired. If pointwise values are needed at a point, where a node does not exist but the point is within the planar space occupied by a finite element, then one way to find the pointwise values would be by planar interpolation using known pointwise values (which would be from the nodal locations of the planar finite element). The described situation gives rise to the term S' . The shape function S is defined for any point given its planar coordinates within each planar element. If a planar element in one section is identical to another element from its adjacent section in all aspects, including the physical x_2 - and x_3 -coordinates that define their planar elemental boundaries, then S is not a function of x_1 within the x_2 - x_3 space of that element. In other words, variations of S in the x_1 -direction appear if mismatches in elements and nodes exist between adjacent sections.

In situations where corresponding points cannot exist between meshes, then either a forward- or backward-difference approximation will instead be applied. A good example is the tapered beam from Fig. 1. It is clear there that for points on the upper and lower edges, there are no corresponding points if a mesh is generated to the right. The pointwise derivative for these points would have to be approximated by differencing with a mesh to the left.

A subtle yet important point, related to the previous paragraph, concerns that of nonuniform beams composed of multiple materials. Figure 5 illustrates an example of a beam composed of two different materials. Location of points forming the outer boundary of each section does not vary along the span, but spanwise nonuniformity exists from having a spanwise shift in the location of the boundary between materials. One must realize that pointwise derivatives, for points located on the boundary between two materials, are discontinuous with respect to any direction which causes a discontinuity in material. It is unclear how to determine derivatives at these boundary points. It is clear, however, that usage of the approximation by finite differences

to calculate pointwise derivatives must not involve points composed of different materials. Even for points that are merely located near a boundary, care must be taken so that derivatives are approximated using only points from the common material as that of the points of interest. These thoughts imply that pointwise derivatives near the material boundaries would likely be approximated by either a forward- or a backward-difference scheme, depending on which is appropriate. Note that undefined pointwise derivatives prevent calculations of the 3D recovery relations, however, section properties such as inertial and stiffness matrices may still be calculated. Recall that these section properties are found by integration over the cross-section. Therefore, the cross-section may be treated as multiple sections without material boundaries so that section properties of the original section are found by summation of properties from each smaller section. The lesson of this simple example is easily applicable to rotary and fixed wings, where a spanwise shift in location of the boundary of two adjacent components is a definite possibility.

It should be evident now that approximating derivatives by finite differences requires deliberation. As an example, the end of Sec. 2.7 provides detailed decisions on how to perform these derivative approximations for a tapered beam with the geometry as shown in Fig. 1.

2.7 Numerical Solution Procedure

The theory presented is admittedly complicated, so an overview of its solution procedure is presented. Figure 6 illustrates the entire procedure from preprocessing of cross-sectional finite element meshes to application of recovery relations. A version of VABS featuring nonuniformity effects has not officially been released, so boxes within Fig. 6 having the label of “VABS” refer to a modified version of VABS featuring nonuniformity effects.

A brief description of each step from Fig. 6 is now given. The “PreProcess” step

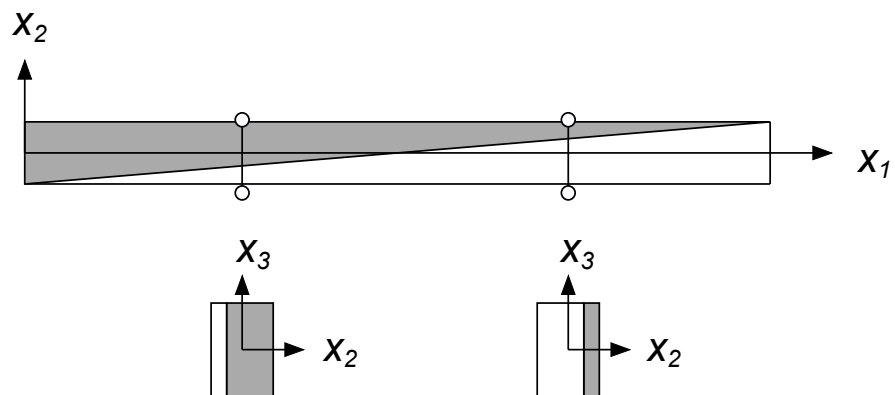


Figure 5: Example of spanwise nonuniformity from material boundary

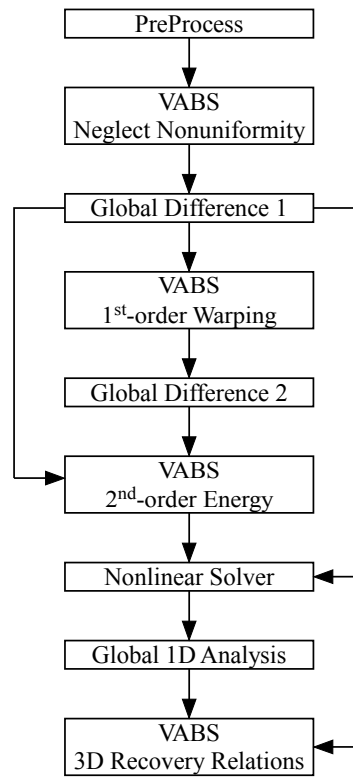


Figure 6: Solution procedure

refers to generation of the finite element meshes for not only the cross-section(s) of interest, where elastic stiffness constants are desired, but also for all other cross-sections needed for the derivative approximations. An analysis, neglecting nonuniformity effect, is then performed by VABS on each cross-section. A nonlinear solver, separate from VABS, may be needed to find the generalized Timoshenko stiffness matrices from Eq. (46) even when nonuniformity effects are neglected (to be discussed in Chap. 3). The “Global Difference 1” step then performs derivative approximations to approximate both pointwise derivatives needed in Eqs. (16) and (26), as well as sectionwise derivatives needed in Eqs. (51) and (52). A second round of VABS analysis is performed for each section to solve for the 1st-order warping fields. The “Global Difference 2” step then approximates derivatives of the 1st-order warping fields, which are needed as inputs to Eqs. (29) and (30). A third round of VABS analysis is then performed only at the section(s) of interest to attain A , B , C , and D . For the section(s) of interest, a nonlinear solver is then applied to solve Eq. (46) for the generalized Timoshenko stiffness matrices. In the case of rotating beams such as rotor blades, the generalized Timoshenko stiffness matrices, inertial properties, and stiffness matrices associated with rotational effects (see pp. 88–96 of Ref. [18]) then complete the beam properties for use as inputs into a blade structural dynamics analysis. Outputs from the 1D global analysis, the flexibility matrix, applied loading terms as well as its derivatives are needed as inputs to VABS in the recovery relations.

Aside from the approximation inherently associated with finite differences, there is an additional approximation with the procedure shown due to nonuniformity. Recall that Eq. (46) is to be solved to attain the generalized Timoshenko stiffness matrices and that it represents a nonlinear system of ODEs, which may be simplified to a nonlinear system of algebraic equations at each particular section presuming knowledge of the derivatives of the generalized Timoshenko stiffness matrices. Figure 6 shows that these particular derivatives are found from “Global Difference 1,” which

means that the derivatives are approximated from applying finite differences based on stiffness matrices neglecting nonuniformity effects. Nonuniformity effects represent higher-order corrections to the 0th-order solution, found for the cross-section as if the beam is prismatic. Therefore, the accuracy of approximating derivatives of stiffness matrices in this manner may be characterized as being 0th-order accurate in terms of small parameters of the cross-sectional analysis. Upon solving for the generalized Timoshenko stiffness matrices from “Nonlinear Solver,” one may update the derivative approximations and will likely not find it to match the original approximations. While it may be possible for one to form an outer loop to the procedure described in an attempt to achieve convergence in the derivatives, this author is not in favor of this action. The formation of this outer loop would be an attempt to solve the original nonlinear system of ODEs, but not having any boundary conditions means that uniqueness of the solution cannot be guaranteed. One could find a solution, to the system of ODEs, and that it could well be a poor representation of the actual stiffness matrices.

With the numerical solution procedure presented, decisions regarding how to perform the derivative approximations may be explained by taking the linearly tapered beam from Fig. 1 as an example. In this paragraph, keep in mind that only derivative approximations that are at least 2nd-order accurate are used. Also keep in mind that central-difference approximations are preferred over forward- and backward-difference approximations. Assuming that only accurate stiffness matrices at one section are desired, then use of Eq. (61) to approximate $V'_{1R\tau}$ and V'_{1S} from “Global Difference 2” would require knowledge of $V_{1R\tau}$ and V_{1S} at both sections adjacent to the section of interest. In order for $V_{1R\tau}$ and V_{1S} to be accurate at the two adjacent sections would require that their pointwise derivatives, calculated from “Global Difference 1,” should be at least 2nd-order accurate. For the section to the left of our section of interest, this last requirement may be satisfied by applying Eq. (61) using values from its own

two adjacent sections. For the section to the right of our section of interest, 2nd-order accurate pointwise derivatives from “Global Difference 1” may also use Eq. (61) for most points. Points for which Eq. (61) is not applicable, e.g. those lying on the upper and lower edges, 2nd-order accurate pointwise derivatives may only be attained by the backward-difference approximation of

$$f'(m) \approx \frac{3f(m) - 4f(m - h) + f(m - 2h)}{2h} \quad (62)$$

From this discussion, it appears that the “PreProcess” step requires generation of finite element meshes for sections located at $x_1 = (m - 2h), (m - h), m$, and $(m + h)$ to attain stiffness matrices at $x_1 = m$ that are based on 2nd-order approximations. This simple example is by no means sufficiently general to apply its decisions on finite differences to all sections, but only serves to exemplify the type of reasoning involved.

CHAPTER III

TRANSFORMATION TO GENERALIZED TIMOSHENKO FORM FOR UNIFORM BEAMS

Issues in obtaining the generalized Timoshenko stiffness matrix for uniform beams are identified and discussed herein. These issues must be resolved for the uniform case before it can be applied to the nonuniform case. The procedure to obtain the generalized Timoshenko stiffness matrix for nonuniform beams, described in Sec. 2.3, remains valid for uniform beams. Without spanwise nonuniformity, solving stiffness matrices X , Y , and G is reduced to solving a set of nonlinear algebraic equations. For uniform beams, the system of equations to be solved is

$$\begin{aligned} X &= X_A + X_B + X_C + X_D \\ Y &= Y_A + Y_B + Y_C + Y_D \\ G &= G_A + G_B + G_C + G_D \end{aligned} \tag{63}$$

These individual contributions may be written as

$$\begin{aligned} X_A &= (\Delta_4 - Q[Z]_{21})^T A (\Delta_4 - Q[Z]_{21}) \\ X_B &= 2 (\Delta_4 - Q[Z]_{21})^T B (Q[Z_2]_{21} - [Z]_{11} - P[Z]_{21}) \\ X_C &= (Q[Z_2]_{21} - [Z]_{11} - P[Z]_{21})^T C (Q[Z_2]_{21} - [Z]_{11} - P[Z]_{21}) \\ X_D &= 2 (\Delta_4 - Q[Z]_{21})^T D ([Z_2]_{11} - Q[Z_3]_{21} + P[Z_2]_{21}) \end{aligned} \tag{64}$$

$$\begin{aligned}
Y_A &= (\Delta_4 - Q[Z]_{21})^T A (P - Q[Z]_{22}) \\
Y_B &= (\Delta_4 - Q[Z]_{21})^T B (Q[Z_2]_{22} - [Z]_{12} - P[Z]_{22}) \\
&\quad + ([Z]_{11} - Q[Z_2]_{21} + P[Z]_{21})^T B^T (Q[Z]_{22} - P) \\
Y_C &= (Q[Z_2]_{21} - [Z]_{11} - P[Z]_{21})^T C (Q[Z_2]_{22} - [Z]_{12} - P[Z]_{22}) \\
Y_D &= (\Delta_4 - Q[Z]_{21})^T D ([Z_2]_{12} - Q[Z_3]_{22} + P[Z_2]_{22}) \\
&\quad + (Q[Z_3]_{21} - [Z_2]_{11} - P[Z_2]_{21})^T D^T (Q[Z]_{22} - P)
\end{aligned} \tag{65}$$

and

$$\begin{aligned}
G_A &= (P - Q[Z]_{22})^T A (P - Q[Z]_{22}) \\
G_B &= 2 (P - Q[Z]_{22})^T B (Q[Z_2]_{22} - [Z]_{12} - P[Z]_{22}) \\
G_C &= (Q[Z_2]_{22} - [Z]_{12} - P[Z]_{22})^T C (Q[Z_2]_{22} - [Z]_{12} - P[Z]_{22}) \\
G_D &= 2 (P - Q[Z]_{22})^T D ([Z_2]_{12} - Q[Z_3]_{22} + P[Z_2]_{22})
\end{aligned} \tag{66}$$

where $[Z_2] = [Z]^2$, $[Z_3] = [Z]^3$. Matrix $[Z]$, which is reduced from its form in Eq. (43), is now simply

$$[Z] = \begin{bmatrix} R & S \\ S^T & T \end{bmatrix} \begin{bmatrix} D_3 & D_4 \\ D_2 & D_1 \end{bmatrix} \begin{bmatrix} X & Y \\ Y^T & G \end{bmatrix} \tag{67}$$

This particular problem is then restated as finding X , Y , and G to satisfy Eq. (63).

The solution to this problem inside VABS is given in Ref. [53] and is based on a perturbation technique. Its idea is that matrices X , Y , and G may be expanded into asymptotic series, thus these matrices may be satisfactorily solved up to the desired order of accuracy. This desired order of accuracy is two in terms of the small parameters, because the transformation process started with an energy that is asymptotically-correct up to 2nd-order. This means that X , Y , and G all need to be accurate up to 2nd-order. As with typical perturbation methods, the solutions are obtained successively from 0th-order up to higher orders. Note that the 0th-order solution corresponds to the stiffness constants of a uniform beam that is prismatic, i.e. having no twist and curvatures such that $k_1 = k_2 = k_3 = 0$. The impetus, from Ref.

[53], to using the perturbation method is that the equations become simple enough that analytical solutions are derived.

3.1 *Prismatic Beams*

Two issues are identified with the 0th-order solution in VABS. The first issue is that the system of equations to be solved, i.e. Eqs. (63), (64), (65), and (66), is missing some terms. A convenient relationship, which may be proved and used in lieu of Eq. (64), is written as

$$X = A + YG^{-1}Y^T \quad (68)$$

The above relationship is used in VABS, regardless if the beam is prismatic or not, and is discussed more in the next section. Contributions to Y and G by the known stiffness matrices, A , B , C , and D , may be written as

$$\begin{aligned} Y_A &= AQG^{-1}Y^TA^{-1}QG + \underline{YQ^TA^{-1}YG^{-1}Q^TAQG^{-1}Y^TA^{-1}QG} \\ Y_B &= -BA^{-1}QG - \underline{YQ^TA^{-1}YG^{-1}Q^TBA^{-1}QG} - \underline{YQ^TA^{-1}B^TQG^{-1}Y^TA^{-1}QG} \\ Y_C &= YQ^TA^{-1}CA^{-1}QG \\ Y_D &= 0 \end{aligned} \quad (69)$$

and

$$\begin{aligned} G_A &= \underline{GQ^TA^{-1}YG^{-1}Q^TAQG^{-1}Y^TA^{-1}QG} \\ G_B &= -\underline{2GQ^TA^{-1}YG^{-1}Q^TBA^{-1}QG} \\ G_C &= GQ^TA^{-1}CA^{-1}QG \\ G_D &= 0 \end{aligned} \quad (70)$$

where the underlined terms represent terms that are missing in the current VABS formulation. There are cases where these underlined terms are negligible, but the terms cannot be neglected in general. Note that the addition of these underlined terms means that a simple 0th-order analytical solution may not exist. Therefore, the

original impetus to using the perturbation method is somewhat lost. Note that these terms are purposely dropped in the current VABS formulation as they are thought to be higher-order terms. The second issue is that the 0th-order solution in VABS is only an approximation. In general, it is an approximation even in cases where the underlined terms may be neglected. The derivation to the solution involves a projection, which reduces the order of the system, and renders the resulting solution as merely an approximation. The intention of pointing out this projection is not to pass judgment on whether or not it is a good approximation, but rather to point out that it is an approximation and should be recognized as such (it was previously thought to be the exact solution). In spite of these two issues, the VABS prediction amazingly does satisfy the system of equations given here for all isotropic cross-sections examined by this author. Reference [31] also reports similar success for the VABS prediction to isotropic prismatic cross-sections. To avoid confusions that may develop with the passage of time, all results in this chapter listed as VABS results are from VABS 3.1.

Two composite box beam cross-sections are now introduced to illustrate the two issues. Both sections have the same geometry, but with different material properties. The geometry is given by Fig. 7 with the dimensions $b = 0.9530$ in, $a = 0.5300$ in, and $t = 0.030$ in. The beam reference line is chosen to coincide with the centroid of the section. The x_2 - and x_3 -axes are parallel to the line segments defining lengths b and a , respectively, while the positive x_1 -direction is coming out of the page. Naming conventions of the two sections are CUS and CAS1, which follow names given on pages 73 and 70 from Ref. [53], respectively. Both sections are made of AS4/3501-6 graphite/epoxy. This material has the properties $E_{11} = 20.59 \times 10^6$ psi, $E_{22} = E_{33} = 1.420 \times 10^6$ psi, $G_{12} = G_{13} = 0.8700 \times 10^6$ psi, and $G_{23} = 0.6960 \times 10^6$ psi. Poisson's ratios are $\nu_{12} = \nu_{13} = 0.30$ and $\nu_{23} = 0.34$ for the CUS section. Poisson's ratios are $\nu_{12} = \nu_{13} = \nu_{23} = 0.42$ for the CAS1 section. The density is $\rho = 0.001774$ slug/in³.

Layup angles for all walls are $[15^\circ]_6$ for the CUS section. Layup angles are $[15^\circ]_6$ in the upper wall, $[-15^\circ]_6$ in the lower wall, $[\pm 15^\circ]_6$ in the left wall, and $[\mp 15^\circ]_6$ in the right wall for the CAS1 section. Results to experimental testing of these two sections are found in Ref. [7]. In addition to Ref. [53], these two sections have also been studied theoretically in Refs. [7], [23], [31], and [35]. VABS input files to both sections are taken from the example files, which are part of the package in the distribution of VABS.

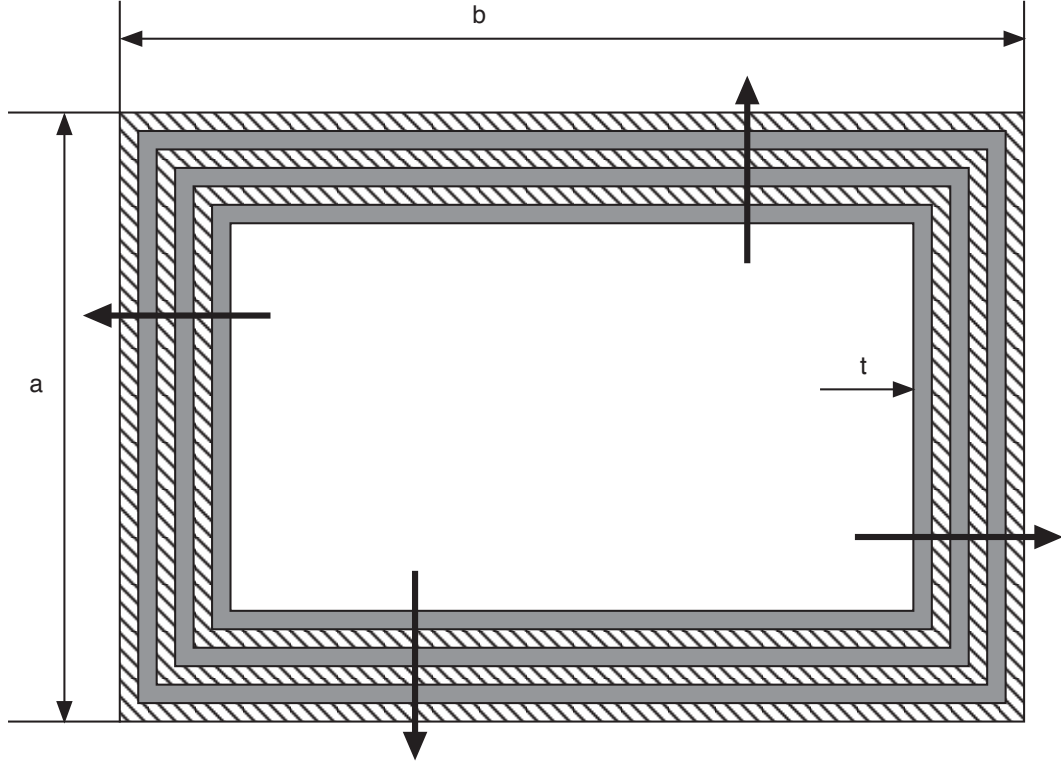


Figure 7: CUS and CAS1 cross-sectional geometry (courtesy of Dewey H. Hodges)

The prismatic CUS section is a case where the missing terms are not negligible. Tables (1) and (2) demonstrate this point by displaying calculations that neglect and include the underlined terms, respectively. The column labeled “VABS” is the VABS prediction. The five rightmost columns are calculated using Eqs. (63), (69), and (70) while using values from the VABS prediction. Some columns are indicated by a letter, where the letter signifies the origin of the contribution. The rightmost

column shows the total values of X , Y , and G calculated from the equations. It is clear that contributions by some of the underlined terms, such as $G_B(1,1)$ are not negligible. Note also that the true solution to X , Y , and G must match the calculated results. The VABS prediction may be considered a solution if the underlined terms are neglected, but is not acceptable as the solution if including those terms. Table (3) shows the prediction, from the nonlinear solver “fsolve” in Matlab, by directly solving the equations iteratively without applying the perturbation method. The default search option within “fsolve”, which is the trust-region dogleg method, is the iterative method used in solving the equations. According to the Matlab documents, this “algorithm is a variant of the Powell dogleg method described in” Ref. [36] and “is similar in nature to the algorithm implemented in” Ref. [29]. Note that the Matlab prediction to X_{33} , X_{44} , Y_{31} , Y_{42} , G_{11} , and G_{22} are drastically different than the VABS prediction. The prediction from the Matlab solver does satisfy the equations including underlined terms, so it is considered a numerical solution. Table (3) also shows the prediction from NABSA, which gives outstanding agreement with the Matlab solver. The NABSA results are taken from Ref. [53].

The prismatic CAS1 cross-section is a case where the VABS prediction is not the true solution despite having all underlined terms being negligible. This is evident from Table (4), which displays calculations of X , Y , and G while using values from the VABS prediction. Only results including the underlined terms are shown (since neglecting those terms yield no difference) and the organization is in the same format as Table (2). A few of the calculated stiffness constants, such as Y_{11} , does not match the original VABS prediction, so the VABS prediction is not the true solution. Note that the Matlab solver could not find a solution in this example.

Table 1: Stiffness for the prismatic CUS cross-section, neglecting underlined terms

stiffness	VABS	A	B	C	D	total
X_{11}, lb	1.437E+06	-	-	-	-	1.437E+06
$X_{21}, \text{lb} \cdot \text{in}$	1.074E+05	-	-	-	-	1.074E+05
$X_{31}, \text{lb} \cdot \text{in}$	1.589E-08	-	-	-	-	1.600E-08
$X_{41}, \text{lb} \cdot \text{in}$	-1.116E-07	-	-	-	-	-1.120E-07
$X_{22}, \text{lb} \cdot \text{in}^2$	1.679E+04	-	-	-	-	1.679E+04
$X_{32}, \text{lb} \cdot \text{in}^2$	1.132E-09	-	-	-	-	1.000E-09
$X_{42}, \text{lb} \cdot \text{in}^2$	-1.100E-08	-	-	-	-	-1.100E-08
$X_{33}, \text{lb} \cdot \text{in}^2$	5.298E+04	-	-	-	-	5.298E+04
$X_{43}, \text{lb} \cdot \text{in}^2$	-2.075E-08	-	-	-	-	-2.100E-08
$X_{44}, \text{lb} \cdot \text{in}^2$	1.340E+05	-	-	-	-	1.340E+05
Y_{11}, lb	-6.807E-08	-1.827E-08	-9.414E-07	-6.807E-08	0	-1.028E-06
$Y_{21}, \text{lb} \cdot \text{in}$	-5.063E-09	-1.400E-09	-1.474E-07	-5.060E-09	0	-1.539E-07
$Y_{31}, \text{lb} \cdot \text{in}$	-2.905E+04	2.841E+04	-2.841E+04	-2.905E+04	0	-2.905E+04
$Y_{41}, \text{lb} \cdot \text{in}$	2.811E-08	-4.210E-09	4.210E-09	2.811E-08	0	2.811E-08
Y_{12}, lb	2.183E-08	-2.631E-08	2.023E-07	2.183E-08	0	1.979E-07
$Y_{22}, \text{lb} \cdot \text{in}$	2.221E-09	-2.560E-09	2.972E-08	2.220E-09	0	2.938E-08
$Y_{32}, \text{lb} \cdot \text{in}$	9.983E-10	-1.193E-08	1.193E-08	1.000E-09	0	1.000E-09
$Y_{42}, \text{lb} \cdot \text{in}$	-2.941E+04	3.008E+04	-3.008E+04	-2.941E+04	0	-2.941E+04
G_{11}, lb	5.042E+04	0	0	5.042E+04	0	5.043E+04
G_{21}, lb	-6.524E-09	0	0	-6.520E-09	0	-6.520E-09
G_{22}, lb	2.058E+04	0	0	2.058E+04	0	2.058E+04

Table 2: Stiffness for the prismatic CUS cross-section, including underlined terms

stiffness	VABS	A	B	C	D	total
X_{11} , lb	1.437E+06	1.437E+06	0.000E+00	0.000E+00	0	1.437E+06
X_{21} , lb · in	1.074E+05	1.074E+05	0.000E+00	0.000E+00	0	1.074E+05
X_{31} , lb · in	1.589E-08	-3.400E-08	4.206E-08	3.921E-08	0	5.510E-07
X_{41} , lb · in	-1.116E-07	-2.600E-08	-3.398E-08	-3.119E-08	0	-3.480E-07
X_{22} , lb · in ²	1.679E+04	1.679E+04	0.000E+00	0.000E+00	0	1.679E+04
X_{32} , lb · in ²	1.132E-09	-3.000E-09	3.130E-09	2.920E-09	0	8.600E-08
X_{42} , lb · in ²	-1.100E-08	-2.000E-09	-3.460E-09	-3.170E-09	0	-4.800E-08
X_{33} , lb · in ²	5.298E+04	1.091E+04	1.795E+04	1.674E+04	0	4.560E+04
X_{43} , lb · in ²	-2.075E-08	8.000E-09	2.308E-08	-1.225E-08	0	-1.100E-08
X_{44} , lb · in ²	1.340E+05	2.608E+04	4.579E+04	4.203E+04	0	1.139E+05
Y_{11} , lb	-6.807E-08	-4.832E-08	-8.813E-07	-6.807E-08	0	-9.977E-07
Y_{21} , lb · in	-5.063E-09	-3.630E-09	-1.429E-07	-5.060E-09	0	-1.516E-07
Y_{31} , lb · in	-2.905E+04	1.558E+04	-2.758E+03	-2.905E+04	0	-1.623E+04
Y_{41} , lb · in	2.811E-08	1.630E-08	-3.682E-08	2.811E-08	0	7.600E-09
Y_{12} , lb	2.183E-08	-1.587E-08	1.815E-07	2.183E-08	0	1.874E-07
Y_{22} , lb · in	2.221E-09	-1.500E-09	2.760E-08	2.220E-09	0	2.832E-08
Y_{32} , lb · in	9.983E-10	-8.330E-09	4.719E-09	1.000E-09	0	-2.610E-09
Y_{42} , lb · in	-2.941E+04	1.602E+04	-1.957E+03	-2.941E+04	0	-1.535E+04
G_{11} , lb	5.042E+04	2.226E+04	-4.452E+04	5.042E+04	0	2.817E+04
G_{21} , lb	-6.524E-09	-8.550E-09	1.710E-08	-6.520E-09	0	2.030E-09
G_{22} , lb	2.058E+04	9.839E+03	-1.968E+04	2.058E+04	0	1.074E+04

Table 3: Comparison of stiffness for the prismatic CUS cross-section between Matlab solver, VABS, and NABSA

stiffness	Matlab	VABS	NABSA
X_{11}, lb	1.437E+06	1.437E+06	1.437E+06
$X_{21}, \text{lb} \cdot \text{in}$	1.074E+05	1.074E+05	1.074E+05
$X_{31}, \text{lb} \cdot \text{in}$	-1.001E+01	1.589E-08	6.510E-08
$X_{41}, \text{lb} \cdot \text{in}$	2.704E+00	-1.116E-07	-8.916E-08
$X_{22}, \text{lb} \cdot \text{in}^2$	1.679E+04	1.679E+04	1.679E+04
$X_{32}, \text{lb} \cdot \text{in}^2$	-1.461E+00	1.132E-09	4.618E-09
$X_{42}, \text{lb} \cdot \text{in}^2$	8.708E-01	-1.100E-08	-6.856E-09
$X_{33}, \text{lb} \cdot \text{in}^2$	6.621E+04	5.298E+04	6.621E+04
$X_{43}, \text{lb} \cdot \text{in}^2$	-4.500E-08	-2.075E-08	-1.708E-08
$X_{44}, \text{lb} \cdot \text{in}^2$	1.725E+05	1.340E+05	1.725E+05
Y_{11}, lb	1.737E+01	-6.807E-08	-7.747E-08
$Y_{21}, \text{lb} \cdot \text{in}$	2.536E+00	-5.063E-09	-6.156E-09
$Y_{31}, \text{lb} \cdot \text{in}$	-5.201E+04	-2.905E+04	-5.201E+04
$Y_{41}, \text{lb} \cdot \text{in}$	7.739E-08	2.811E-08	1.895E-08
Y_{12}, lb	-1.892E+00	2.183E-08	5.235E-08
$Y_{22}, \text{lb} \cdot \text{in}$	-6.094E-01	2.221E-09	3.777E-09
$Y_{32}, \text{lb} \cdot \text{in}$	1.187E-08	9.983E-10	1.015E-08
$Y_{42}, \text{lb} \cdot \text{in}$	-5.635E+04	-2.941E+04	-5.635E+04
G_{11}, lb	9.027E+04	5.042E+04	9.024E+04
G_{21}, lb	-3.042E-08	-6.524E-09	-1.018E-08
G_{22}, lb	3.943E+04	2.058E+04	3.940E+04

Table 4: Stiffness for the prismatic CAS1 cross-section

stiffness	VABS	A	B	C	D	total
X_{11} , lb	1.367E+06	9.851E+05	-5.839E+04	3.822E+05	0	1.309E+06
X_{21} , lb · in	2.655E-08	-1.550E-08	-3.890E-06	1.330E-08	0	-1.948E-06
X_{31} , lb · in	-7.072E-08	-1.800E-07	-3.899E-06	1.180E-08	0	-2.118E-06
X_{41} , lb · in	1.411E-07	6.090E-08	3.633E-07	-6.690E-08	0	1.800E-07
X_{22} , lb · in ²	1.696E+04	1.696E+04	0.000E+00	0.000E+00	0	1.696E+04
X_{32} , lb · in ²	1.761E+04	1.761E+04	0.000E+00	0.000E+00	0	1.761E+04
X_{42} , lb · in ²	-3.506E+02	-3.506E+02	0.000E+00	0.000E+00	0	-3.506E+02
X_{33} , lb · in ²	5.912E+04	5.912E+04	0.000E+00	0.000E+00	0	5.912E+04
X_{43} , lb · in ²	-3.705E+02	-3.705E+02	0.000E+00	0.000E+00	0	-3.705E+02
X_{44} , lb · in ²	1.415E+05	1.415E+05	0.000E+00	0.000E+00	0	1.415E+05
Y_{11} , lb	-1.838E+05	-1.127E-19	1.404E+04	-1.838E+05	0	-1.697E+05
Y_{21} , lb · in	-6.380E-09	1.385E-08	9.353E-07	-6.400E-09	0	9.428E-07
Y_{31} , lb · in	-5.643E-09	4.689E-08	9.375E-07	-5.600E-09	0	9.787E-07
Y_{41} , lb · in	3.214E-08	7.070E-08	-8.736E-08	3.210E-08	0	1.550E-08
Y_{12} , lb	-1.326E+02	-1.534E-19	3.751E+02	-1.326E+02	0	2.425E+02
Y_{22} , lb · in	-8.563E-09	1.604E-08	7.432E-07	-8.600E-09	0	7.507E-07
Y_{32} , lb · in	2.842E-08	5.400E-08	7.344E-07	2.840E-08	0	8.169E-07
Y_{42} , lb · in	-4.913E-08	2.563E-08	-4.125E-08	-4.910E-08	0	-6.470E-08
G_{11} , lb	8.836E+04	7.282E-20	1.405E-18	8.836E+04	0	8.836E+04
G_{21} , lb	7.302E+01	5.586E-20	1.682E-18	7.302E+01	0	7.302E+01
G_{22} , lb	3.878E+04	5.408E-20	1.328E-18	3.878E+04	0	3.878E+04

3.2 *Initially Twisted and Curved Beams*

The two issues with VABS, which are identified in the last section related to prismatic beams, are amplified with uniform beams featuring initial twist and/or curvature. Solutions to X , Y , and G are now sought up to 2nd-order. One of the issues from the prismatic case is that the VABS formulation is missing some terms, which are underlined in Eqs. (69) and (70) for Y and G , respectively. In the case of initially twisted and/or curved beams, the VABS formulation is also missing 1st- and 2nd-order terms. This means that even if the 0th-order prediction from VABS is acceptable, its formulation to the 1st- and 2nd-order corrections to X , Y , and G cannot be correct in general due to not including all terms. The other issue from the prismatic case is that the VABS prediction is a mere approximation. Having an error in the 0th-order solution of a perturbation method has the undesirable property that the error will be propagated into its higher-order calculations.

A third issue, which pertains to beams that are not prismatic, is the VABS usage of Eq. (68) to calculate X . In the case of a prismatic beam, the 4×4 stiffness matrix A is what is recovered from the 6×6 generalized Timoshenko stiffness matrix by a “condensation” of shear strain measures. In other words, $A = A_{cl}$ in the case of prismatic beams. Equation (68) is not valid if the beam is not prismatic, because the described “condensation” procedure implicitly assumes that all geometric corrections to classical theory are embodied in A . An examination of Eq. (30) shows that geometric effects from initial twist and curvatures also affect stiffness matrix B . In fact, nonuniformity effects also appear in Eq. (30), so Eq. (68) is neither valid in the case of nonuniform beams. For beams that are not prismatic, one must then calculate X from Eq. (64).

Nonzero stiffness constants, for the CUS section, are plotted as functions of k_1 to demonstrate the discrepancy between solutions from VABS and the Matlab solver. The axis of twist is set to coincide with the beam reference line. Figures 8, 9, 10,

11, 12, 13, 14, 15, and 16 show the plots of X_{11} , X_{22} , X_{33} , X_{44} , X_{21} , Y_{31} , Y_{42} , G_{11} and G_{22} , respectively. Of the different values of k_1 examined, the least value for the radius of twist is $R = 1/k_1 = 10$ in, so the largest value of the ratio of characteristic length to R is 0.0953 if b is taken as the characteristic length. Excellent agreement exists between the two solutions for the extension stiffness X_{11} , the torsional stiffness X_{22} , and the extension-twist coupling X_{21} . The other plotted quantities do not share such excellent agreement. Some of the curves, such as bending stiffness X_{33} and shear stiffness G_{11} , do not even share the same sign in its derivative, with respect to k_1 , between the two solutions. The plots of bending stiffness X_{33} , bending-shear coupling Y_{31} , and shear stiffness G_{11} are indications that the VABS solution is missing 2nd-order terms. The plots of bending stiffness X_{44} and shear stiffness G_{22} are fairly linear, so the discrepancy between solutions from VABS and the Matlab solver there seem mostly due to the offset between their prismatic values.

It is known that the global behavior of beams with similar reduced classical stiffness matrices can be closely matched even if their generalized Timoshenko stiffness matrices are quite different. As already discussed, the VABS solution incorrectly uses Eq. (68) even when the beam is not prismatic. The reduced classical stiffness matrix from VABS is then simply equal to A . Figures 17, 18, 19, 20, and 21 show the extensional stiffness, torsional stiffness, bending stiffness about x_2 , bending stiffness about x_3 , and extension-twist coupling, respectively, from the reduced classical stiffness matrix. Components to the reduced classical stiffness matrix not plotted are negligible. Results between the Matlab solver and VABS here are exactly equal for the extensional stiffness, torsional stiffness, and extension-twist coupling for all values of k_1 . For the prismatic case, even the two bending stiffness terms are exactly equal. The departure in the bending stiffness terms from the prismatic case reflects the error from usage of Eq. (68). The results of these figures are to be kept in mind for the discussion of results in Sec. 3.4.

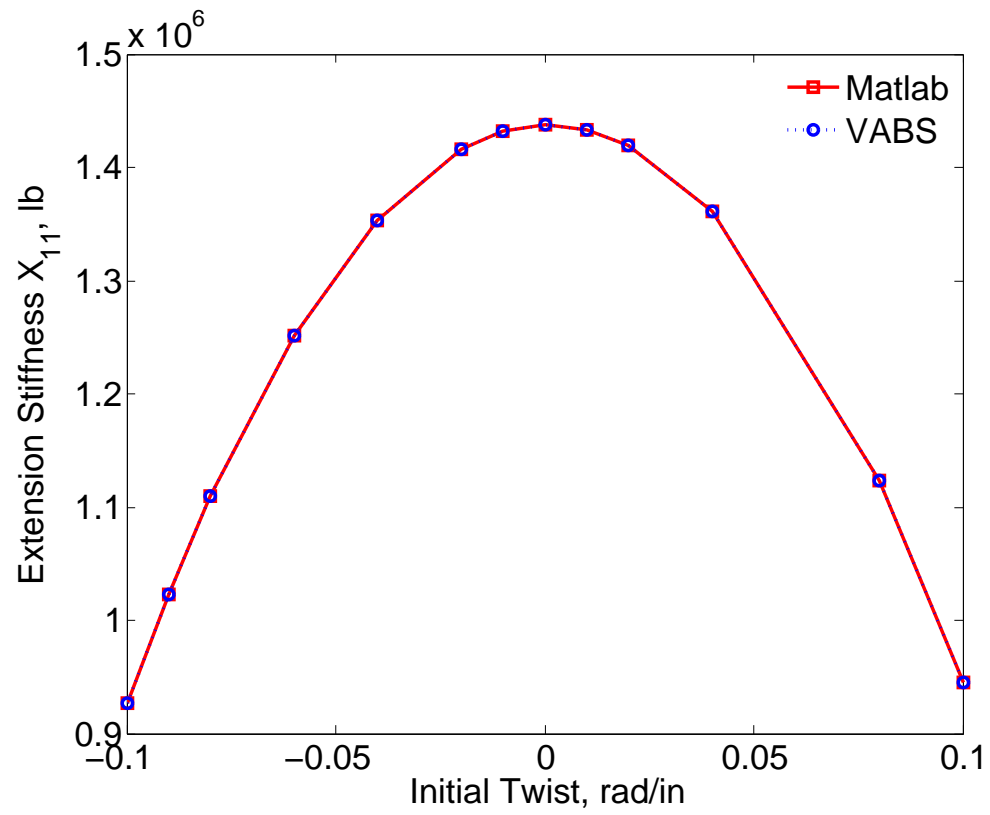


Figure 8: Generalized Timoshenko extension stiffness, X_{11} , for the CUS section featuring initial twist

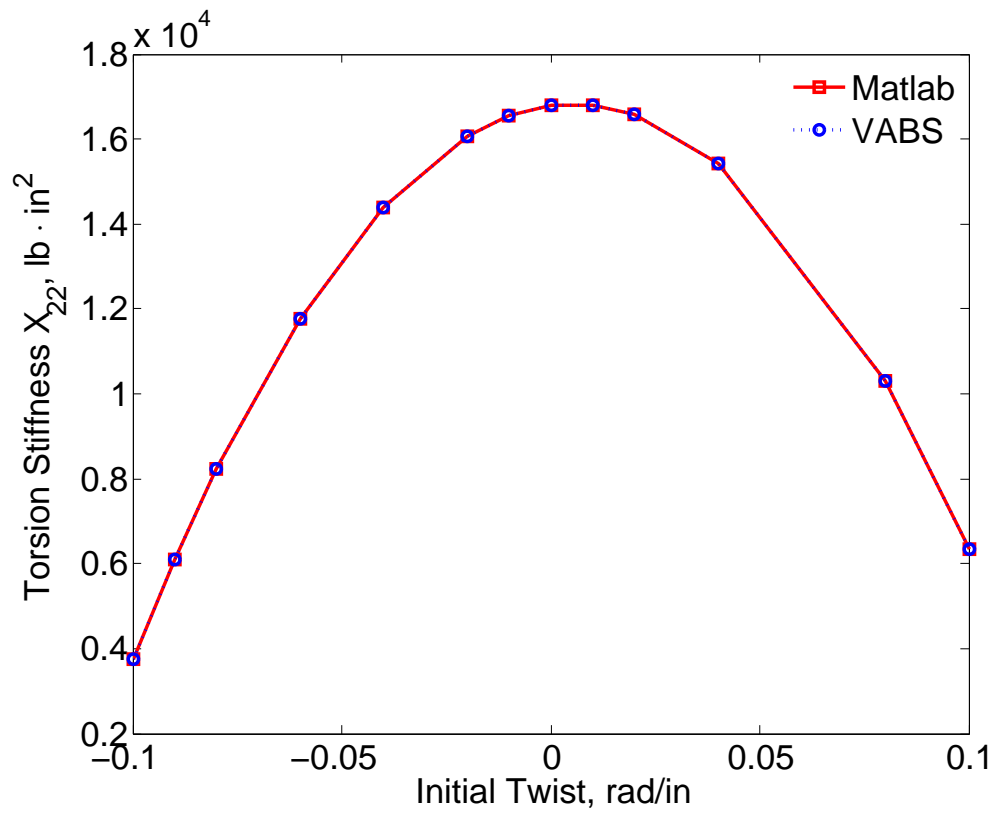


Figure 9: Generalized Timoshenko torsional stiffness, X_{22} , for the CUS section featuring initial twist

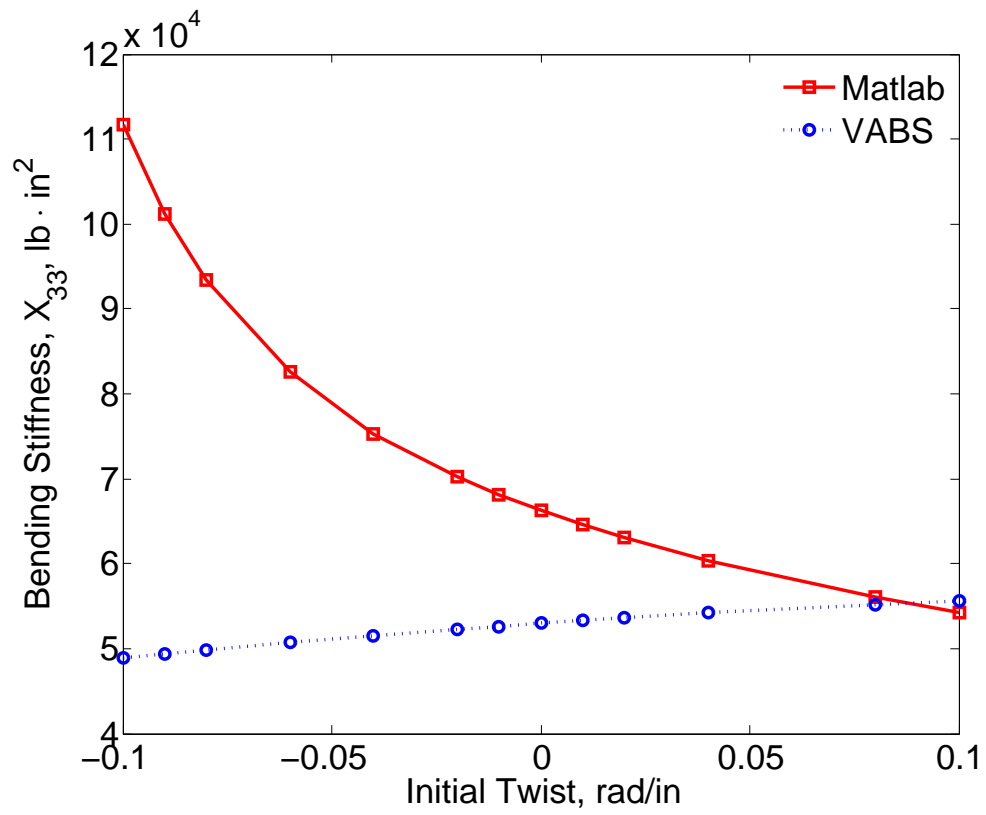


Figure 10: Generalized Timoshenko bending stiffness, X_{33} , for the CUS section featuring initial twist

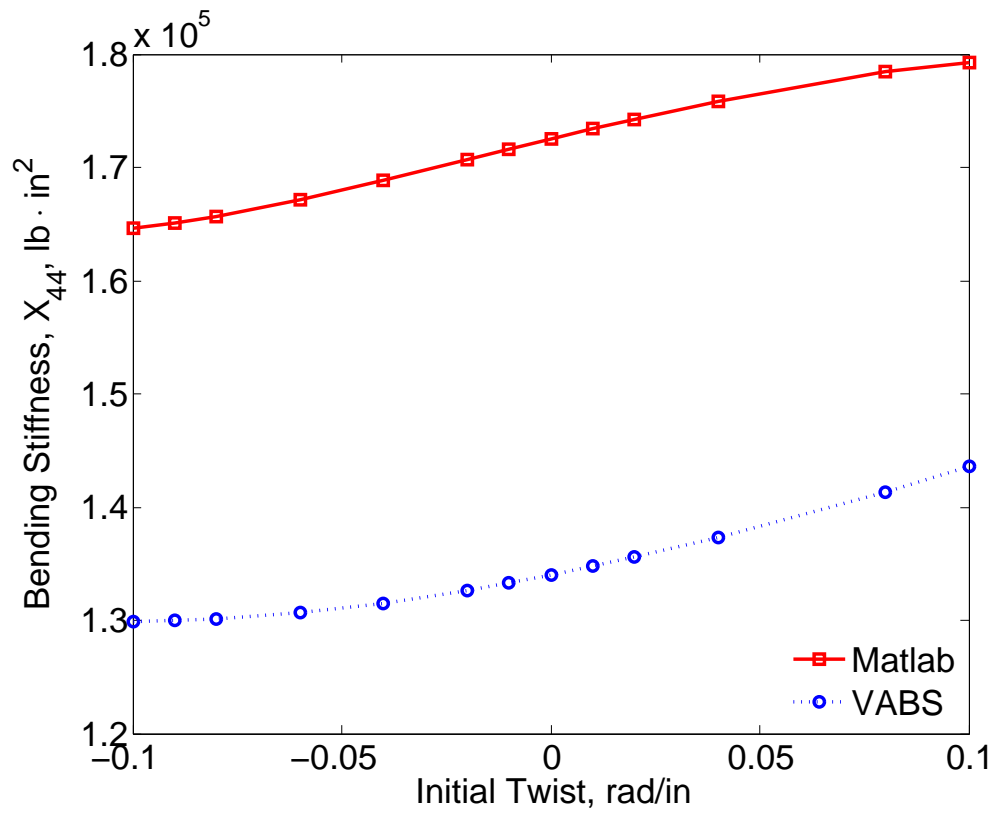


Figure 11: Generalized Timoshenko bending stiffness, X_{44} , for the CUS section featuring initial twist

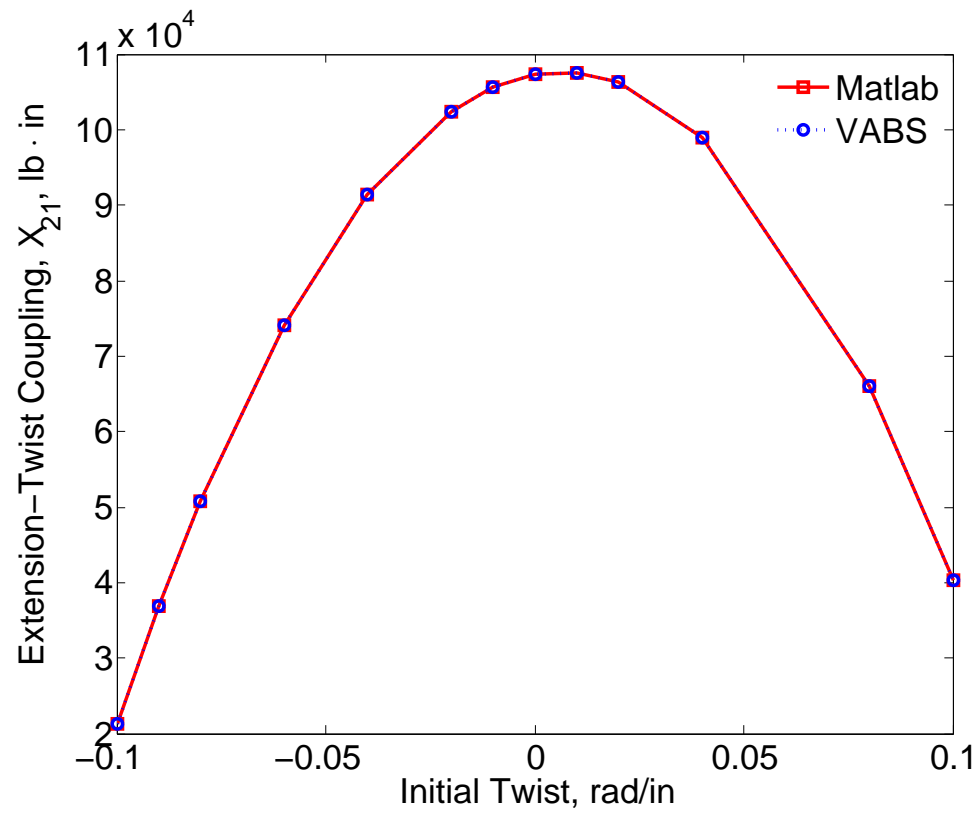


Figure 12: Generalized Timoshenko extension-twist coupling, X_{21} , for the CUS section featuring initial twist

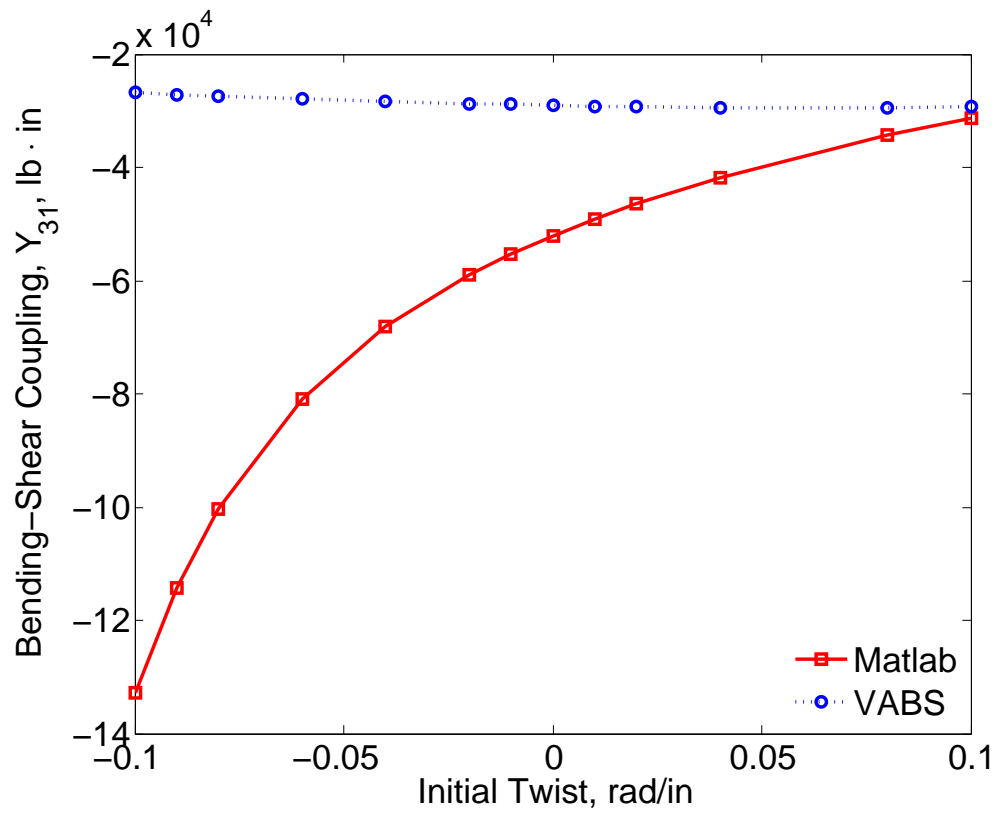


Figure 13: Generalized Timoshenko bending-shear coupling, Y_{31} , for the CUS section featuring initial twist

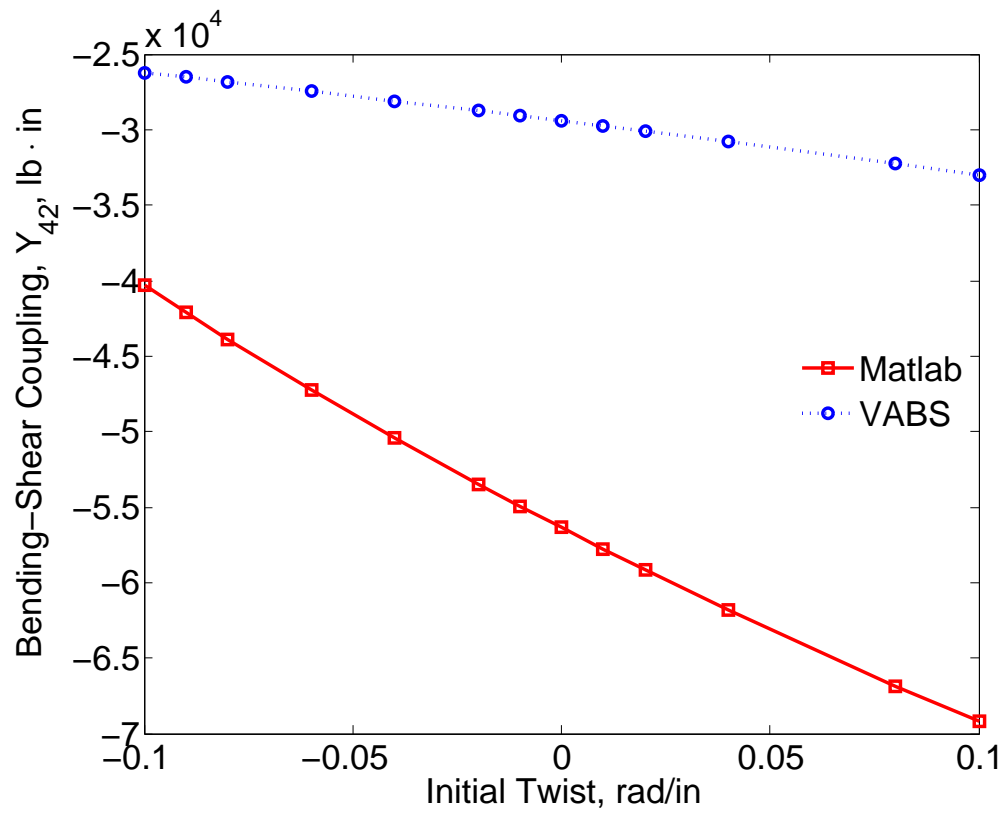


Figure 14: Generalized Timoshenko bending-shear coupling, Y_{42} , for the CUS section featuring initial twist

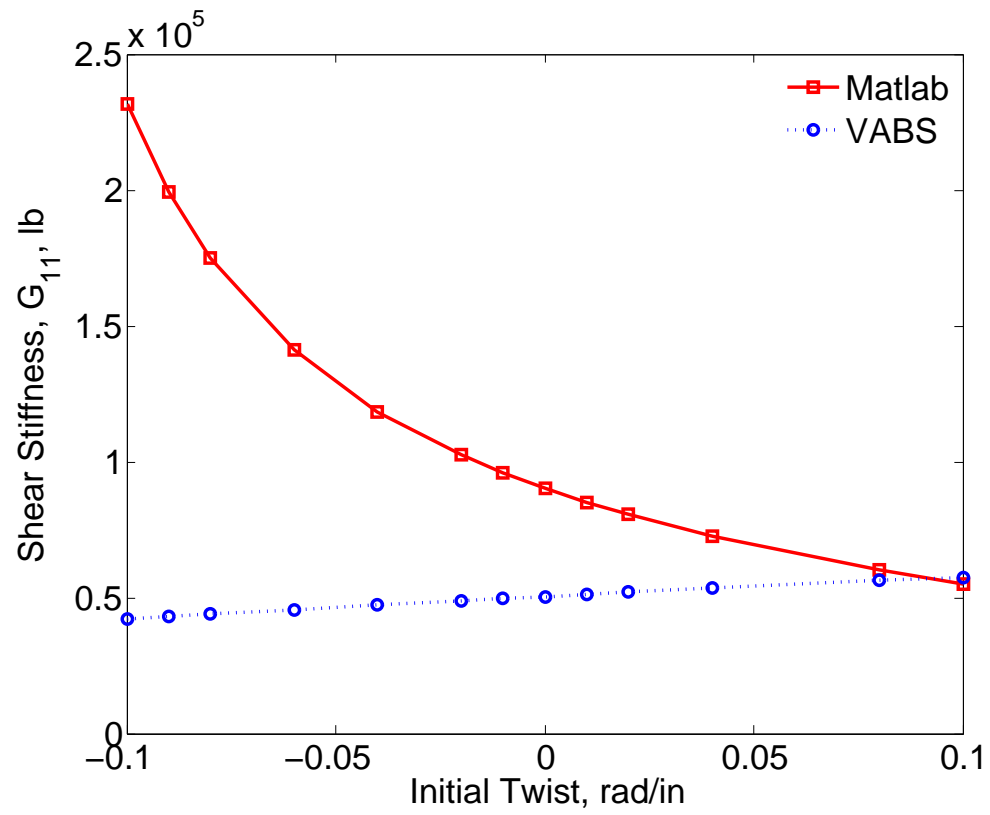


Figure 15: Generalized Timoshenko shear stiffness, G_{11} , for the CUS section featuring initial twist

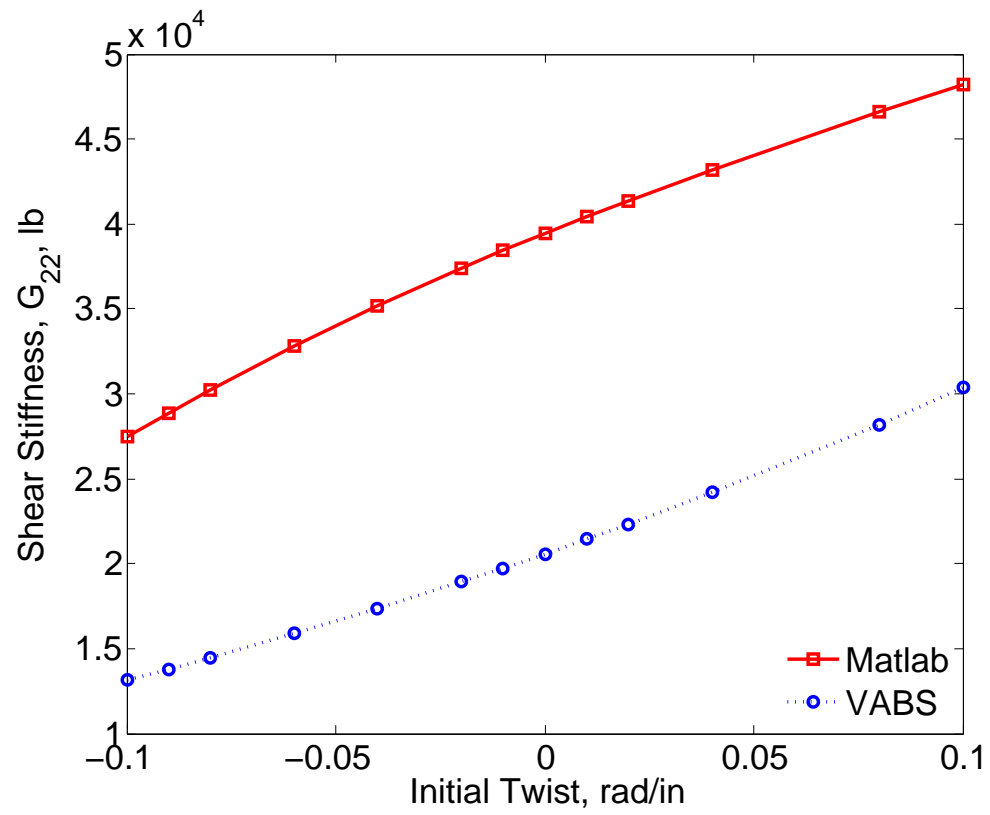


Figure 16: Generalized Timoshenko shear stiffness, G_{22} , for the CUS section featuring initial twist

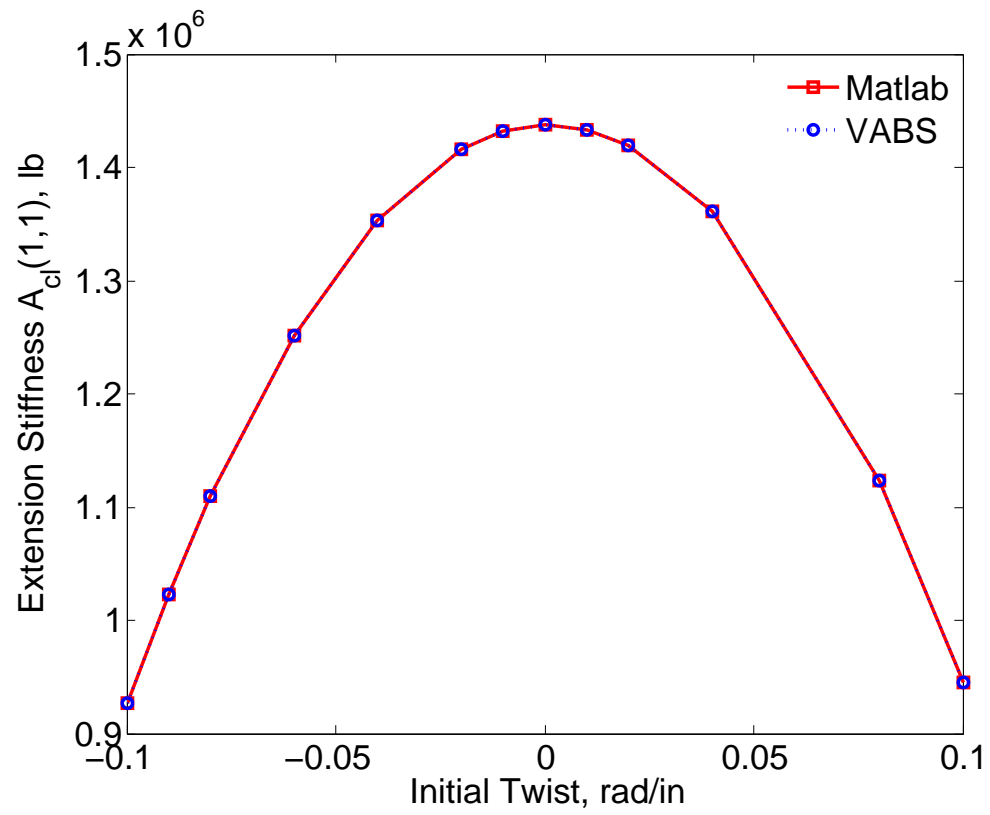


Figure 17: Reduced classical extension stiffness, $A_{cl}(1,1)$, for the CUS section featuring initial twist

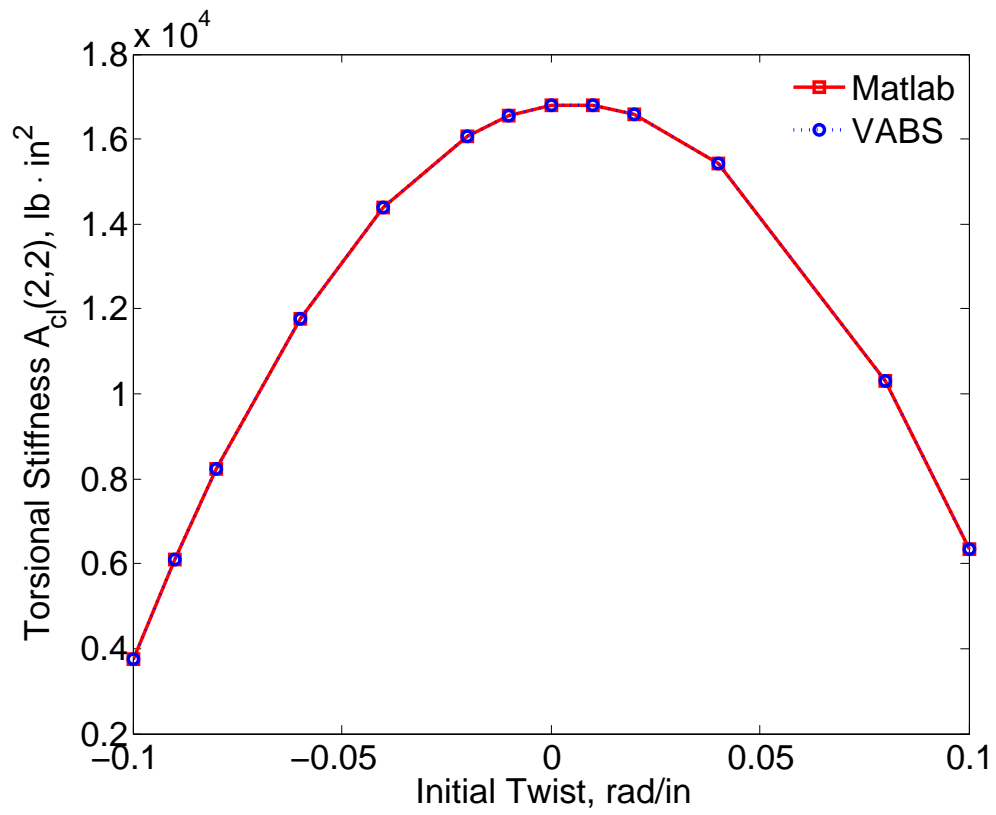


Figure 18: Reduced classical torsional stiffness, $A_{cl}(2,2)$, for the CUS section featuring initial twist

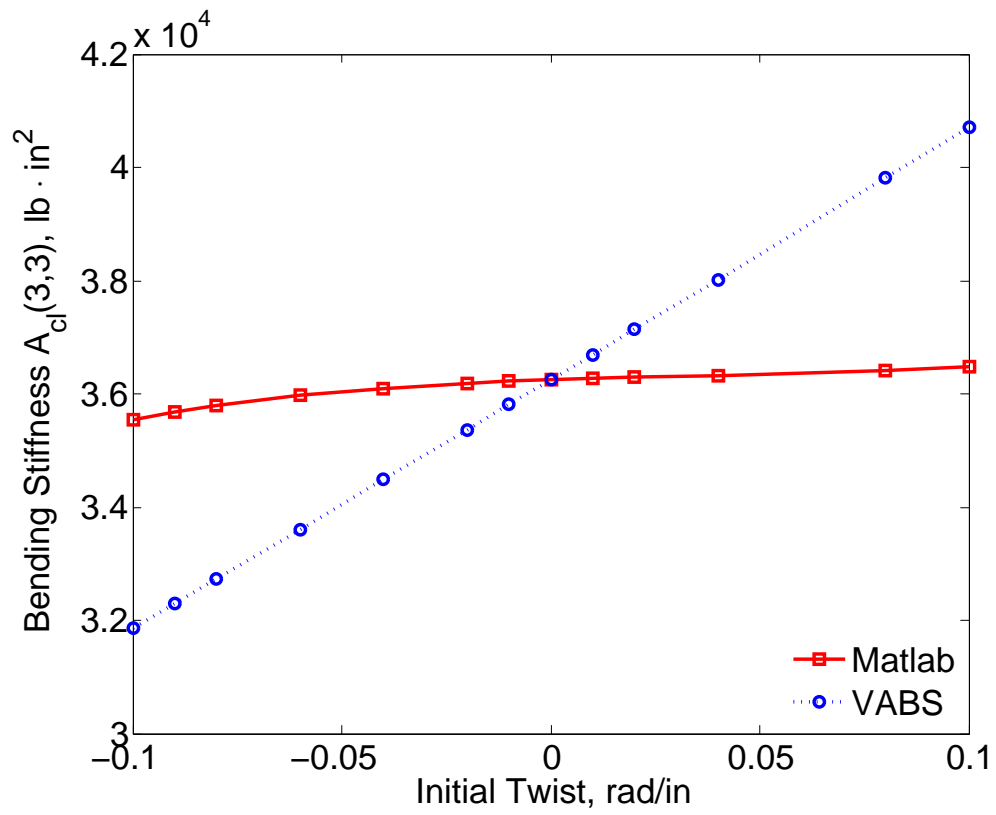


Figure 19: Reduced classical bending stiffness, $A_{cl}(3,3)$, for the CUS section featuring initial twist

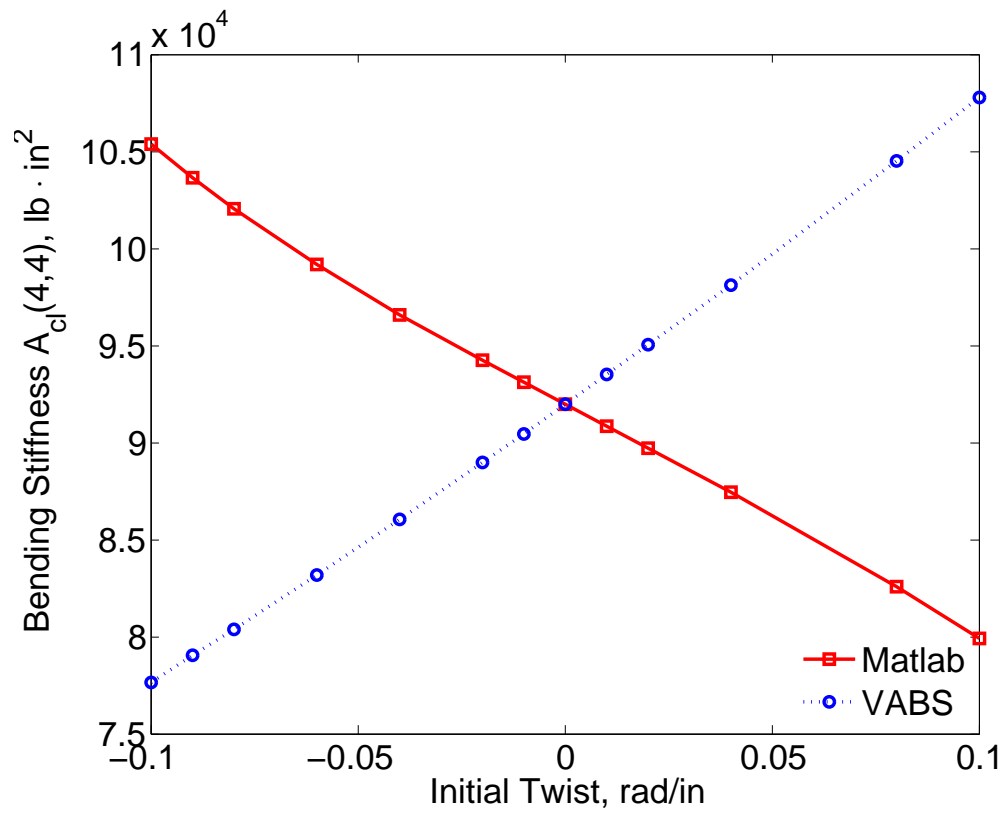


Figure 20: Reduced classical bending stiffness, $A_{cl}(4,4)$, for the CUS section featuring initial twist

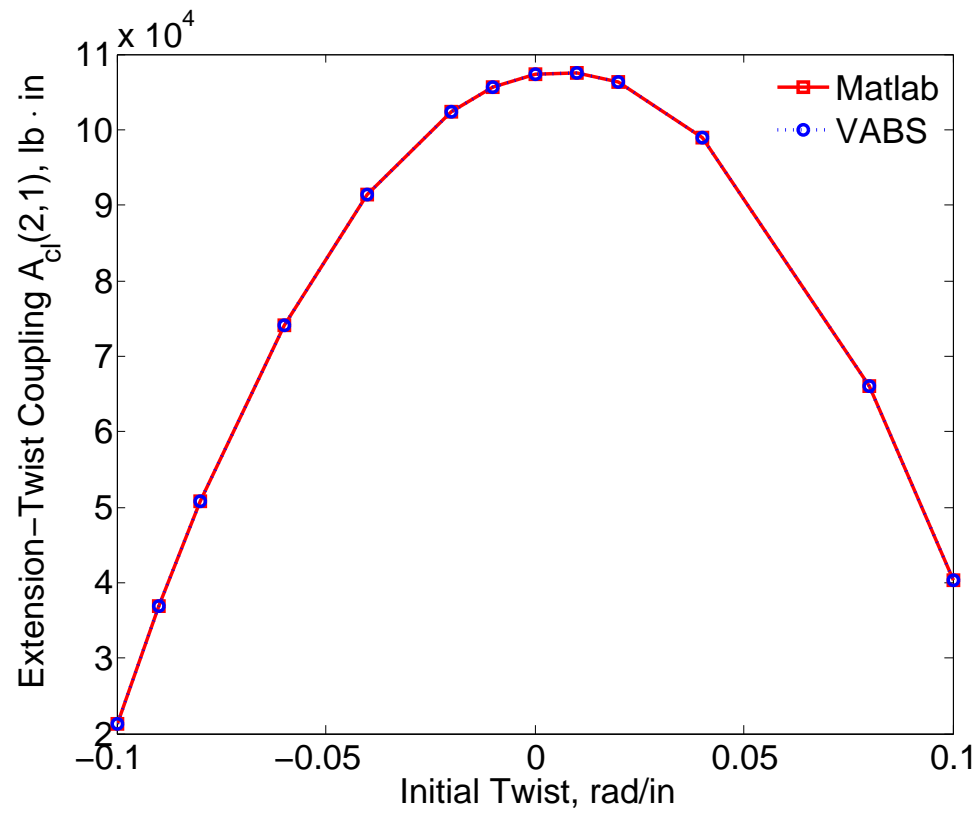


Figure 21: Reduced classical extension-twist coupling, $A_{cl}(2,1)$, for the CUS section featuring initial twist

Excellent agreement exists, between the solutions from VABS and the Matlab solver, for the case of an isotropic square cross-section with initial twist. The section of interest has sides of length 0.500 in with material properties of $E = 2.600 \times 10^7$ psi and $\nu = 0.30$. The axis of twist and the beam reference line are both set to coincide with the locus of cross-sectional centroids. The x_2 - and x_3 -axes are parallel to the two line segments defining the sides, while the positive x_1 -direction forms an orthogonal right-handed coordinate system with the x_2 - and x_3 -axes. The stiffness constants are tabulated in Tables 5 and 6 for solutions from VABS and the Matlab solver, respectively. If the length of the side is taken as the characteristic length a , then the largest value of a/R chosen here is 0.05. Both solutions share the same trends with k_1 as a result of the excellent agreement.

An observation, from inspecting results to both the CUS section and the isotropic square section, is that the effects of initial twist are different for the two sections. An example of this difference is that the curve of X_{22} , as a function of k_1 , has a downward concavity for the CUS section whereas it has an upward concavity for the isotropic square section. Since both sections are geometrically symmetric about both the x_2 - and x_3 -axes, the difference in the effects brought on by k_1 for the two sections are due to material properties. In particular, material properties for the CUS section are direction-dependent whereas they are not for the isotropic square section. Therefore, the effects of k_1 on stiffness constants may be understood for specific sections, but it cannot be easily described in general especially for sections composed of direction-dependent materials and lacking geometric symmetry.

Results from the Matlab solver confirm that Eq. (68), which is derived from a “condensation” of shear strain measures, is not valid unless the beam is prismatic. One may verify this by substituting solutions from the Matlab solver into Eq. (68) and see that the equation is not satisfied. The equation is always satisfied by the VABS solution, because there X is incorrectly calculated from Eq. (68) and satisfaction

Table 5: Stiffness for initially twisted isotropic square cross-sections from VABS

stiffness	$k_1=-0.10$ rad/in	$k_1=-0.01$ rad/in	$k_1=0.00$	$k_1=0.01$ rad/in	$k_1=0.10$ rad/in
X_{11} , lb	6.4989E+06	6.5000E+06	6.5000E+06	6.5000E+06	6.4989E+06
X_{21} , lb · in	-4.2395E+03	-4.2395E+02	0.0000E+00	4.2395E+02	4.2395E+03
X_{31} , lb · in	8.6253E-09	8.6554E-09	8.6558E-09	8.6554E-09	8.6253E-09
X_{41} , lb · in	8.1783E-09	8.1294E-09	8.1289E-09	8.1294E-09	8.1783E-09
X_{22} , lb · in ²	8.7883E+04	8.7861E+04	8.7861E+04	8.7861E+04	8.7883E+04
X_{32} , lb · in ²	3.1149E-12	2.7335E-13	0.0000E+00	-2.7335E-13	-3.1149E-12
X_{42} , lb · in ²	-4.5107E-11	-4.5215E-12	0.0000E+00	4.5215E-12	4.5107E-11
X_{33} , lb · in ²	1.3532E+05	1.3542E+05	1.3542E+05	1.3542E+05	1.3532E+05
X_{43} , lb · in ²	1.3275E-09	1.3384E-09	1.3385E-09	1.3384E-09	1.3275E-09
X_{44} , lb · in ²	1.3532E+05	1.3542E+05	1.3542E+05	1.3542E+05	1.3532E+05
Y_{11} , lb	2.4411E-09	2.4836E-10	0.0000E+00	-2.4836E-10	-2.4411E-09
Y_{21} , lb · in	5.3840E-09	5.3888E-09	5.3889E-09	5.3888E-09	5.3840E-09
Y_{31} , lb · in	2.7129E+03	2.7149E+02	0.0000E+00	-2.7149E+02	-2.7129E+03
Y_{41} , lb · in	9.0109E-10	8.8713E-11	0.0000E+00	-8.8713E-11	-9.0109E-10
Y_{12} , lb	1.4776E-09	1.4768E-10	0.0000E+00	-1.4768E-10	-1.4776E-09
Y_{22} , lb · in	1.6987E-09	1.7095E-09	1.7096E-09	1.7095E-09	1.6987E-09
Y_{32} , lb · in	-2.8107E-10	-2.8453E-11	0.0000E+00	2.8453E-11	2.8107E-10
Y_{42} , lb · in	2.7129E+03	2.7149E+02	0.0000E+00	-2.7149E+02	-2.7129E+03
G_{11} , lb	2.0674E+06	2.0705E+06	2.0705E+06	2.0705E+06	2.0674E+06
G_{21} , lb	-1.4948E-08	-1.5371E-08	-1.5375E-08	-1.5371E-08	-1.4948E-08
G_{22} , lb	2.0674E+06	2.0705E+06	2.0705E+06	2.0705E+06	2.0674E+06

Table 6: Stiffness for initially twisted isotropic square cross-sections from Matlab

stiffness	$k_1=-0.10$ rad/in	$k_1=-0.01$ rad/in	$k_1=0.00$	$k_1=0.01$ rad/in	$k_1=0.10$ rad/in
X_{11} , lb	6.4989E+06	6.5000E+06	6.5000E+06	6.5000E+06	6.4989E+06
X_{21} , lb · in	-4.2395E+03	-4.2395E+02	0.0000E+00	4.2395E+02	4.2395E+03
X_{31} , lb · in	-3.9229E-04	-1.2441E-04	9.0000E-09	1.6708E-04	5.8860E-04
X_{41} , lb · in	4.0874E-04	-4.3970E-05	8.0000E-09	2.5469E-04	5.2141E-04
X_{22} , lb · in ²	8.7883E+04	8.7861E+04	8.7861E+04	8.7861E+04	8.7883E+04
X_{32} , lb · in ²	2.1830E-06	1.9257E-05	0.0000E+00	-1.9242E-05	-1.5430E-06
X_{42} , lb · in ²	1.9400E-07	4.6040E-06	0.0000E+00	-4.5850E-06	-1.2100E-07
X_{33} , lb · in ²	1.3537E+05	1.3542E+05	1.3542E+05	1.3542E+05	1.3537E+05
X_{43} , lb · in ²	1.0000E-09	1.0000E-09	1.0000E-09	1.0000E-09	1.0000E-09
X_{44} , lb · in ²	1.3537E+05	1.3542E+05	1.3542E+05	1.3542E+05	1.3537E+05
Y_{11} , lb	7.4984E-02	2.3794E-01	0.0000E+00	3.1951E-01	1.1250E-01
Y_{21} , lb · in	-4.1726E-04	-3.6827E-02	9.8032E-01	-3.6799E-02	-2.9496E-04
Y_{31} , lb · in	2.7139E+03	2.7149E+02	0.0000E+00	-2.7149E+02	-2.7139E+03
Y_{41} , lb · in	9.1200E-10	8.8300E-11	0.0000E+00	-5.2100E-11	-8.8700E-10
Y_{12} , lb	-7.8125E-02	8.4104E-02	0.0000E+00	4.8705E-01	9.9661E-02
Y_{22} , lb · in	-3.7125E-05	-8.8040E-03	1.9742E-01	-8.7685E-03	-2.3076E-05
Y_{32} , lb · in	-2.7000E-10	-2.8900E-11	0.0000E+00	6.5100E-11	2.9600E-10
Y_{42} , lb · in	2.7139E+03	2.7149E+02	0.0000E+00	-2.7149E+02	-2.7139E+03
G_{11} , lb	2.0689E+06	2.0705E+06	2.0705E+06	2.0705E+06	2.0689E+06
G_{21} , lb	-1.5000E-08	-1.5000E-08	-1.5000E-08	-1.5000E-08	-1.5000E-08
G_{22} , lb	2.0689E+06	2.0705E+06	2.0705E+06	2.0705E+06	2.0689E+06

of the equation is forced. Let the residual matrix of Eq. (68) be defined as the difference between its right-hand and left-hand sides. For both the CUS and isotropic square sections, magnitudes of components of the residual increases as k_1 deviates from being prismatic. For the isotropic square section, at least the magnitudes are negligibly small (in comparison to magnitudes of its respective components in A) so that usage of Eq. (68) is decent.

Lastly, it is significant to note that the Matlab solver could not find a solution to its system of equations for cases inspected by this author whenever a nonzero value of either k_2 or k_3 exists. Along with the inability of the Matlab solver to find a solution to the prismatic CAS1 section, it seems that consistency in finding the solution to the system of equations is still elusive at this point.

3.3 Solution by Iterative Method

If the solution to the system of equations from Eq. (63) is to be found with no approximations, then a direct iterative method seems to have advantages over the perturbation method. For the general case of a beam with nonzero k_1 , k_2 , and k_3 values, the perturbation method entails successively solving three systems of nonlinear algebraic equations. Each system represents a problem to be solved for the solution to be accurate up to a certain order. As with most nonlinear systems of equations, the systems in this case do not appear to have simple analytical solutions. It would then seem that each system would have to be solved with an iterative method. The perturbation method is clearly impractical considering that only one system needs to be solved by directly solving the original system prior to applying the perturbation method.

Quite a few issues do exist with trying to solve Eq. (63) with no approximations. A nonlinear system of equations may have a unique solution, multiple solutions, or no solution. While it has been presumed here that a structure would deform in a

repeatable manner when loaded under the same conditions, the uniqueness that a set of stiffness constants exist may be found for each condition is lost here by the approximation of equating the 2nd-order asymptotically-correct refined and generalized Timoshenko energies. The iterative method may not find a solution (assuming one exists) and has no obvious way of deciding if a found solution is reasonable.

The perturbation method may still be useful, especially if approximations are allowed. For example, allowing a least squares approximation to be called the solution makes it possible that analytical formulae may be found for such a least squares solution. The perturbation method may then facilitate the derivation to the analytical formulae, because it would decompose the original system into smaller systems. Unlike finding solutions iteratively, having analytical formulae removes the issue of not finding a solution (assuming that issues such as having to take the inverse of a singular matrix does not arise).

3.4 Implications on Global Analysis

This section shows the differences, in results to the 1D global beam analysis, between calculations using stiffness constants from the Matlab solver and from VABS for a specific example. It is a cantilevered beam with the CUS cross-section. The external applied loading is the weight, but with a gravitational acceleration that is ten times that near our planet's surface. This loading is chosen as a crude representation for loading on wings of a commercial fixed-wing aircraft. For example, the Boeing 747-8 has a maximum takeoff-weight to wing weight ratio that is slightly greater than ten. The direction of the loading is always along the negative x_3 -direction. The beam length is $L = 0.953$ ft, so that the ratio of beam length to the length of its dominant cross-sectional side is $L/b = 12$. To be consistent with the properties shown on Figs. 8, 9, 10, 11, 12, 13, 14, 15, and 16, the axis of twist and beam reference line both coincide with the locus of cross-sectional centroids. At the root section, the orientation

is set such that the local x_3 -axis coincides with the x_3 -axis from the global absolute reference frame. In other words, the local x_3 -axis at the root section is in the opposite direction as the direction of loading. The beam axial coordinate has values $x_1 = 0$ at the fixed end and $x_1 = L$ at the free end.

The 1D global beam analysis is performed using NATASHA [32]. The beam theory embedded in NATASHA is nonlinear, geometrically-exact, based on fully intrinsic variables, and fully compatible with the generalized Timoshenko theory presented in this thesis. To ensure convergence in results, 25 beam elements and 26 nodes are chosen for the 1D analysis.

3.4.1 Static Analysis

The tip displacements of the beam are now shown. Figures 22 and 23 show the lateral displacement u_2 and the vertical displacement u_3 , respectively, as functions of initial twist k_1 . Due to the loading chosen, the extensional displacement u_1 and elastic twist are negligible. Displacements reported here are in the global absolute reference frame. Note that the calculated displacements here are small enough so that predictions from a linearized beam theory may be adequate.

Results of the lateral displacement, from Fig. 22, show decent correlation between calculations from the two different sets of stiffness constants. Both curves show a highly linear relation with k_1 . The asymmetry in the cross-section, that occur from introducing an initial twist without changing the direction of the applied loading vector, causes the lateral deflection to increase as the twist increases. The correlation between the two curves decreases as the beam deviates from the prismatic case, which reflects that the prismatic case shows the best correlation in the reduced classical bending stiffness about the x_2 -axis from Fig. 19.

A striking observation from results of the vertical displacement, from Fig. 23, is that calculations from the two different sets of stiffness constants result in different

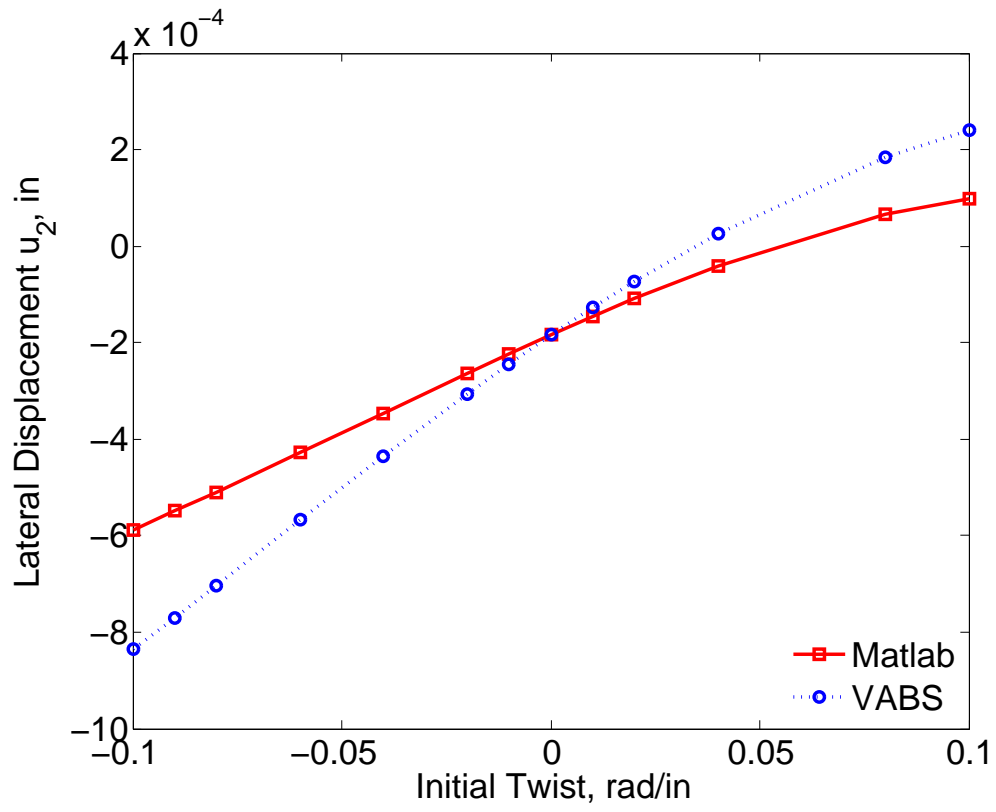


Figure 22: Lateral displacement at the tip, $u_2(L)$, for the CUS section featuring initial twist

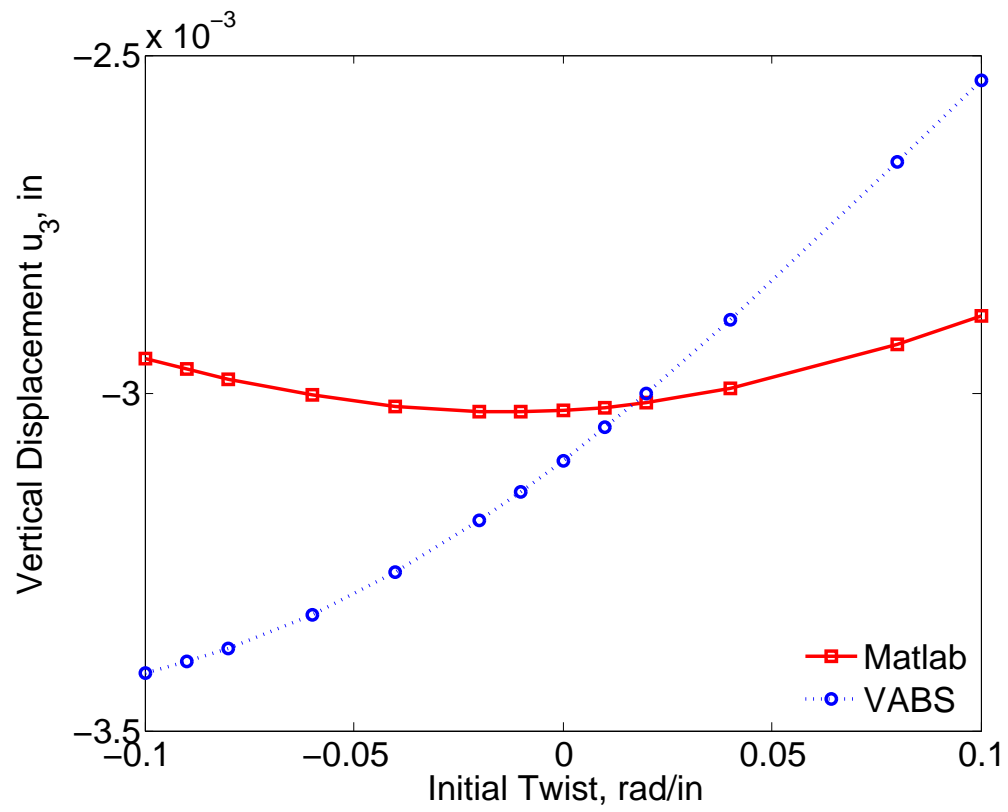


Figure 23: Vertical displacement at the tip, $u_3(L)$, for the CUS section featuring initial twist

behaviors with respect to k_1 . The curve predicted using the Matlab properties is fairly symmetric about a value of k_1 that is in the interval of $-0.02 \text{ rad/in} < k_1 < 0.0$. The curve predicted using VABS properties always shows a positive correlation between u_2 and k_1 . For the prismatic case, the two curves are very close due to the excellent correlation in the reduced classical bending stiffness about the x_3 -axis from Fig. 20.

It should be stressed here that these results have not been validated. A valid form of validation would be results from an analysis performed without dimensional reduction, such as finite element analysis to the 3D elasticity equations.

3.4.2 Dynamic Analysis

Results of dynamic analysis are in the form of natural frequency calculations. The frequencies are calculated from solving the eigenvalue problem associated with the linearized equations of motion, which are linearized about the static equilibrium state. The deflections caused by the loading are apparently so small that frequency calculations, through the first five digits of the lowest eight modes, are equal between calculations about either the undeformed or deformed states. It should nevertheless be remembered that this is not a general rule and that frequencies may be strongly influenced by the static equilibrium position [20].

The frequency results are plotted in Fig. 24 for the first five modes. The five lowest modes are first flapwise bending (F1), first chordwise bending (C1), second flapwise bending (F2), first torsion (T1), and a coupled mode between chordwise bending and flapwise bending (CF). For the F1 mode, the frequency calculations follow the trends in the reduced classical bending stiffness about the x_2 -axis from Fig. 19. Namely, frequencies calculated using VABS properties have a positive slope with respect to k_1 while those using Matlab solver properties are relatively flat. Likewise, frequencies from the C1 mode follow the reduced classical stiffness behaviors from Fig. 20. Modes above the first two are all highly coupled. As a result of the excellent agreement in

torsional stiffness predictions between the Matlab solver and VABS from Figs. 9 and 18, frequency predictions of the T1 mode are also in excellent agreement between using the two different sets of properties. As with the static analysis results, the message here is that significantly different behaviors to the 1D global analysis may be predicted between using properties from the Matlab solver and VABS.

3.5 Latest Implementation to VABS

The identification of the issues, with VABS, in this chapter has initiated efforts to address these issues. Changes have already been implemented to a modified version of VABS that has not been officially released yet. The changes implemented are still based on the ideas of (1) finding an analytical solution with a reduction in the order of the system of equations, and (2) applying the perturbation approach for beams featuring initial twist and/or curvature. The motivation for applying these two ideas have been discussed at the end of Sec. 3.3. The changes implemented thus far have focused on the prismatic case. Specifically, the focus is on incorporating the underlined terms from Eqs. (69) and (70). With this latest implementation, VABS results to the prismatic CUS section are now in agreement with those from the Matlab solver and NABSA. When it is determined that the solution to the prismatic case is satisfactory, the focus will then shift to addressing the issues surrounding beams featuring initial twist and/or curvature.

3.6 Validation of Initially Twisted Beams

This author is not aware of any previous validation studies on initially twisted beams other than validations in stiffness constants, so this section digresses briefly to provide a form of validation. An initially twisted beam with a constant value of k_1 may be analyzed as a uniform beam if the beam local in-plane coordinates, x_2 and x_3 , are continuously rotating along the beam by following the twist. The same beam may also be analyzed as a beam, whose local in-plane coordinates do not change

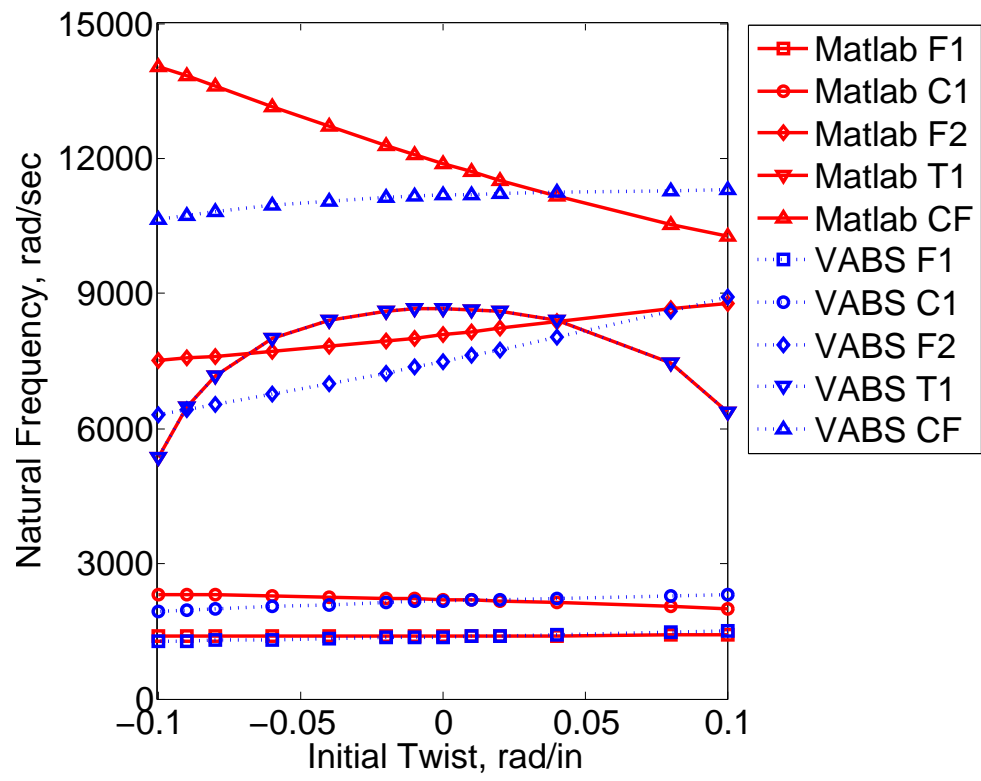


Figure 24: Natural frequencies for the CUS section featuring initial twist

their orientations, such that its sectional properties do vary along the length. The former approach requires only one sectional analysis to attain the section properties, while the latter may require numerous sectional analyses to properly describe the varying nature in the section properties. The former approach performs analyses with a nonzero value of k_1 while the latter approach sets $k_1 = 0.0$. Results from the 1D global analysis, such as displacement vector of the beam reference line and natural frequencies, cannot differ between the two approaches. The validation in mind here is to verify that calculated results from 1D global analyses using the two different approaches are indeed invariant of the chosen coordinates, which would be a validation on the correct modeling of initial twist effects to both the 1D global analysis embedded in NATASHA and stiffness constants from the 2D cross-sectional analysis. Results from 1D global analysis in Sec. 3.4 are all calculated from the first approach.

The twisted beam configuration, under consideration, is again a cantilevered beam subject to a gravitational force that is ten times the gravity on Earth. The cross-section is isotropic and rectangular with sides of lengths $a = 1$ in and $b = 2$ in. The beam reference line and the axis of twist coincide with the locus of cross-sectional centroids. The beam axial coordinate has value $x_1 = 0$ at the fixed end and is positive towards the free end. At the fixed end, in-plane coordinates x_2 and x_3 are parallel to the line segments defining the sides of lengths b and a , respectively, regardless if these axes are rotating along the length. The gravitational force always acts in the negative x_3 -direction in the global absolute reference frame. The length of the beam is set as $L = 2$ ft, so that the ratio of beam length to length of its dominant side is $L/b = 12$. The described beam is analyzed for values of $k_1 = -0.05, -0.025, 0.0, 0.025$, and 0.05 rad/in. Choosing b as the characteristic length, then the largest value of characteristic length to radius of twist is $b/R = 0.10$. The material is chosen to have properties of $E = 2.6 \times 10^7$ psi, $\nu = 0.30$, and $\rho = 14.125$ slug/ft³, which are close to

that of malleable ASTM A-197 (an often used cast iron alloy).

The two different approaches entail different procedures to attaining section properties. All of the stiffness constants from VABS are verified to be accurate by the Matlab nonlinear solver. In the first approach, where the in-plane coordinates rotate along the span, section properties are uniform and are taken from a single analysis using VABS.

In the second approach, where the in-plane coordinates do not rotate along the span, properties are taken from a combination of VABS and usage of analytical formulae. Inertial and stiffness properties at the fixed end are taken from a single VABS analysis. To avoid the need to perform VABS analysis at other locations, formulae from Mohr's circle are applied to find the sectional mass moments and mass mixed moment of inertia, the bending stiffnesses and the bending-bending coupling, and the shear stiffnesses and the shear-shear coupling. The extension stiffness, torsional stiffness, sectional mass, and mass moment associated with twist are constant. Other inertial properties and terms from the stiffness matrix are confirmed, with another VABS run at the free end and a few more in the interior, to be negligible.

Note that stiffness constants attained by the second approach neglects spanwise nonuniformity effects, which are hypothesized to be negligible and possibly even nonexistent for such a beam. Points located on the surface boundaries follow the paths of a circular helix as it moves along the span. It is known from differential geometry that the normal vector of a point on a circular helix is always horizontal and points towards its axis of rotation. This means that the outward-directed normal vectors to the surface lack the out-of-plane component in the cross-sectional plane. Therefore, stresses at the boundaries may satisfy the traction boundary conditions. This is the motivation behind the hypothesis that nonuniformity effects may be neglected for this case.

Lateral and vertical displacements at the tip and natural frequencies, calculated

about the equilibrium state, are plotted as functions of k_1 on Figs. 25, 26, and 27, respectively. The results are from using 25 beam elements and 26 nodes in NATASHA. Results from performing calculations with k_1 set to zero and with a nonzero value of k_1 are labeled “Cartesian” and “curvilinear”, respectively. The displacements are calculated in the global absolute reference frame. For the frequency figure, the first five modes are in the order of first flapwise bending (F1), first chordwise bending (C1), second flapwise bending (F2), second chordwise bending (C2), and first torsion (T1). Calculations by both approaches correlate well in all quantities, so the intended validation is successful. Due to the symmetry in the cross-section, the lateral displacement and the vertical displacement are perfectly antisymmetric and symmetric, respectively, about the prismatic case. Frequencies here are shown for the lowest five modes. It may be difficult to perceive due to the scale of Fig. 27, but the frequency calculations, between the two different sets of coordinates, are in full agreement up to at least the first three digits. The next five modes correlate just as well as the modes shown.

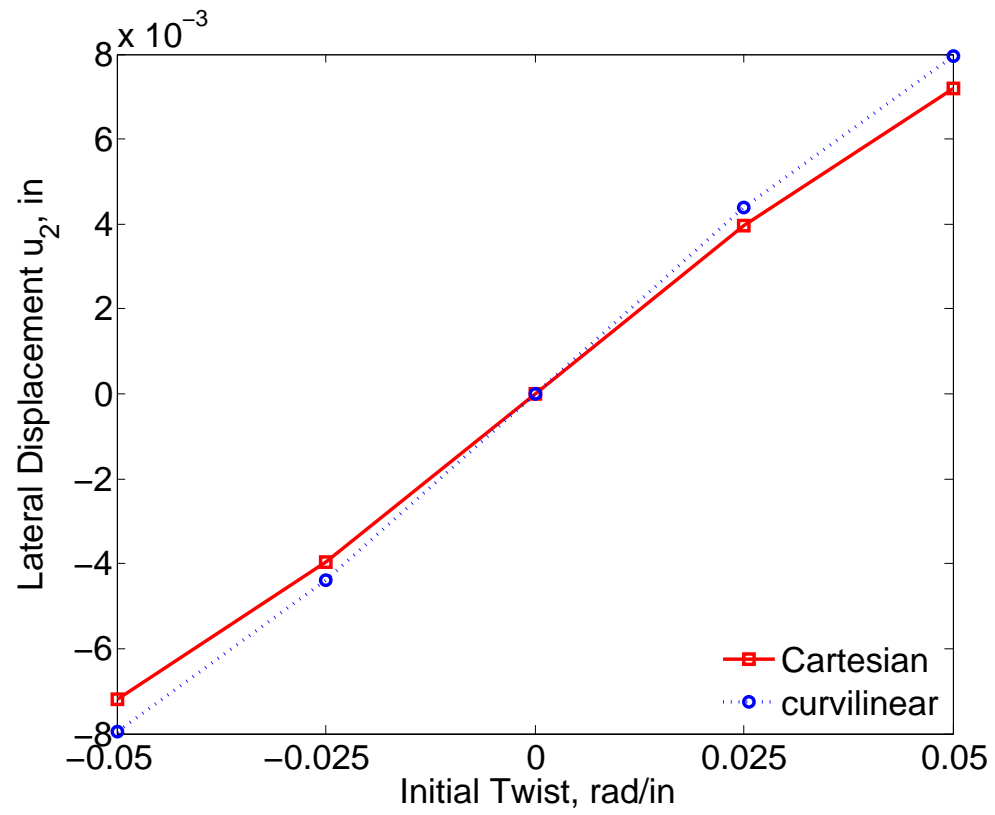


Figure 25: Lateral displacement at the tip, $u_2(L)$, for the isotropic rectangular section featuring initial twist

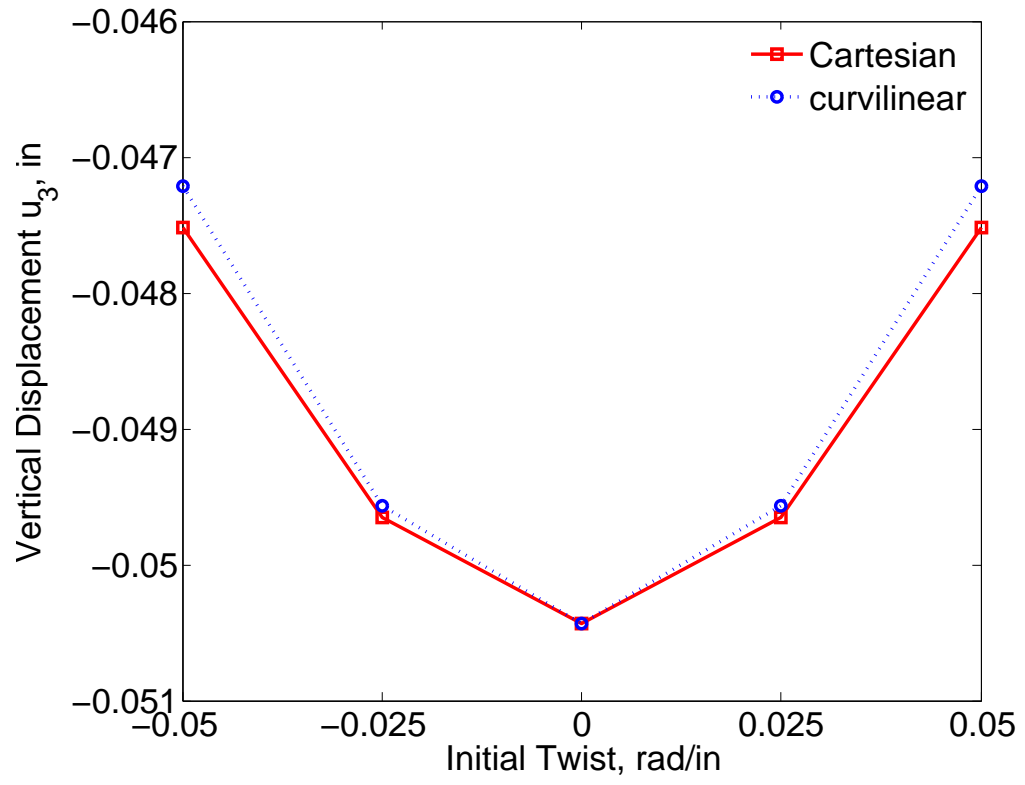


Figure 26: Vertical displacement at the tip, $u_3(L)$, for the isotropic rectangular section featuring initial twist

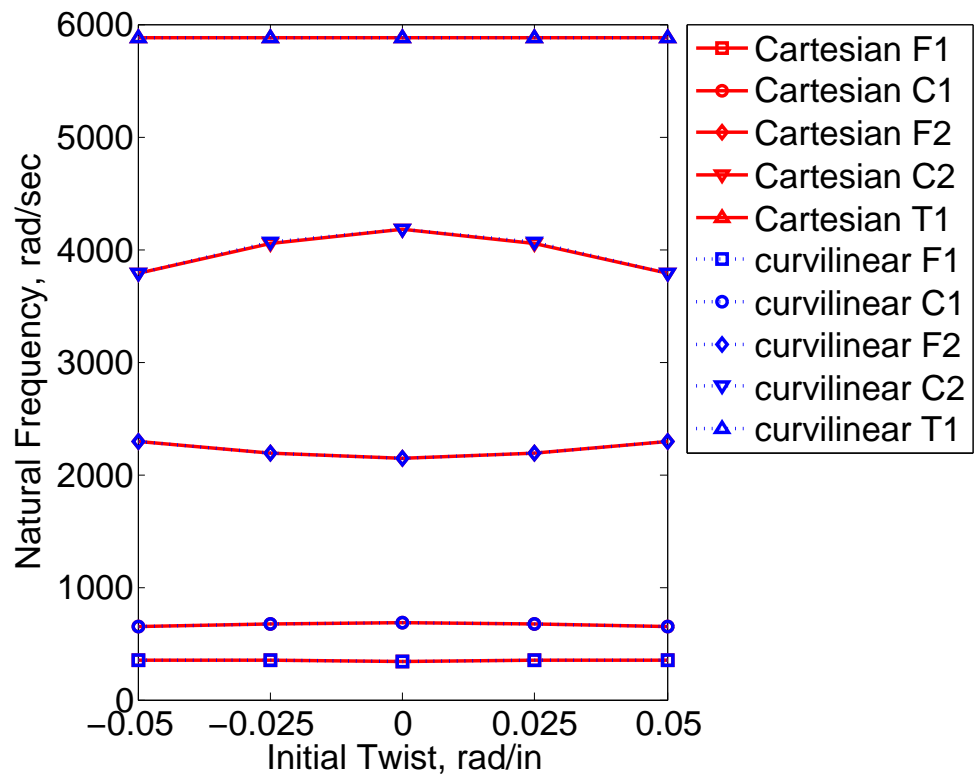


Figure 27: Natural frequencies for the isotropic rectangular section featuring initial twist

CHAPTER IV

LINEARLY TAPERED ISOTROPIC STRIP

As a demonstration of the nonuniformity effect, the VAM is now used to obtain an analytical, asymptotically-correct expression for the strain energy of a linearly tapered isotropic strip beam. The strip is assumed to be sufficiently thin to warrant the use of 2D plane stress elasticity. The taper is represented by a nondimensional constant, which is of the same order as the ratio of the maximum cross-sectional width to the wavelength of deformation along the beam. The resulting asymptotically-correct stiffness constants, being functions of the taper parameter, are then used to find stiffness constants for a generalized Timoshenko beam theory. These generalized Timoshenko stiffness constants are then used in the associated 1D beam equations to obtain solutions for the deformation of a linearly tapered beam subject to three classical loading conditions. These beam solutions are then compared with plane stress elasticity solutions, developed for these three classical loading cases. The agreement is excellent, and the results show that correction of the stiffness constants using the taper parameter is necessary in order for beam theory to yield accurate results if the taper parameter is sufficiently large.

A correlation study of this strip beam is next shown between the analytical and numerical VAM results. Unfortunately, the level of correlation to the stiffness constants, from the 2nd-order asymptotically-correct refined theory, is not high enough for the numerical VAM results to be adequate. At least the numerical VAM results to the generalized Timoshenko transformation, performed while using formulae from the analytical VAM, show perfect correlation with the analytical VAM results.

This chapter is written with care so that notations are consistent with what is

written in Chap. 2.

4.1 *Analytical Beam Solution*

This section shows the derivation to the energy of a linearly tapered isotropic strip beam undergoing in-plane deformations. It begins with an introduction to the 2D kinematics and its energy prior to dimensional reduction. Small parameters are then identified. The VAM is then applied to rigorously split the 2D plane stress problem into a 1D global analysis and a 1D cross-sectional analysis. This results in a sectional energy that is asymptotically-correct up to 2nd-order in terms of the small parameters. The energy is then transformed into generalized Timoshenko form.

4.1.1 Asymptotically-Correct Refined Theory

The kinematics of the beam, which has the same geometry as the one shown on the right side of Fig. 1, are now presented. These quantities follow directly from Chap. 2 while keeping in mind that the dimension along the thickness is now neglected. The position vector to an arbitrary point in the undeformed beam is taken to be

$$\hat{\mathbf{r}} = x_1 \mathbf{a}_1 + x_2 \mathbf{a}_2 = \mathbf{r} + x_2 \mathbf{a}_2 \quad (71)$$

The x_1 -axis is the reference line of the undeformed beam, taken for convenience as the locus of cross-sectional centroids. The position vector to an arbitrary point in the deformed beam can be written as

$$\hat{\mathbf{R}} = \mathbf{R} + x_2 \mathbf{T}_2 + w_1(x_1, x_2) \mathbf{T}_1 + w_2(x_1, x_2) \mathbf{T}_2 \quad (72)$$

where $\mathbf{R} = (x_1 + u_1) \mathbf{a}_1 + u_2 \mathbf{a}_2$, \mathbf{T}_1 is a unit vector tangent to the deformed reference line, and \mathbf{T}_2 is normal to \mathbf{T}_1 in the plane. If only linear terms are kept, then $\mathbf{T}_1 = \mathbf{a}_1 + u'_2 \mathbf{a}_2$ and $\mathbf{T}_2 = -u'_2 \mathbf{a}_1 + \mathbf{a}_2$. The displacement field is thus described in terms of beam variables $u_1(x_1)$, $u_2(x_1)$ along with warping functions $w_1(x_1, x_2)$ and $w_2(x_1, x_2)$. Two constraints on the warping are needed to make the displacement field unique.

Choosing the constraints so that average warping displacements of the cross-sections are zero means that

$$\langle \hat{\mathbf{R}} \rangle = 2b\mathbf{R} \quad (73)$$

where

$$\langle (\bullet) \rangle = \int_{-b(x_1)}^{b(x_1)} (\bullet) dx_2 \quad (74)$$

Eq. (73) implies that

$$\langle w_1 \rangle = \langle w_2 \rangle = 0 \quad (75)$$

The beam is assumed to be homogeneous and isotropic, and the entire development is linear throughout. Under assumption of plane stress, appropriate for a thin body such as this one, twice the strain energy per unit length is given by

$$2U = \frac{Et}{1-\nu^2} \left\langle \Gamma_{11}^2 + \Gamma_{22}^2 + 2\nu\Gamma_{11}\Gamma_{22} + \frac{(1-\nu)}{2}\Gamma_{12}^2 \right\rangle \quad (76)$$

where ν is Poisson's ratio. According to the displacement field spelled out in Eq. (72), the 2D strain components are

$$\begin{aligned} \Gamma_{11} &= \bar{\gamma}_{11} - x_2 \bar{\kappa}_3 + w_1' \\ \Gamma_{22} &= w_{2,2} \\ \Gamma_{12} &= w_{1,2} + w_2' \end{aligned} \quad (77)$$

The only classical 1D generalized strains are $\bar{\gamma}_{11}$ and $\bar{\kappa}_3$, which are both functions of x_1 . Here $\bar{\kappa}_3 = u_2''(x_1)$ is the usual curvature of the reference line from Euler-Bernoulli beam theory, and $\bar{\gamma}_{11} = u_1'(x_1)$ is the stretching of the reference line.

There are three small parameters that can be identified. First, the strain is small compared to unity. It is straightforward to show that both $\bar{\gamma}_{11}$ and $a\bar{\kappa}_3$ are $O(\hat{\epsilon})$, where $\hat{\epsilon}$ denotes the maximum strain and $a = b(0)$, the maximum value taken on by x_2 in the structure. The second small parameter is a/ℓ where ℓ is the wavelength of deformation along the beam, such that $\partial(\bullet)/\partial x_1 = O(\bullet/\ell)$. Finally, in this study the nondimensional taper parameter τ is also selected as a small parameter. The fact

that the problem is linear, the strain will only enter quadratically, so the smallness of strain has no real effect on the formulation. For convenience, a/ℓ and τ are taken to be of the same order, $O(a)$. Despite the abuse in notations, the context should easily dictate what is meant. In this work, terms which are $O(a^3)$ when compared to unity are neglected.

The VAM procedure is summarized as follows:

1. Identify and remove all terms $O(a)$ and higher in the strain.
2. Use this resulting 0th-order approximation of strain to form the 0th-order approximation of strain energy in terms of warping.
3. Minimize the 0th-order approximation of strain energy with respect to warping to obtain the 0th-order approximation of warping.
4. Perturb the resulting 0th-order warping by one order of a and use the perturbed warping to express strain components to a sufficiently high order of approximation, such that the energy contains all $O(a^2)$ terms while all higher-order terms are dropped.
5. Minimize this 2nd-order approximation of the energy with respect to the warping function perturbations.
6. Substitute the result for the warping back into the original strain energy and discard all terms of orders higher than $O(a^2)$.

The result is the asymptotically-correct strain energy per unit length.

To begin, twice the 0th-order approximation of the energy, tantamount to ignoring a altogether, is written as

$$2U_0 = \left\langle \frac{Et}{1-\nu^2} \left[(\bar{\gamma}_{11} - x_2 \bar{\kappa}_3)^2 + 2\nu w_{2,2} (\bar{\gamma}_{11} - x_2 \bar{\kappa}_3) + \frac{(1-\nu)w_{1,2}^2}{2} + w_{2,2}^2 \right] - 2\lambda_1 w_1 - 2\lambda_2 w_2 \right\rangle \quad (78)$$

where Lagrange multipliers λ_1 and λ_2 are used to enforce constraints on the warping. The warping field that minimizes U_0 can be found as

$$\begin{aligned} w_1 &= 0 \\ w_2 &= -\nu \bar{\gamma}_{11} x_2 + \frac{\nu \bar{\kappa}_3}{2} \left(x_2^2 - \frac{b^2}{3} \right) \end{aligned} \quad (79)$$

Plugging this warping field back into the expression for $2U_0$, one obtains twice the 0th-order energy as

$$2U_0 = 2Ebt\bar{\gamma}_{11}^2 + \frac{2}{3}Etb^3\bar{\kappa}_3^2, \quad (80)$$

which is consistent with Euler-Bernoulli theory. Note that Eq. (80) is derived without *ad hoc* assumptions such as assuming the cross-section to be rigid in its own plane or assuming that $\nu = 0$. Such assumptions are sometimes used to derive classical beam theory, but they are neither necessary nor correct.

For the next approximation to the sectional energy, the above approximation of warping is perturbed to arrive at

$$\begin{aligned} w_1 &= v_1 \\ w_2 &= -\nu \bar{\gamma}_{11} x_2 + \frac{\nu \bar{\kappa}_3}{2} \left(x_2^2 - \frac{b^2}{3} \right) + v_2 \end{aligned} \quad (81)$$

where v_1 is the perturbation of w_1 and v_2 is the perturbation of w_2 ; v_1 and v_2 are of one order higher in a than w_1 and w_2 .

This new warping field is then substituted into the strain components from Eq. (77), at which point a new expression for the strain energy arises from Eq. (76) by virtue of the new strain components. Here one must be careful to retain all terms up through $O(a^2)$ and drop all terms of higher order in the energy, which now becomes

$$\begin{aligned} 2U_2 &= \frac{Et}{1-\nu^2} \left\{ \frac{1-\nu}{2} \left\langle \left[\frac{\nu \tau b \bar{\kappa}_3}{3} - x_2 \nu \bar{\gamma}'_{11} + \frac{\nu (3x_2^2 - b^2) \bar{\kappa}'_3}{6} + v_{1,2} \right]^2 \right\rangle \right. \\ &\quad \left. + \langle v_{2,2}^2 + 2v'_1(1-\nu^2)(\bar{\gamma}_{11} - x_2 \bar{\kappa}_3) \rangle \right\} \end{aligned} \quad (82)$$

Expressions for the perturbation variables, v_1 and v_2 , that minimize U_2 subject to the constraints in Eq. (75) must be found. The constraints are enforced by use of

Lagrange multipliers Λ_1 and Λ_2 . The stationary point of U_2 is found by setting its first variation equal to zero, which leads to the two Euler-Lagrange equations

$$\begin{aligned}\frac{\partial U_2}{\partial v_1} - \left(\frac{\partial U_2}{\partial v'_1} \right)' - \left(\frac{\partial U_2}{\partial v_{1,2}} \right)_{,2} &= \Lambda_1 \\ \frac{\partial U_2}{\partial v_2} - \left(\frac{\partial U_2}{\partial v_{2,2}} \right)_{,2} &= \Lambda_2\end{aligned}\tag{83}$$

along with corresponding natural boundary conditions

$$\begin{aligned}\left. \frac{\partial U_2}{\partial v_{1,2}} \right|_{x_2=\pm b(x_1)} &= 0 \\ \left. \frac{\partial U_2}{\partial v_{2,2}} \right|_{x_2=\pm b(x_1)} &= 0\end{aligned}\tag{84}$$

According to Saint-Venant's principle, boundary conditions on the warping at the beam ends do not affect the behavior of the warping in the interior of the beam. Therefore, boundary conditions on warping at the beam ends are not used in the solution of Eqs. (83) and (84).

Although both the Euler-Lagrange equations and boundary conditions for v_1 and v_2 look almost identical, the actual equations obtained are not. The Euler-Lagrange equation for v_2 , i.e. the second of Eq. (83), reduces simply to $v_{2,22} = 0$; from this and the second of Eq. (84), which requires $v_{2,2}$ to vanish at $x_2 = \pm b$, one obtains by inspection that $\Lambda_2 = v_2 = 0$. On the other hand, the resulting Euler-Lagrange equation in v_1 , i.e. the first of Eq. (83), can be simplified to

$$Et [(2 + \nu)(\bar{\gamma}'_{11} - x_2 \bar{\kappa}'_3) + v_{1,22}] + 2(1 + \nu)\Lambda_1 = 0\tag{85}$$

and the natural boundary conditions simplify to

$$\frac{x_2 \tau (\bar{\gamma}_{11} - x_2 \bar{\kappa}_3)}{b} + \frac{2\nu (\tau b \bar{\kappa}_3 - 3x_2 \bar{\gamma}'_{11}) + \nu (3x_2^2 - b^2) \bar{\kappa}'_3 + 6v_{1,2}}{12(1 + \nu)} \Big|_{x_2=\pm b(x_1)} = 0\tag{86}$$

Solving Eqs. (85) and (86) simultaneously gives Λ_1 as

$$\Lambda_1 = Et \left(\frac{\tau \bar{\gamma}_{11}}{b} - \bar{\gamma}'_{11} \right)\tag{87}$$

and v_1 as

$$v_1 = \frac{\tau}{3b} [(1 + \nu) (b^2 - 3x_2^2) \bar{\gamma}_{11} + x_2(5\nu + 6)b^2 \bar{\kappa}_3] + \frac{1}{6} \{ \nu (3x_2^2 - b^2) \bar{\gamma}'_{11} + [x_2^3(\nu + 2) - x_2(5\nu + 6)b^2] \bar{\kappa}'_3 \} \quad (88)$$

Note that the first line is $O(\tau)$ and the second is $O(a/\ell)$, so that the perturbation is indeed $O(a)$. It can also be easily checked that the traction-free boundary conditions are satisfied asymptotically to the order of the perturbation variables, $O(a)$.

With both perturbation variables now known, the 2nd-order energy is also known. The strain energy per unit length, asymptotically-correct up to 2nd-order in a , is then the sum of U_0 and U_2 and is equal to

$$U = Etb \left[1 - \frac{2}{3}(\nu + 1)\tau^2 \right] \bar{\gamma}_{11}^2 + \frac{2Et\nu\tau b^2}{3} \bar{\gamma}_{11} \bar{\gamma}'_{11} + \frac{Etb^3}{9} [3 + 2(14\nu + 15)\tau^2] \bar{\kappa}_3^2 - \frac{4Et\tau(8\nu + 9)b^4}{9} \bar{\kappa}_3 \bar{\kappa}'_3 + \frac{4Et(1 + \nu)b^5}{15} \bar{\kappa}_3'^2 + \frac{2Et(11\nu + 12)b^5}{45} \bar{\kappa}_3 \bar{\kappa}_3'' \quad (89)$$

This energy is equivalent to that given by Eq. (28) for this particular problem. The coefficients multiplying the products, of the 1D strain measures and its derivatives, are the stiffness constants for this theory. These stiffness constants are implicit functions of x_1 through the varying width $b(x_1)$ and explicit functions of τ . It is easy to see that the coefficients multiplying $\bar{\gamma}_{11}^2$ and $\bar{\kappa}_3^2$ correspond to those of Euler-Bernoulli theory if its terms from τ are neglected. Terms with τ represent the corrections from taper. Stiffness constants, which lack the influence from τ , pertain to shear deformation of prismatic beams.

4.1.2 Generalized Timoshenko Beam Theory

The strain energy function developed in the previous section is not suitable for use as an engineering beam theory because of the presence of derivatives of $\bar{\gamma}_{11}$ and $\bar{\kappa}_3$. It is known, however, that the form of Eq. (89) can be transformed into a generalized Timoshenko theory, which is the main objective of this section. Thus, the strain energy will be put into the form

$$2U^* = X_{44}\kappa_3^2 + 2Y_{41}\kappa_3(2\gamma_{12}) + G_{11}(2\gamma_{12})^2 + X_{11}\gamma_{11}^2 \quad (90)$$

In general, the sectional energy may include contributions from the coupling between extension and other modes of deformation, but an inspection of the asymptotically-correct refined energy reveals that is not the case here. In other words, inspecting Eq. (89) shows that γ_{11} is coupled only with its own derivative, hence it is decoupled from both κ_3 and $2\gamma_{12}$. The shear strain measure $2\gamma_{12}$ turns out to be one order higher in a than the classical measures of strain; therefore the 2nd-order correct energy from Eq. (89) is sufficient to construct a generalized Timoshenko model. Also because $2\gamma_{12}$ is $O(a)$, G_{11} will not have corrections from the taper parameter in a 2nd-order correct strain energy. Note that after being put in this form, the energy will no longer be asymptotically-correct because information is lost in the conversion process.

The relationships between classical and generalized Timoshenko beam theories are established here. In an analogous manner to the situation shown by Fig. 3, \mathbf{T}_1 and \mathbf{T}_2 collectively represent the dyad associated with classical theory whereas \mathbf{B}_1 and \mathbf{B}_2 represent the dyad associated with generalized Timoshenko theory. \mathbf{T}_1 and \mathbf{T}_2 are aligned parallel to and normal to the beam reference axis. \mathbf{B}_1 and \mathbf{B}_2 are then rotated clockwise by an angle from \mathbf{T}_1 and \mathbf{T}_2 so that \mathbf{B}_1 is normal to the cross-sectional plane (which may be either defined as an average or at a point). The relationship between the basis vectors is then

$$\begin{aligned}\mathbf{B}_1 &= \mathbf{T}_1 - 2\gamma_{12} \mathbf{T}_2 \\ \mathbf{B}_2 &= 2\gamma_{12} \mathbf{T}_1 + \mathbf{T}_2\end{aligned}\tag{91}$$

The extensional strain measure is identical for the two theories so that

$$\bar{\gamma}_{11} = \gamma_{11}\tag{92}$$

The relationship of the bending strain measure between the two theories is given by

$$\bar{\kappa}_3 = \kappa_3 + (2\gamma_{12})'\tag{93}$$

Due to the presence of the derivatives in $\bar{\kappa}_3$ from Eq. (89), the derivatives are

$$\begin{aligned}\bar{\kappa}'_3 &= \kappa'_3 + (2\gamma_{12})'' \\ \bar{\kappa}''_3 &= \kappa''_3 + (2\gamma_{12})'''\end{aligned}\tag{94}$$

and also that $u'_2 = \theta + 2\gamma_{12}$ where θ is the total section rotation, and $\kappa_3 = \theta'$.

The derivatives of γ_{11} , κ_3 , and $2\gamma_{12}$ must be written in terms of γ_{11} , κ_3 , and $2\gamma_{12}$, since the form of Eq. (90) contains no derivatives. The approach for “eliminating” the derivatives is to make use of the equilibrium equations. At each section, the internal axial force F_1 , shear force F_2 , and bending moment M_3 are, respectively,

$$\begin{aligned}F_1 &= \frac{\partial U^*}{\partial \gamma_{11}} = X_{11} \gamma_{11} \\ F_2 &= \frac{\partial U^*}{\partial (2\gamma_{12})} = Y_{41} \kappa_3 + G_{11} (2\gamma_{12}) \\ M_3 &= \frac{\partial U^*}{\partial \kappa_3} = X_{44} \kappa_3 + Y_{41} (2\gamma_{12})\end{aligned}\tag{95}$$

In the absence of applied loading within the beam, the equilibrium equations are then

$$\begin{aligned}F'_1 &= X_{11} \gamma'_{11} + X'_{11} \gamma_{11} = 0 \\ F'_2 &= G_{11} (2\gamma_{12})' + Y_{41} \kappa'_3 + G'_{11} (2\gamma_{12}) + Y'_{41} \kappa_3 = 0 \\ M'_3 + F_2 &= Y_{41} (2\gamma_{12})' + X_{44} \kappa'_3 + (Y'_{41} + G_{11}) (2\gamma_{12}) + (X'_{44} + Y_{41}) \kappa_3 = 0\end{aligned}\tag{96}$$

The above represents a system of equations which can be used to solve for γ'_{11} , $(2\gamma_{12})'$, and κ'_3 in terms of γ_{11} , $2\gamma_{12}$, and κ_3 . The higher derivatives can then be obtained, in terms of γ_{11} , $2\gamma_{12}$, and κ_3 , by directly taking derivatives of Eq. (96). The resulting expressions are too lengthy to include here, but suffice it to say that the procedure is not at all challenging for symbolic computational tools such as Mathematica.

The desired strain energy of the beam, in the form of Eq. (90), can now be obtained by substituting Eqs. (93) and (94), along with the described approach for “eliminating” derivatives, into Eq. (89). Equating the resultant 2nd-order approximation to the

strain energy with Eq. (90), one obtains the stiffness constants as

$$\begin{aligned}
X_{44} &= \frac{2 E t b^3}{3} \left[1 + \frac{(\nu - 48)\nu - 45}{45(\nu + 1)} \tau^2 \right] \\
Y_{41} &= \frac{E t (5\nu + 3) b^2 \tau}{9(\nu + 1)} \\
G_{11} &= \frac{5 E t b}{6(\nu + 1)} \\
X_{11} &= 2 E t b \left(1 - \frac{2\tau^2}{3} \right)
\end{aligned} \tag{97}$$

The terms involving $\tau = -b'(x_1)$ are the corrections from having included taper. From these expressions, one can observe that X_{44} is proportional to b^3 and is a quadratic polynomial in τ , Y_{41} is proportional to b^2 and is linear in τ , G_{11} is proportional to b and independent of τ , and X_{11} is proportional to b and is a quadratic polynomial in τ .

According to Ref. [40], there is no consensus on the precise definition of shear stiffness. Even though the expression for G_{11} corresponds to results by Refs. [40], [50], and [52], it may not necessarily match those of other definitions.

Note that the stiffness constants from both Eqs. (89) and (97) are either symmetric or antisymmetric with respect to $\tau = 0$. This feature is a reflection of the symmetry in both material properties and geometry for this section. The feature is also a similarity that is shared by the initially twisted isotropic square section, whose stiffness constants are shown to be either symmetric or antisymmetric about $k_1 = 0$ in Table 6. As shown on Figs. 8 to 16, the initially twisted CUS section does not share this feature due to its dependency on directions in material properties.

4.2 Classical Loading Cases

Now that analytical formulae of stiffness constants to the generalized Timoshenko beam theory are known, the next step is to use these stiffness constants as inputs into the 1D global analysis. Analytical beam theory solutions are first established for the three classical loading conditions such that (1) the internal axial force, (2)

bending moment, or (3) shear force is constant along the span. As mentioned in Sec. 1.2, exact elasticity solutions exist for these three cases under 2D plane stress assumptions. These elasticity solutions are next presented. This section concludes with the comparison of results between beam theory and elasticity.

4.2.1 Analytical Beam Solutions

4.2.1.1 Constant Axial Force

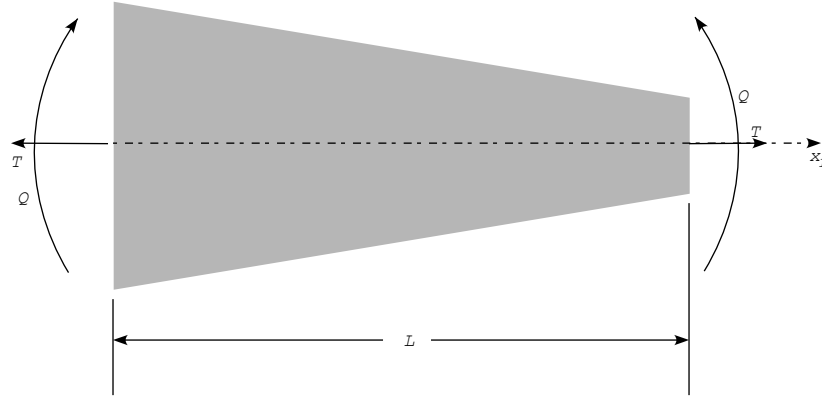


Figure 28: Schematic of beam loaded for either pure extension or pure bending

In the constant axial force case, a beam of length L is loaded at each end by equal and opposite axial tensile forces of magnitude T , depicted in Fig. 28 for $Q = 0$. The potential of the applied loads is thus

$$\Phi = -T[u_1(L) - u_1(0)] = -T \int_0^L u_1' dx_1 = -T \int_0^L \gamma_{11} dx_1 \quad (98)$$

According to the principle of virtual work, the system is in equilibrium if and only

if the variation of its total potential is zero. Upon setting the variation of the total potential equal to zero without imposing any geometric boundary conditions, one obtains

$$\int_0^L [X_{44}\kappa_3\delta\kappa_3 + Y_{41}(2\gamma_{12})\delta\kappa_3 + Y_{41}\kappa_3\delta(2\gamma_{12}) + G_{11}(2\gamma_{12})\delta(2\gamma_{12}) + X_{11}\gamma_{11}\delta\gamma_{11} - T\delta\gamma_{11}] dx_1 = 0 \quad (99)$$

The above equation requires that the internal axial force, F_1 , to be

$$F_1 = X_{11}\gamma_{11} = T \quad (100)$$

One can easily see that the elongation strain is

$$\gamma_{11} = \frac{T}{X_{11}} \quad (101)$$

knowledge of which allows one to then integrate the kinematical differential equation $u'_1 = \gamma_{11}$ to obtain $u_1(x_1)$ for any given spanwise variation of the stiffness constant X_{11} . According to the model obtained from the VAM, the displacement $u_1(x_1)$ can be related directly to the elasticity solution in terms of the average axial displacement over the section.

4.2.1.2 Constant Bending Moment

To solve the constant bending moment problem, one may use the kinematical differential equation $\kappa_3 = \theta'$ and apply equal and opposite moments of magnitude Q on the ends of the beam. Figure 28, with $T = 0$, illustrates this case. This yields a potential of the applied loads of the form

$$\Phi = -Q[\theta(L) - \theta(0)] = -Q \int_0^L \theta' dx_1 = -Q \int_0^L \kappa_3 dx_1 \quad (102)$$

Equilibrium equations can then be found by minimizing the total potential subject to no geometric boundary conditions. The result is

$$\int_0^L [X_{44}\kappa_3\delta\kappa_3 + Y_{41}(2\gamma_{12})\delta\kappa_3 + Y_{41}\kappa_3\delta(2\gamma_{12}) + G_{11}(2\gamma_{12})\delta(2\gamma_{12}) + X_{11}\gamma_{11}\delta\gamma_{11} - Q\delta\kappa_3] dx_1 = 0 \quad (103)$$

The resulting Euler-Lagrange equations require that the bending moment and shear force are, respectively,

$$\begin{aligned} M_3 &= X_{44}\kappa_3 + Y_{41}(2\gamma_{12}) = Q \\ F_3 &= Y_{41}\kappa_3 + G_{11}(2\gamma_{12}) = 0 \end{aligned} \quad (104)$$

Thus, using $2\gamma_{12} = -Y_{41}\kappa_3/G_{11}$, one obtains

$$\left(X_{44} - \frac{Y_{41}^2}{G_{11}}\right) \kappa_3 = Q \quad (105)$$

The solution can then be written as

$$\kappa_3 = \frac{Q}{X_{44} - \frac{Y_{41}^2}{G_{11}}} \quad (106)$$

which allows one to integrate the kinematical differential equation, $\kappa_3 = \theta'$, to obtain $\theta(x_1)$ for any given spanwise variation of X_{44} , Y_{41} , and G_{11} . Unlike the prismatic case, even though Q is constant, κ_3 is not. Moreover, the transverse displacement $u_2(x_1)$ can then be obtained by integration of another kinematical differential equation, $u_2' = \theta + 2\gamma_{12} = \theta - Y_{41}\kappa_3/G_{11}$. It is clear that loading by a constant bending moment along the span produces shear deformation in a tapered beam.

4.2.1.3 Constant Shear Force

For the flexure problem, the beam is loaded with an equal and opposite transverse force P at each end, and a moment PL at the left end to counteract the moment of the force at the right end; see Fig. 29. For this loading the potential of the applied

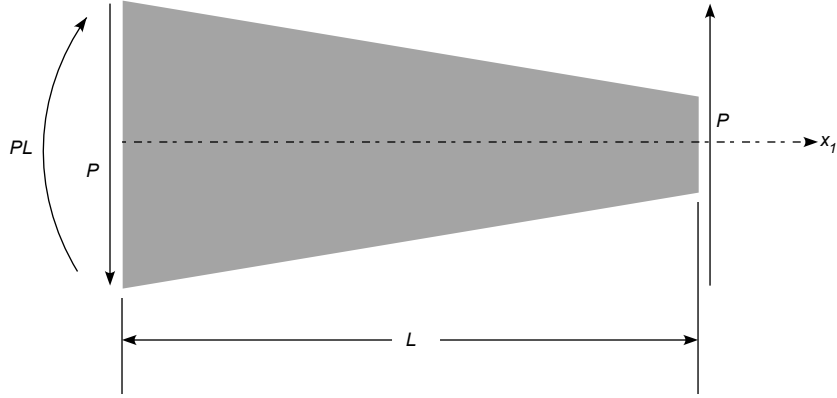


Figure 29: Schematic of beam loaded for flexure

loads takes the form

$$\begin{aligned}
 \Phi &= -P[u_2(L) - u_2(0)] + PL\theta(0) \\
 &= -P \int_0^L [(u'_2 - \theta) + (L - x_1)\theta'] dx_1 \\
 &= -P \int_0^L [2\gamma_{12} + (L - x_1)\kappa_3] dx_1
 \end{aligned} \tag{107}$$

Equilibrium equations can then be found by minimizing the total potential subject to no geometric boundary conditions. The result is

$$\begin{aligned}
 \int_0^L \{ &X_{44}\kappa_3\delta\kappa_3 + Y_{41}(2\gamma_{12})\delta\kappa_3 + Y_{41}\kappa_3\delta(2\gamma_{12}) + G_{11}(2\gamma_{12})\delta(2\gamma_{12}) + X_{11}\gamma_{11}\delta\gamma_{11} \\
 &-P[\delta(2\gamma_{12}) + (L - x_1)\delta\kappa_3]\} dx_1 = 0
 \end{aligned} \tag{108}$$

The resulting Euler-Lagrange equations and boundary conditions require that the bending moment and shear force are, respectively,

$$\begin{aligned} M_3 &= X_{44}\kappa_3 + Y_{41}(2\gamma_{12}) = P(L - x_1) \\ F_3 &= Y_{41}\kappa_3 + G_{11}(2\gamma_{12}) = P \end{aligned} \tag{109}$$

Thus, one obtains

$$\begin{aligned} \kappa_3 &= \frac{P}{X_{44}G_{11} - Y_{41}^2} [G_{11}(L - x_1) - Y_{41}] \\ 2\gamma_{12} &= \frac{P}{X_{44}G_{11} - Y_{41}^2} [X_{44} - Y_{41}(L - x_1)] \end{aligned} \tag{110}$$

which allows one to integrate the same kinematical differential equations, as in the constant bending moment case, to obtain the total section rotation $\theta(x_1)$ and the displacement of the neutral axis $u_2(x_1)$ for any given spanwise variation of X_{44} , Y_{41} , and G_{11} . Unlike the prismatic case, although the bending moment is linear along the span, κ_3 is not. Likewise, although the shear force is constant along the span, $2\gamma_{12}$ is not.

4.2.2 Exact Elasticity Solutions

This section presents exact solutions for the purpose of comparing with the above beam theory solutions. These solutions are appropriately based on linear, plane stress elasticity theory for a linearly tapered strip for the constant axial force, constant bending moment, and constant shear force loading cases. For all three cases, the components of the stress tensor are given. Components of the strain tensor may then be obtained from the plane stress form of Hooke's law. Lastly, the strains can be integrated to obtain displacements, $u_x(x_1, x_2)$ and $u_y(x_1, x_2)$. The displacement fields from elasticity are denoted by $u_x(x_1, x_2)$ and $u_y(x_1, x_2)$ to distinguish it from $u_1(x_1)$ and $u_2(x_1)$, which are the displacements from the 1D global beam analysis. In the formulae that ensue, $h = a - L\tau$ is the half-width of the strip at $x_1 = L$ and s is defined by $s = L - x_1$.

A way to extract information from the elasticity solutions is now set forth, so that the results can be compared with those from beam theory. The displacement fields from elasticity can be related to beam theory by making use of Eq. (72), yielding

$$\begin{aligned} u_x &= u_1 - x_2 u_2' + w_1 \\ u_y &= u_2 + w_2 \end{aligned} \tag{111}$$

where the warping displacements are approximated from the derivations of earlier. Integration of both sides of Eq. (111) over x_2 while using the constraints on warping yields

$$\begin{aligned} u_1 &= \frac{1}{2b} \langle u_x \rangle \\ u_2 &= \frac{1}{2b} \langle u_y \rangle \end{aligned} \tag{112}$$

Multiplying both sides of the first of Eq. (111) by x_2 and then integrating allows one to write

$$\begin{aligned} \theta &= \frac{3}{2b^3} \langle -x_2 u_x \rangle \\ 2\gamma_{12} &= u_2' - \theta = \frac{3}{2b^3} \langle x_2 w_1 \rangle \end{aligned} \tag{113}$$

Finally, the stretching and bending strain measures, $\gamma_{11} = u_1'$ and $\kappa_3 = \theta'$, along with the shear strain measure $2\gamma_{12}$, can now be compared directly with results from the beam analysis.

4.2.2.1 Constant Axial Force

The solution for the deformation of a wedge, described by polar coordinates r_p and ϕ_p , is presented on p. 110 of Ref. [45]. The stresses for this case are $\sigma_\phi = \sigma_{r\phi} = 0$ and

$$\sigma_r = \frac{T \cos \phi_p}{r_p t (\alpha + \cos \alpha \sin \alpha)} \tag{114}$$

where, referring back to Fig. 28, $Q = 0$ and T is nonzero. Here $\alpha = \tan^{-1} \tau$,

$$r_p = \sqrt{x_2^2 + \frac{b^2}{\tau^2}} \tag{115}$$

and

$$\phi_p = \tan^{-1} \left(\frac{x_2 \tau}{b} \right) \tag{116}$$

The stresses in the Cartesian system can be found as

$$\begin{aligned}
\sigma_{11} &= \sigma_r \cos^2 \phi_p - \sigma_{r\phi} \sin 2\phi_p \\
\sigma_{12} &= -\sigma_{r\phi} \cos 2\phi_p - \frac{1}{2}\sigma_r \sin 2\phi_p \\
\sigma_{22} &= \sigma_r \sin^2 \phi_p + \sigma_{r\phi} \cos 2\phi_p
\end{aligned} \tag{117}$$

In terms of the geometric parameters and loads, the stresses finally become

$$\begin{aligned}
\sigma_{11} &= \frac{T\tau b^3 (\tau^2 + 1)}{t (b^2 + x_2^2 \tau^2)^2 [\tau + (\tau^2 + 1) \tan^{-1}(\tau)]} \\
\sigma_{12} &= -\frac{T x_2 \tau^2 b^2 (\tau^2 + 1)}{t (b^2 + x_2^2 \tau^2)^2 [\tau + (\tau^2 + 1) \tan^{-1}(\tau)]} \\
\sigma_{22} &= \frac{T x_2^2 \tau^3 b (\tau^2 + 1)}{t (b^2 + x_2^2 \tau^2)^2 [\tau + (\tau^2 + 1) \tan^{-1}(\tau)]}
\end{aligned} \tag{118}$$

4.2.2.2 Constant Bending Moment

This case is also shown on Fig. 28, here with $T = 0$ and Q nonzero. The stresses in polar coordinates are given on pp. 112, 113 of Ref. [45] as $\sigma_\phi = 0$ and

$$\begin{aligned}
\sigma_r &= \frac{2Q \sin 2\phi_p}{r_p^2 t (2\alpha \cos 2\alpha - \sin 2\alpha)} \\
\sigma_{r\phi} &= -\frac{Q (\cos 2\phi_p - \cos 2\alpha)}{r_p^2 t (2\alpha \cos 2\alpha - \sin 2\alpha)}
\end{aligned} \tag{119}$$

Making the above transformation to Cartesian coordinates, one may obtain the stresses as

$$\begin{aligned}
\sigma_{11} &= -\frac{2bQx_2\tau^3 [b^2 (2\tau^2 + 1) - x_2^2 \tau^2]}{t (b^2 + x_2^2 \tau^2)^3 [\tau + (\tau^2 - 1) \tan^{-1}(\tau)]} \\
\sigma_{12} &= -\frac{Q\tau^4 [b^4 - 3x_2^2 (\tau^2 + 1) b^2 + x_2^4 \tau^2]}{t (b^2 + x_2^2 \tau^2)^3 [\tau + (\tau^2 - 1) \tan^{-1}(\tau)]} \\
\sigma_{22} &= \frac{2bQx_2\tau^5 [b^2 - x_2^2 (\tau^2 + 2)]}{t (b^2 + x_2^2 \tau^2)^3 [\tau + (\tau^2 - 1) \tan^{-1}(\tau)]}
\end{aligned} \tag{120}$$

To visualize the deformed shape, the results from finite element analysis using ABAQUS are shown. The deformed shape of the structure is shown in Fig. 30. To eliminate rigid body modes, two geometric boundary conditions are set. The first condition is $u_x = u_y = 0$ at the point with coordinates of $x_1 = 0$ and $x_2 = 0$. The second condition is $u_y = 0$ at the point with coordinates of $x_1 = L$ and $x_2 = 0$.

Modeling in ABAQUS is done using its CPS8R elements and its results are validated with the elasticity solution. The specific dimensions, material properties, and loading chosen are given in Table 7. It is clear that κ_3 increases as the width of the structure decreases.

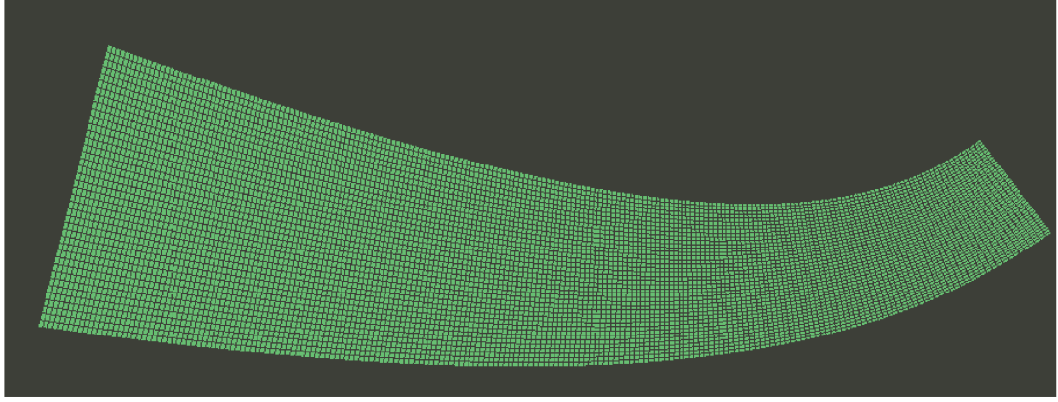


Figure 30: Deformed shape of the tapered strip loaded under a constant bending moment

Table 7: Dimensions and material properties for the tapered strip evaluated for ABAQUS calculations

L (m)	a (m)	τ	t (m)	E (GPa)	ν
20	3	0.1	$\frac{3}{16}$	200	0.3

4.2.2.3 Constant Shear Force

The stresses of this case, shown on Fig. 29, are given in polar coordinates by Ref. [26] to be $\sigma_\phi = 0$ and

$$\begin{aligned}\sigma_r &= \frac{2P}{r_p^2 t} \left[\frac{r_p \sin \phi_p}{\sin 2\alpha - 2\alpha} + \frac{(L - a \cot \alpha) \sin 2\phi_p}{2\alpha \cos 2\alpha - \sin 2\alpha} \right] \\ \sigma_{r\phi} &= - \frac{P(\cos 2\phi_p - \cos 2\alpha) \cot \alpha (a - L \tan \alpha)}{r_p^2 t (\sin 2\alpha - 2\alpha \cos 2\alpha)}\end{aligned}\tag{121}$$

(It is noted that several small printing mistakes in Ref. [26] had to be corrected in order to obtain this result.) Making the transformation to Cartesian coordinates, one

finds the stresses to be

$$\begin{aligned}
\sigma_{11} &= \frac{bPx_2\tau^2}{t(b^2 + x_2^2\tau^2)^3} \left\{ \frac{2h[b^2 + (2b^2 - x_2^2)\tau^2]}{\tau + (\tau^2 - 1)\tan^{-1}(\tau)} - \frac{b(\tau^2 + 1)(b^2 + x_2^2\tau^2)}{(\tau^2 + 1)\tan^{-1}(\tau) - \tau} \right\} \\
\sigma_{12} &= -\frac{P\tau^4[b^5 - s\tau b^4 - 4x_2^2(\tau^2 + 1)b^3 + 3sx_2^2\tau(\tau^2 + 1)b^2 - x_2^4\tau^4b - sx_2^4\tau^3]}{t(b^2 + x_2^2\tau^2)^3 \left\{ 2\tau\tan^{-1}(\tau) + (\tau^4 - 1)[\tan^{-1}(\tau)]^2 - \tau^2 \right\}} \\
&\quad + \frac{P\tau^3(\tau^2 + 1)[b^5 - s\tau b^4 - 2x_2^2(\tau^2 + 2)b^3 + 3sx_2^2\tau(\tau^2 + 1)b^2 + x_2^4\tau^4b - sx_2^4\tau^3]\tan^{-1}(\tau)}{t(b^2 + x_2^2\tau^2)^3 \left\{ 2\tau\tan^{-1}(\tau) + (\tau^4 - 1)[\tan^{-1}(\tau)]^2 - \tau^2 \right\}} \\
\sigma_{22} &= -\frac{Px_2\tau^4}{t(b^2 + x_2^2\tau^2)^3} \left\{ \frac{(\tau^2 + 1)(b^2 + x_2^2\tau^2)x_2^2}{(\tau^2 + 1)\tan^{-1}(\tau) - \tau} + \frac{2bh[b^2 - x_2^2(\tau^2 + 2)]}{\tau + (\tau^2 - 1)\tan^{-1}(\tau)} \right\}
\end{aligned} \tag{122}$$

4.2.3 Validation of Analytical Beam Solutions: Stiffness

In this section the stiffness constants, obtained by the VAM, are compared with results for the same quantities extracted from the elasticity solutions. To do so, the 1D displacement and rotation variables u_1 , u_2 , and θ are extracted from the elasticity solutions above by averaging 2D displacements over x_2 in accordance with Eqs. (112) and (113). Then, these quantities are differentiated with respect to x_1 , leading to the values of 1D generalized strains γ_{11} , $2\gamma_{12}$, and κ_3 . Finally, effective stiffnesses are found by dividing appropriate applied loads by corresponding 1D generalized strains. These effective stiffnesses are then compared directly with effective stiffnesses determined by beam theory.

4.2.3.1 Constant Axial Force

For the constant axial force case, it is appropriate to compare the quantity T/γ_{11} using stiffness constants obtained from the VAM with an expansion of the elasticity solution in τ . The beam solution, from Eq. (101), and the 2nd-order asymptotic expansion of the elasticity solution both agree that this quantity is

$$\frac{T}{\gamma_{11}} = X_{11} = 2Et b \left(1 - \frac{2\tau^2}{3} \right) \tag{123}$$

The term involving τ^2 represents the correction to taper. The perfect agreement by both solutions reflects that the strain energy from the refined model is asymptotically-correct for this problem, which is expected because shear deformations are not involved in this case. This effective extension stiffness, which is normalized by dividing through by values which neglect the taper effect, is plotted as a function of τ on Fig. 31. For a section with a taper of $\tau = 0.1763$, which corresponds to 10° taper and is not uncommon as local taper on rotor blades, the extension stiffness is overpredicted by 2.12% if the taper effect is neglected.

4.2.3.2 Constant Bending Moment

The quantity to be compared for this problem is Q/κ_3 . The beam solution, from Eq. (106) is

$$\frac{Q}{\kappa_3} = X_{44} - \frac{Y_{41}^2}{G_{11}} = \frac{2 E t b^3}{3} - \frac{4 E t b^3 (4\nu + 9) \tau^2}{45} \quad (124)$$

whereas the 2nd-order asymptotic expansion of the elasticity solution yields

$$\frac{Q}{\kappa_3} = \frac{2 E t b^3}{3} - \frac{4 E t b^3 (\nu + 3) \tau^2}{15} \quad (125)$$

This effective bending stiffness, again normalized by dividing through by values which neglect the taper effect, is plotted as a function of τ on Fig. 32 for $\nu=0.3$. For a taper of $\alpha = 10^\circ$, the taper effect reduces the bending stiffness by 4.28% and 4.42% from the elasticity and beam solutions, respectively. The relative difference between the beam solution and the elasticity solution is $2\nu \tau^2/15$, with the beam solution being softer. This small difference between the asymptotic expansion of the exact solution versus the beam results can be attributed to having approximated the asymptotically-correct energy, Eq. (89), by forcing it into the mold of the generalized Timoshenko model, Eq. (90). Obviously, the correction due to taper is itself much larger than the difference between the elasticity and beam solutions.

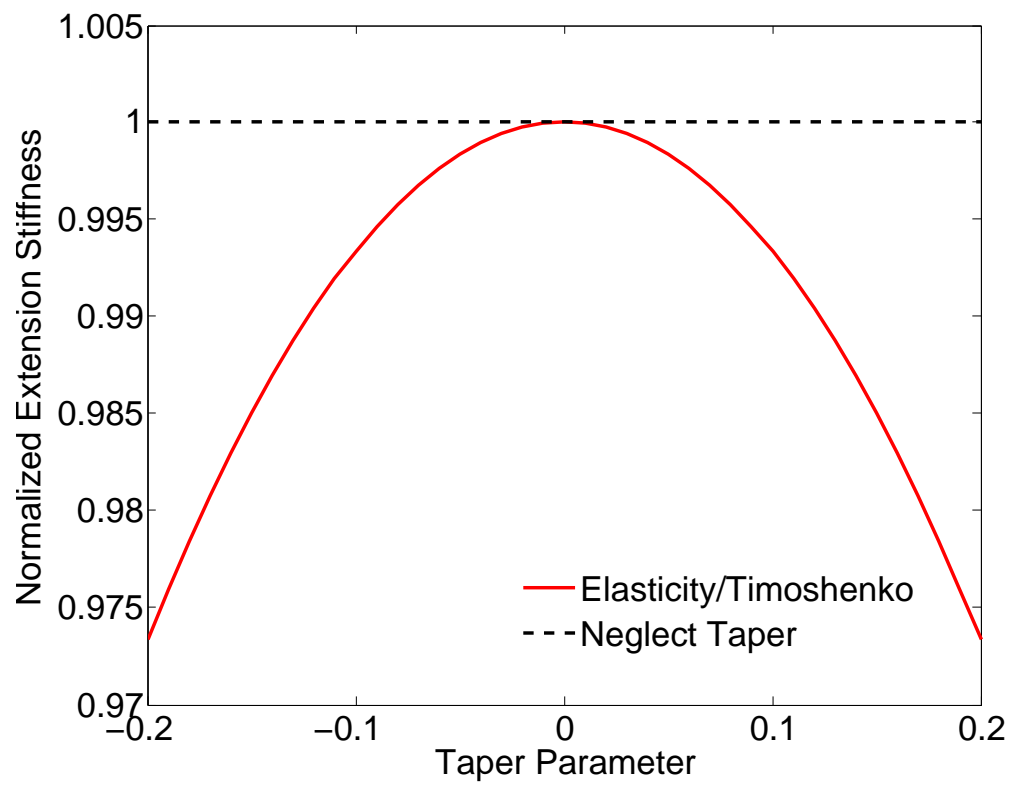


Figure 31: Effective extension stiffness under loading for constant axial force

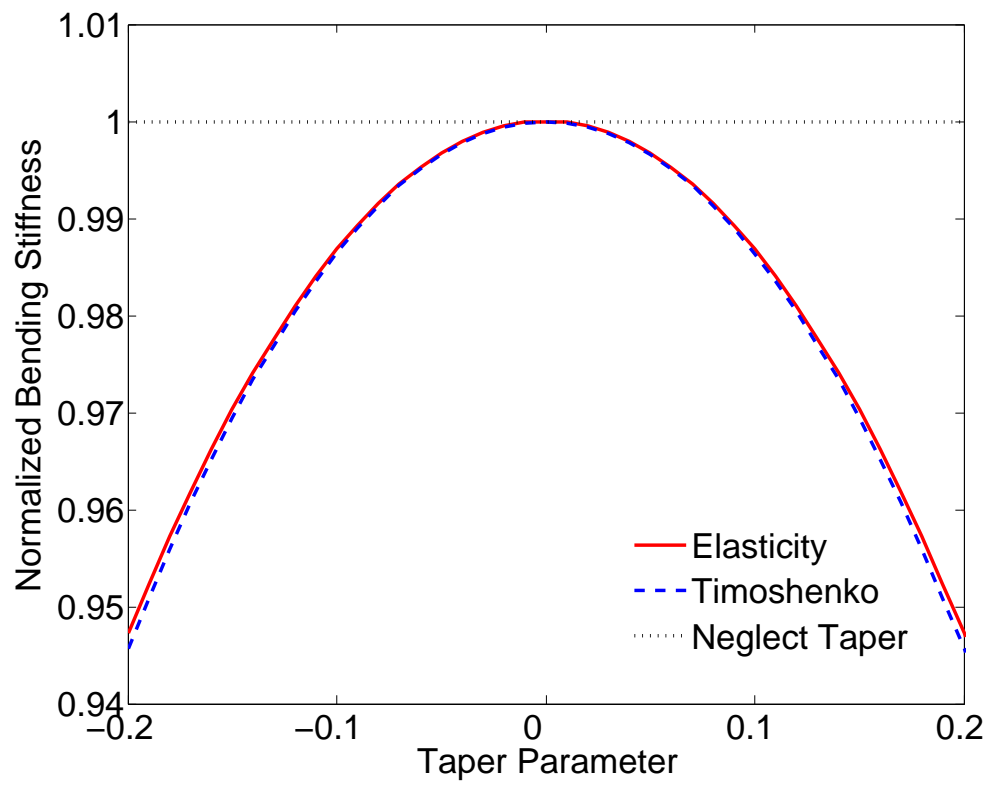


Figure 32: Effective bending stiffness under loading for constant bending moment, $\nu = 0.3$

4.2.3.3 Constant Shear Force

For the flexure problem, relevant quantities for comparison are P/κ_3 and $P/(2\gamma_{12})$ at $x_1 = L$. The beam solution, Eq. (110), yields

$$\begin{aligned}\frac{P}{\kappa_3} &= Y_{41} - \frac{X_{44}G_{11}}{Y_{41}} = -\frac{5 E t b^2}{(3 + 5\nu) \tau} + O(\tau) \\ \frac{P}{2\gamma_{12}} &= G_{11} - \frac{Y_{41}^2}{X_{44}} = \frac{5 E t b}{6(1 + \nu)} + O(\tau^2)\end{aligned}\tag{126}$$

An order of magnitude analysis shows that neither of the correction terms to these results are trustworthy, because there is not sufficient information in the energy to ensure that all contributions are present. That is to say, the VAM solution would have to be extended to include terms of higher order in τ than that is needed in simply constructing a beam model with a 2nd-order asymptotically-correct energy; in particular corrections of 3rd-order to Y_{41} and 2nd-order to G_{11} would be needed. As expected, the elasticity solution is in agreement with the above $P/(2\gamma_{12})$ result since it does not involve taper; it should be noted, however, that there is more than one possible result from this exercise. The method of Ref. [54] is used here. The result for P/κ_3 does involve taper and is given by

$$\frac{P}{\kappa_3} = -\frac{10 E t b^2}{3(2 + 3\nu) \tau} + O(\tau)\tag{127}$$

This effective bending-shear coupling at $x_1 = L$, which is normalized by dividing the beam solution through by the elasticity solution, is plotted as a function of ν on Fig. 33. The beam solution differs from the elasticity solution by less than 4% for practical values of ν . Note that this term tends to infinity as taper decreases and the beam approaches being prismatic.

4.2.4 Validation of Analytical Beam Solutions: Recovery Relations

This section presents analytical formulae to the 2D stress and strain fields from the VAM beam theory and from 2D elasticity. The 2D displacement field may be recovered by integrating the 2D strain field along with appropriate boundary conditions,

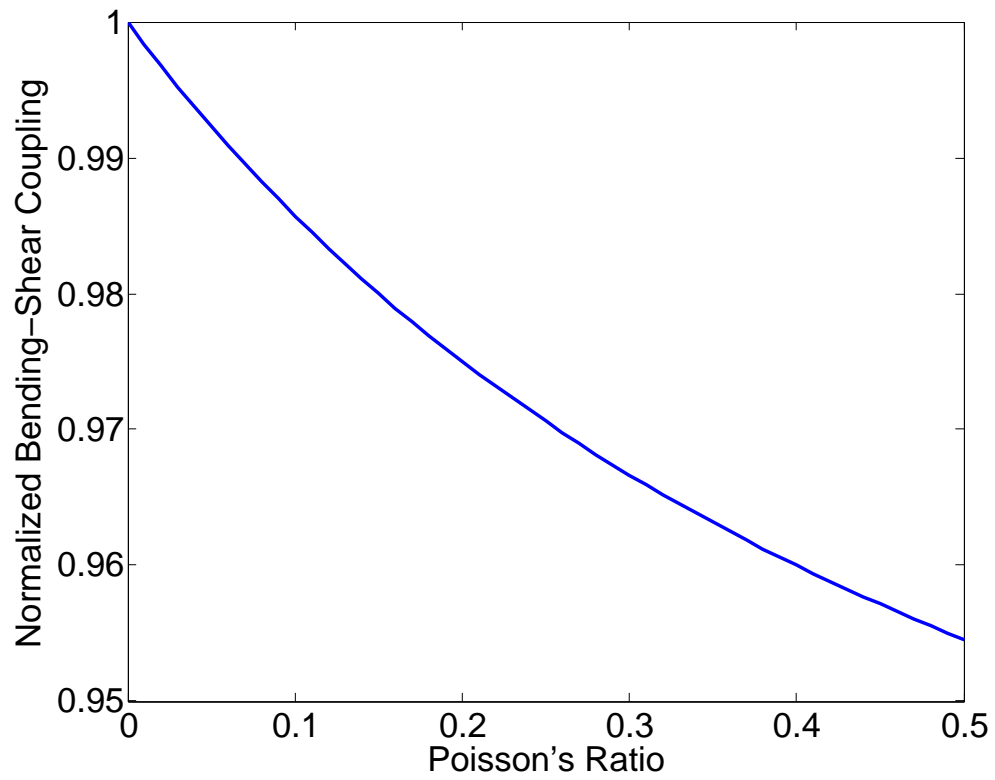


Figure 33: Effective bending-shear coupling under loading for constant shear force, $x_1 = L$

so the accuracy of the displacement field is dependent only upon the accuracy of the strain field. Therefore, there is no need to specify detailed boundary conditions to compare the 2D displacement fields between beam theory and elasticity. In the case of beam theory, the 2D strain field is found from substituting the 1D strain measures and warping fields into Eq. (77) for each specific loading condition. In the case of elasticity, the exact 2D stress field is given for each of the three classical loading cases in Sec. 4.2.2. For both beam theory and elasticity, the 2D stress field is determined from Hooke's law once the 2D strain field is known, and vice versa.

In general, the order of accuracy for these recovered quantities is not as high as that of the energy. Since the refined theory from Eq. (89) is asymptotically-correct up to 2nd-order in its energy, the formulae presented here from both beam theory and elasticity represent 2nd-order series expansions in the small quantity a . If one desires to improve the accuracy of the results from beam theory, then one would need to account for higher-order perturbations to the warping displacements. Note that $\xi = \frac{x_2}{b}$. As mentioned in Sec. 4.1.1, the stress field presented in this section from beam theory do satisfy the traction boundary conditions up to $O(a)$.

4.2.4.1 Constant Axial Force

This case is the most accurate among the three loading cases. Recall that the shear mode of deformation is absent in this case, so the strain energy is 2nd-order asymptotically-correct. The stress and strain components from both beam theory and elasticity theory are given below. For σ_{12} , Γ_{11} , and Γ_{12} , there is accuracy up to 2nd-order while the other components are accurate up to 1st-order. From beam theory, the stress components are

$$\begin{aligned}\sigma_{11} &= \frac{T}{2bt} \left[\left(\frac{(\nu + 2)\xi^2}{\nu^2 - 1} + \frac{2}{3} \right) \tau^2 + 1 \right] \\ \sigma_{22} &= \frac{T\nu(\nu + 2)\xi^2\tau^2}{2bt(\nu^2 - 1)} \\ \sigma_{12} &= -\frac{T\xi\tau}{2bt}\end{aligned}\tag{128}$$

and the strain components are

$$\begin{aligned}\Gamma_{11} &= \frac{T}{2Ebt} \left[\left(\frac{2}{3} - (\nu + 2)\xi^2 \right) \tau^2 + 1 \right] \\ \Gamma_{22} &= -\frac{T\nu}{2Ebt} \left[\frac{2\tau^2}{3} + 1 \right] \\ \Gamma_{12} &= -\frac{T(\nu + 1)\xi\tau}{2Ebt}\end{aligned}\tag{129}$$

From elasticity, the stress components are

$$\begin{aligned}\sigma_{11} &= \frac{T}{2bt} \left[\left(\frac{2}{3} - 2\xi^2 \right) \tau^2 + 1 \right] \\ \sigma_{22} &= \frac{T\xi^2\tau^2}{2bt} \\ \sigma_{12} &= -\frac{T\xi\tau}{2bt}\end{aligned}\tag{130}$$

and the strain components are

$$\begin{aligned}\Gamma_{11} &= \frac{T}{2Ebt} \left[\left(\frac{2}{3} - (\nu + 2)\xi^2 \right) \tau^2 + 1 \right] \\ \Gamma_{22} &= -\frac{T\nu}{2Ebt} \left[\left(\frac{2}{3} - \left(2 + \frac{1}{\nu} \right) \xi^2 \right) \tau^2 + 1 \right] \\ \Gamma_{12} &= -\frac{T(\nu + 1)\xi\tau}{2Ebt}\end{aligned}\tag{131}$$

4.2.4.2 Constant Bending Moment

Unlike the prismatic case, there is deformation from the shear mode for this loading condition. Therefore, the generalized Timoshenko strain energy is no longer asymptotically-correct due to the transformation procedure to generalized Timoshenko form. The beam expressions for σ_{12} and Γ_{12} are only accurate up to 0th-order while the other four quantities are accurate up to 1st-order. From beam theory, the stress components are

$$\begin{aligned}\sigma_{11} &= -\frac{3Q\xi}{2b^2t} \left[\frac{(80\xi^2 + \nu(50\xi^2 + 6(1 - 2\nu)\nu - 43) - 66)\tau^2}{15(\nu^2 - 1)} + 1 \right] \\ \sigma_{22} &= \frac{Q\nu\xi(-10\nu\xi^2 - 16\xi^2 + 11\nu + 12)\tau^2}{2b^2t(\nu^2 - 1)} \\ \sigma_{12} &= \frac{3Q(2\xi^2 - 1)\tau}{2b^2t}\end{aligned}\tag{132}$$

and the strain components are

$$\begin{aligned}
\Gamma_{11} &= -\frac{3Q\xi}{2Eb^2t} \left[\frac{1}{15} (-10(5\nu + 8)\xi^2 + 43\nu + 66) \tau^2 + 1 \right] \\
\Gamma_{22} &= \frac{3Q\nu\xi}{2Eb^2t} \left[\frac{1}{5} (2 - 4\nu)\tau^2 + 1 \right] \\
\Gamma_{12} &= \frac{3Q(\nu + 1)(2\xi^2 - 1)\tau}{2Eb^2t}
\end{aligned} \tag{133}$$

From elasticity, the stress components are

$$\begin{aligned}
\sigma_{11} &= -\frac{3Q\xi}{2b^2t} \left[\frac{4}{5} (3 - 5\xi^2) \tau^2 + 1 \right] \\
\sigma_{22} &= -\frac{3Q\xi(2\xi^2 - 1)\tau^2}{2b^2t} \\
\sigma_{12} &= \frac{3Q(3\xi^2 - 1)\tau}{4b^2t}
\end{aligned} \tag{134}$$

and the strain components are

$$\begin{aligned}
\Gamma_{11} &= -\frac{3Q\xi}{2Eb^2t} \left[\left(-2\nu\xi^2 - 4\xi^2 + \nu + \frac{12}{5} \right) \tau^2 + 1 \right] \\
\Gamma_{22} &= \frac{3Q\nu\xi}{2Eb^2t} \left[\left(-4\xi^2 + \frac{1 - 2\xi^2}{\nu} + \frac{12}{5} \right) \tau^2 + 1 \right] \\
\Gamma_{12} &= \frac{3Q(\nu + 1)(3\xi^2 - 1)\tau}{4Eb^2t}
\end{aligned} \tag{135}$$

4.2.4.3 Constant Shear Force

Compared to the constant bending moment case, the shear mode of deformation is now much more significant. As a result, the correlation has deteriorated further. The beam expressions are now only accurate up to the 0th-order for all six quantities of stress and strain. Already having defined $h = b(L)$, then the term $\frac{b-h}{\tau}$ is equal to

$(L - x_1)$. From beam theory, the stress components are

$$\begin{aligned}
\sigma_{11} &= -\frac{3P}{2b^2t} \left[(L - x_1)\xi + \frac{b((12\nu^3 + 12\nu^2 + 28\nu + 33)\xi - (20\nu + 35)\xi^3)\tau}{15(\nu^2 - 1)} \right] \\
&\quad - \frac{3P}{2b^2t} \left[\frac{(L - x_1)((50\nu + 80)\xi^3 + (-12\nu^3 + 6\nu^2 - 43\nu - 66)\xi)\tau^2}{15(\nu^2 - 1)} \right] \\
\sigma_{22} &= \frac{P\nu}{2bt(\nu^2 - 1)} \left[\frac{(L - x_1)(-10\nu\xi^3 - 16\xi^3 + 11\nu\xi + 12\xi)\tau^2}{b} \right] \\
&\quad + \frac{P\nu}{2bt(\nu^2 - 1)} [((4\nu + 7)\xi^3 + (-8\nu - 9)\xi)\tau] \\
\sigma_{12} &= \frac{3P}{4bt} \left[\frac{2}{5}(8\nu\xi^2 + 5\xi^2 - 4\nu - 1)\tau^2 + \frac{2(x_1 - L)(1 - 2\xi^2)\tau}{b} + (1 - \xi^2) \right]
\end{aligned} \tag{136}$$

and the strain components are

$$\begin{aligned}
\Gamma_{11} &= -\frac{3P}{2Eb^2t} \left[\frac{L - x_1}{15}\xi((50\nu + 80)\xi^2 - 43\nu - 66)\tau^2 \right] \\
&\quad - \frac{3P}{2Eb^2t} \left[\frac{1}{15}b\xi((20\nu + 35)\xi^2 - 28\nu - 33)\tau + (L - x_1)\xi \right] \\
\Gamma_{22} &= \frac{3P\nu}{2Eb^2t} \left[\frac{2}{5}(L - x_1)(1 - 2\nu)\xi\tau^2 + \frac{4}{5}b(\nu + 1)\xi\tau + (L - x_1)\xi \right] \\
\Gamma_{12} &= \frac{3P(\nu + 1)}{4Ebt} \left[\frac{2}{5}((8\nu + 5)\xi^2 - 4\nu - 1)\tau^2 + \frac{2(L - x_1)(2\xi^2 - 1)\tau}{b} + (1 - \xi^2) \right]
\end{aligned} \tag{137}$$

From elasticity, the stress components are

$$\begin{aligned}
\sigma_{11} &= -\frac{3P}{2b^2t} \left[\frac{(b - h)\xi}{\tau} - \frac{2}{5}(b - 2h)\xi(5\xi^2 - 3)\tau \right] \\
\sigma_{22} &= -\frac{3P((b - 2h)\xi^3 + h\xi)\tau}{2b^2t} \\
\sigma_{12} &= \frac{3P}{4bt} \left[\left(6\xi^4 - \frac{24\xi^2}{5} + \frac{2}{5} \right) \tau^2 - \frac{(L - x_1)(1 - 3\xi^2)\tau}{b} + (1 - \xi^2) \right]
\end{aligned} \tag{138}$$

and the strain components are

$$\begin{aligned}
\Gamma_{11} &= -\frac{3P}{2Eb^2t} \left[\frac{(b - h)\xi}{\tau} + \left(-2b\xi^3 + 4h\xi^3 - b\nu\xi^3 + 2h\nu\xi^3 + \frac{6b\xi}{5} - \frac{12h\xi}{5} - h\nu\xi \right) \tau \right] \\
\Gamma_{22} &= \frac{3P\nu}{2Eb^2t} \left[\frac{(b - h)\xi}{\tau} \right] \\
&\quad + \frac{3P\nu}{2Eb^2t} \left[\frac{(-5b\xi^3 + 10h\xi^3 - 10b\nu\xi^3 + 20h\nu\xi^3 - 5h\xi + 6b\nu\xi - 12h\nu\xi)\tau}{5\nu} \right] \\
\Gamma_{12} &= \frac{3P(\nu + 1)}{4Ebt} \left[\frac{2}{5}(15\xi^4 - 12\xi^2 + 1)\tau^2 + \frac{(L - x_1)(3\xi^2 - 1)\tau}{b} + (1 - \xi^2) \right]
\end{aligned} \tag{139}$$

4.3 *Correlation with Numerical Beam Solutions*

The numerical VAM formulation of Chap. 2 is now applied to the linearly tapered isotropic strip. Results from the numerical VAM formulation are correlated against the analytical VAM formulation of Sec. 4.1. Back in Sec. 4.2.3, relationships between 1D stress resultants and 1D strain measures are derived for the three classical loading cases by both beam theory and elasticity theory. In the case of beam theory, these relationships involve only the generalized Timoshenko stiffnesses; therefore excellent correlation in these relationships between beam theory and elasticity theory is a validation of the derived stiffnesses. To validate the numerical VAM formulation, the calculated stiffness constants are now compared against the formulae based on analytical VAM.

The assumption of 2D plane stress elasticity means that many terms, from the general formulation of Chap. 2, may be dropped. Due to the dimensional reduction, the classical 1D strain measures are

$$\bar{\epsilon} = [\bar{\gamma}_{11} \ \bar{\kappa}_3]^T \quad (140)$$

while the 1D strain measures in a generalized Timoshenko model are

$$\epsilon = [\gamma_{11} \ \kappa_3]^T; \quad \gamma_s = [2\gamma_{12}] \quad (141)$$

The kinematic relationships between the strain measures are still given by Eq. (34), but now with

$$Q = \begin{bmatrix} 0 \\ 1 \end{bmatrix}; \quad P = \begin{bmatrix} 0 \\ 0 \end{bmatrix} \quad (142)$$

The 2nd-order asymptotically-correct and generalized Timoshenko sectional strain energies are still given by Eqs. (28) and (36), respectively, but with the modifications

that

$$\begin{aligned}
[A] &= \begin{bmatrix} A_{11} & A_{14} \\ A_{14} & A_{44} \end{bmatrix}; \quad [B] = \begin{bmatrix} B_{11} & B_{14} \\ B_{41} & B_{44} \end{bmatrix} \\
[C] &= \begin{bmatrix} C_{11} & C_{14} \\ C_{14} & C_{44} \end{bmatrix}; \quad [D] = \begin{bmatrix} D_{11} & D_{14} \\ D_{41} & D_{44} \end{bmatrix} \\
[X] &= \begin{bmatrix} X_{11} & X_{14} \\ X_{14} & X_{44} \end{bmatrix}; \quad [Y] = \begin{bmatrix} Y_{11} \\ Y_{41} \end{bmatrix}; \quad [G] = [G_{11}]
\end{aligned} \tag{143}$$

The 1D constitutive law of the generalized Timoshenko model is reduced to

$$\begin{Bmatrix} F_1 \\ M_3 \\ F_2 \end{Bmatrix} = \begin{bmatrix} X & Y \\ Y^T & G \end{bmatrix} \begin{Bmatrix} \epsilon \\ \gamma_s \end{Bmatrix} \tag{144}$$

From Sec. 4.1.1, the analytical formulae to terms in the 2nd-order asymptotically-correct stiffness matrices are

$$\begin{aligned}
A_{11} &= 2Etb \left[1 - \frac{2}{3}(1 + \nu)\tau^2 \right] \\
A_{44} &= \frac{2}{3}Etb^3 \left[1 + \frac{1}{3}(30 + 28\nu)\tau^2 \right] \\
B_{11} &= \frac{2}{3}Et\nu\tau b^2 \\
B_{44} &= -\frac{1}{9}Etb^4\tau(36 + 32\nu) \\
C_{44} &= \frac{8}{15}Etb^5(1 + \nu) \\
D_{44} &= \frac{1}{45}Etb^5(24 + 22\nu) \\
A_{14} &= B_{14} = B_{41} = C_{14} = D_{14} = D_{41} = 0
\end{aligned} \tag{145}$$

while terms of the generalized Timoshenko stiffness matrices are found from Sec. 4.1.2

to be

$$\begin{aligned}
X_{11} &= 2Et b \left(1 - \frac{2}{3} \tau^2 \right) \\
X_{44} &= \frac{2}{3} E t b^3 \left[1 + \frac{(\nu - 48)\nu - 45}{45(\nu + 1)} \tau^2 \right] \\
Y_{41} &= \frac{E t (5\nu + 3) b^2 \tau}{9(\nu + 1)} \\
G_{11} &= \frac{5Et b}{6(1 + \nu)} \\
X_{14} &= Y_{11} = 0
\end{aligned} \tag{146}$$

The equations involved in the transformation procedure to generalized Timoshenko form remain unchanged in its symbolic forms, but are reduced in dimensions. The formulae, given in Eqs (145) and (146), are the standards from which numerical results from this section are compared against.

At this point, it is worthwhile to note that the stiffness constants from Eqs. (145) and (146) do not satisfy Eq. (68), which is used by VABS. Once again, Eq. (68) is developed from a “condensation” of shear strain measures, but it is only applicable to prismatic beams. The analytical transformation procedure to generalized Timoshenko form, from which the analytical stiffness constants in Eq. (146) are derived, represents an independent source apart from the numerical transformation procedure of Sec. 2.3. And this independent source indeed validates the claim that Eq. (68) does not hold unless the beam is prismatic.

4.3.1 Asymptotically-Correct Refined Theory

The numerical solution procedure, described in Sec. 2.7, is applied to find the stiffness constants from the 2nd-order asymptotically-correct refined theory for a correlation study with results from Eq. (145). Finite element meshes are generated for nine equally-spaced sections, so that pointwise derivatives are calculated with enough accuracy that the calculated stiffness constants at the middle section would be an accurate reflection of the numerical solution procedure. Note that the finite element

meshes are generated such that, wherever possible, corresponding nodes exist between all nine meshes. Therefore, all pointwise derivatives associated with S' are identically zero as discussed in Sec. 2.7. Another implication of generating the meshes in this manner is that all pointwise derivatives, calculated from the “Global Difference 1” step from Fig. 6, are identically zero except for those which are located on the upper or lower edge (a physical boundary that is shifting along the span). Pointwise derivatives calculated from the “Global Difference 1” step are as accurate as the order of accuracy used in the derivative approximation from finite differences. Within the section with the widest width (among the nine sections), pointwise derivatives for nodes located on the upper or lower edge may not be approximated by finite differences and are therefore set to zero. Following along in the numerical procedure, $D_{R\tau}$ and D_S are calculated from Eq. (26). Having $D_{R\tau}$ and D_S then leads to finding $V_{1R\tau}$ and V_{1S} , respectively. These 1st-order warping influence coefficients are not trusted for the section with the widest width, because its pointwise derivatives at the edges are erroneously set to zero. At the adjacent section, the accuracy of 1st-order warping influence coefficients is not great, because its pointwise derivatives at the edges are approximated from a mere 1st-order backward-difference approximation in the case of a positive value of τ (or from a 1st-order forward-difference approximation in the case of $\tau < 0$). The “Global Difference 2” step is performed and then stiffness matrices A , B , C , and D are found from Eqs. (29), (30), (31), and (32), respectively. By this described procedure, the order of accuracy from the finite difference approximations should not be an issue for results at the middle section.

Figures 34, 35, 36, and 37 show the results for A_{11} , A_{44} , B_{11} , and B_{44} , respectively, as functions of τ . Normalization is especially important for these figures, because they incorporate results from strip beams of various dimensions (but always with the same material properties, including choosing $\nu = 0.3$). Figures 34 and 35 are normalized by dividing through by values which neglect the taper effect. Figures 36 and 37 are

normalized by dividing through by $2Et\nu b^2/3$ and $Et b^4(36 + 32\nu)/9$, respectively. The curves labeled “Analytical” are calculated using the formulae from Eq. (145). The data points labeled “Calculated” are calculated from Eqs. (29) and (30) through the numerical procedure. The “Calculated” points include values at $\tau = -0.10, -0.01, 0.0, 0.01$, and 0.10 . The curves labeled “Curve Fit” are from a quadratic curve fit from using only the three “Calculated” values at $\tau = -0.01, 0.0$, and 0.01 . Curves labeled “Neglect Taper” are calculated from neglecting the taper effect. The quantities A_{14} , B_{14} , and B_{41} are not shown, because they are correctly calculated to be zero. Quantities in stiffness matrices C and D are not shown, because the taper effect is not needed there for the derivation of a 2nd-order asymptotically-correct energy.

The levels of correlation between “Calculated” and “Analytical” shown are mixed. At the very least, the “Calculated” points do all exhibit the correct general behavior. The level of correlation for B_{11} is perfect while that of A_{11} may be considered acceptable. Unfortunately, the taper effect for both A_{44} and B_{44} are severely underpredicted. Nonuniformity effects are considered higher-order corrections to the prismatic case, so the significant levels of underprediction in A_{44} and B_{44} represent a failure to capture the nonuniformity effects to full satisfaction.

The source(s) to the aforementioned underprediction is not known, but some possibilities are discussed. One possibility could be that an approximation in VABS regarding the use of the classical kernel, ψ , is not good for nonuniform beams. The approximation is that ψ , which is used in minimizing the 0th-order energy, is used again as the kernel for minimizing the 2nd-order energy. Another possibility is that a mistake exists in the theory presented in Chap. 2. Another possibility is that there exist programming mistakes in implementing the theory described. Note, however, that the “Calculated” data points, at $\tau = -0.10$ and 0.10 , virtually coincide with their respective values from “Curve Fit”, as they should due to the normalization. Also,

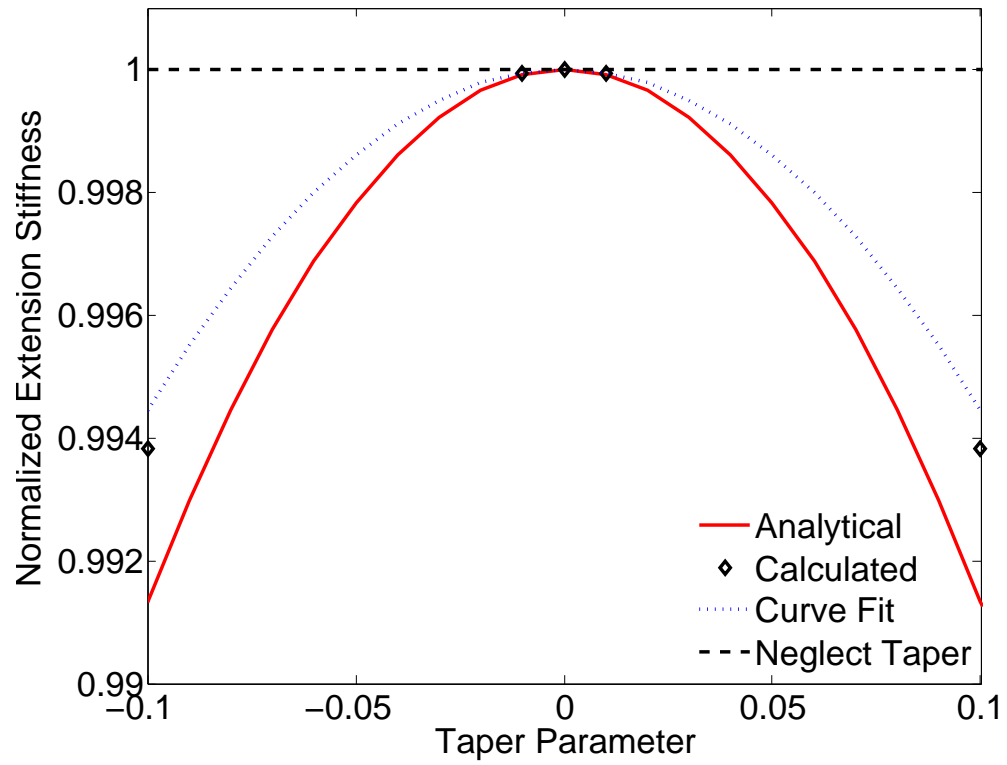


Figure 34: Normalized extension stiffness A_{11} , from the 2nd-order asymptotically-correct refined theory, $\nu = 0.3$

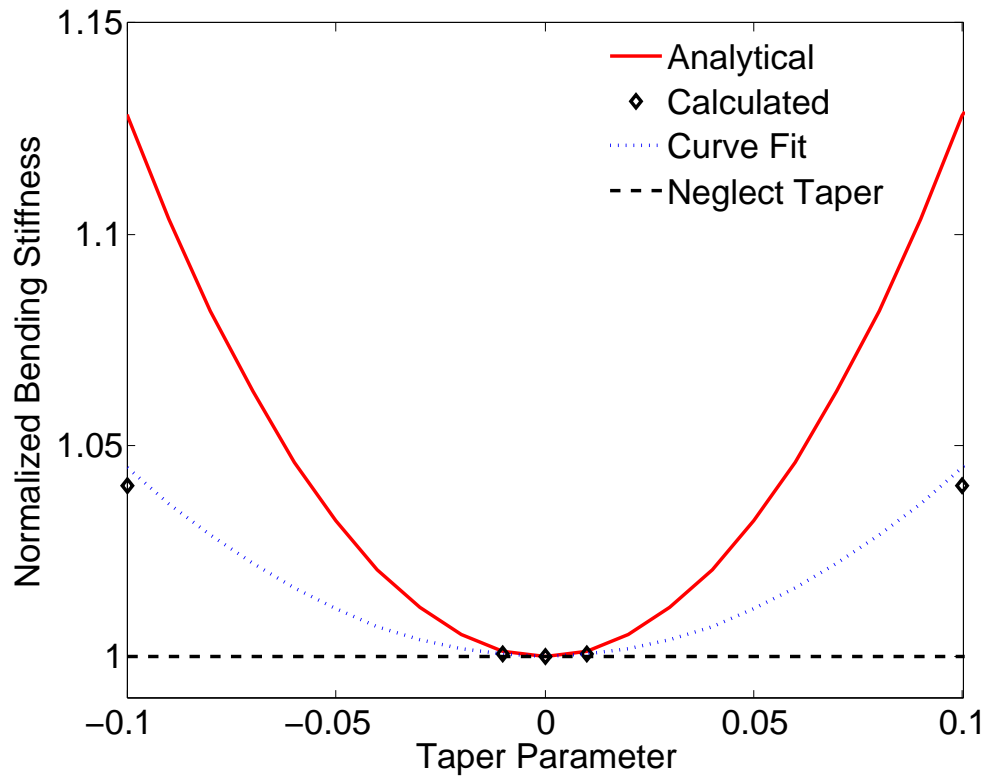


Figure 35: Normalized bending stiffness A_{44} , from the 2nd-order asymptotically-correct refined theory, $\nu = 0.3$

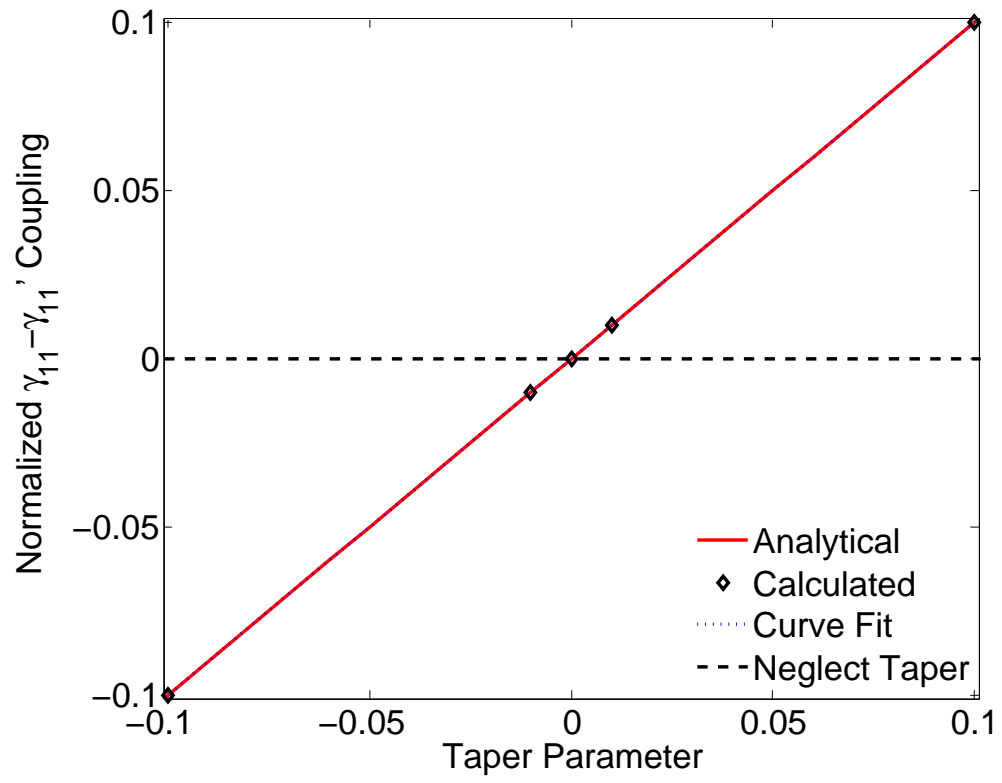


Figure 36: Normalized coupling B_{11} , between γ_{11} and γ_{11}' from the 2nd-order asymptotically-correct refined theory

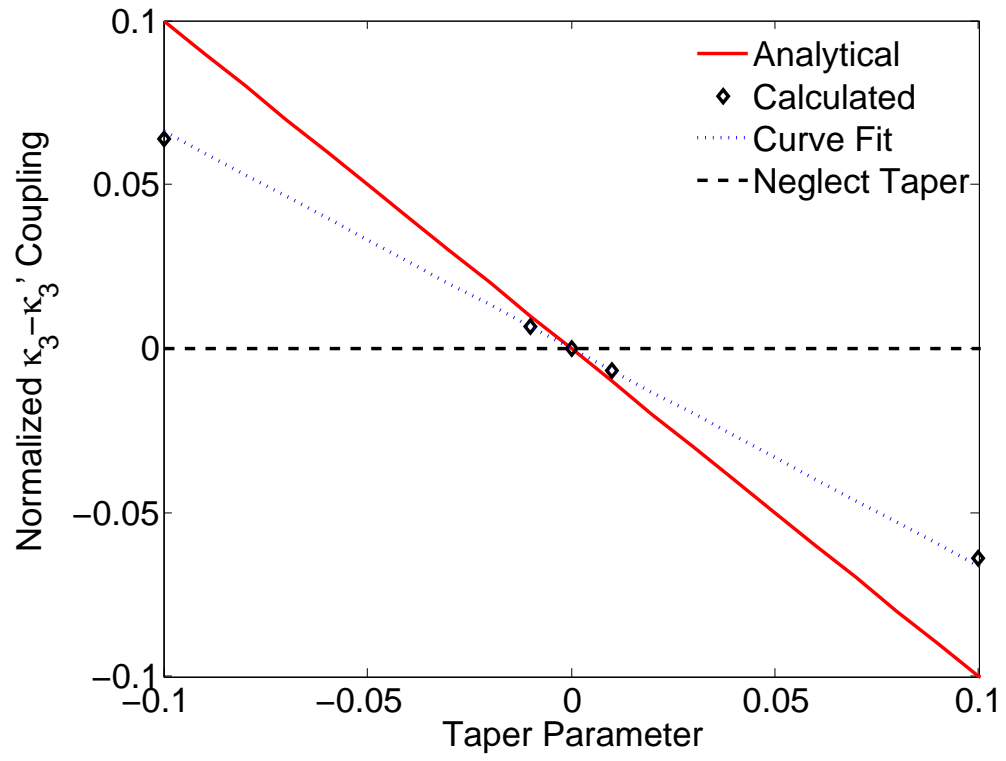


Figure 37: Normalized coupling B_{44} , between κ_3 and κ_3' from the 2nd-order asymptotically-correct refined theory

the “Calculated” data points exhibit the appropriate perfect symmetry or antisymmetry for each stiffness constant. Therefore, the chance that programming mistakes exist is significantly reduced.

The source(s) of the error is difficult to detect, because there does not exist any analytical results for comparison at intermediate steps between calculations of the stiffness matrices from the 0th-order and 2nd-order energies. In particular, analytical formulae to $D_{R\tau}$, $V_{1R\tau}$ would be especially useful but its derivations would likely require analytical formulae to the pointwise derivatives. The pointwise derivatives are difficult to calculate analytically, because they represent derivatives of integrals, whose integrand and limits of integration are all functions of the variable with which differentiation is taken with respect to. In other words, the pointwise derivatives are of the form $\frac{d}{dx_1} \left[\int \int_{g(x_1)}^{h(x_1)} F(x_1, x_2, x_3) dx_2 dx_3 \right]$. An attempt by this author to derive analytical formulae to the pointwise derivatives was unfruitful, but it may be helpful for readers interested in pursuing this task to know that the plane version of the Leibniz rule for differentiating an integral is given by Ref. [14] as

$$\frac{d}{dx_1} \left[\int \int_{A(x_1)} F(x_1, x_2, x_3) dx_2 dx_3 \right] = \int_{\partial A} F(\tau_2 dx_3 - \tau_3 dx_2) + \int \int_{A(x_1)} \frac{\partial F}{\partial x_1} dx_2 dx_3 \quad (147)$$

4.3.2 Generalized Timoshenko Beam Theory

For the sole purpose of validating the transformation procedure to generalized Timoshenko form, the reduced system of equations represented by Eq. (46) is solved while making use of the formulae to matrices A , B , C , D , and derivatives of matrices X , Y , and G from Eqs. (145) and (146). Figures 38 and 39 show the extension stiffness, X_{11} , and bending stiffness, X_{44} , as functions of the taper parameter, τ , respectively, for $\nu = 0.3$. The figures are normalized by dividing through by values which neglect the taper effect. Curves labeled “Analytical” and “Calculated” are from using Eq. (146) and from solving Eq. (46), respectively. Figure 40 shows the bending-shear coupling,

Y_{41} , as a function of τ for $\nu = 0.3$, $E = 200 \text{ GPa}$, $t = 0.1 \text{ m}$, and $b = 3 \text{ m}$. Note that the energy derived is 2nd-order. Therefore, the orders of accuracy to matrices X , Y , and G , are two, one, and zero, respectively, due to γ_s itself being a 1st-order quantity. Formulae given in Eq. (146) are found by truncation in a series expansion by discarding terms of higher order than the highest order of accuracy. To reflect this truncation in the numerical VAM results, curves shown on Figs. 38 and 39 are from a quadratic curve fit from using only the three values at $\tau = -0.01, 0.0$, and 0.01 . Meanwhile, curves shown on Fig. 40 is from a linear curve fit from using only the two values at $\tau = -0.01$ and 0.01 . The curve fit is justified, because the underlying principle of the asymptotic method is that higher-order corrections are found by an expansion about the 0th-order solution, which is the prismatic case. Results from “Analytical” and “Calculated” are visibly indistinguishable, so the numerical transformation procedure is a success. The curves labeled “Neglect Taper” represent calculated stiffnesses from neglecting the taper effect, so its departures from the other curves represent the errors from neglecting the taper effect. The “Calculated” results for X_{14} , Y_{11} , and G_{11} , which are quantities that are independent of τ , are all correctly predicted and are not shown.

Results, discussed from the previous paragraph, validate the system of equations for the transformation procedure to generalized Timoshenko form, but it does not validate the entire numerical procedure. Recall that the suggested procedure, from Sec. 2.7, approximates derivatives to the generalized Timoshenko stiffness matrices by applying finite difference formulae based on stiffness matrices while neglecting nonuniformity effects. When this 0th-order approximation to the derivatives is used, there is a deterioration in the level of correlation with analytical results. In particular, the correlation with analytical results remains visibly indistinguishable for X_{11} and Y_{41} , but the calculated results for X_{44} are significantly softer than the analytical results. Calculated results for X_{14} , Y_{11} , and G_{11} are still correctly predicted.

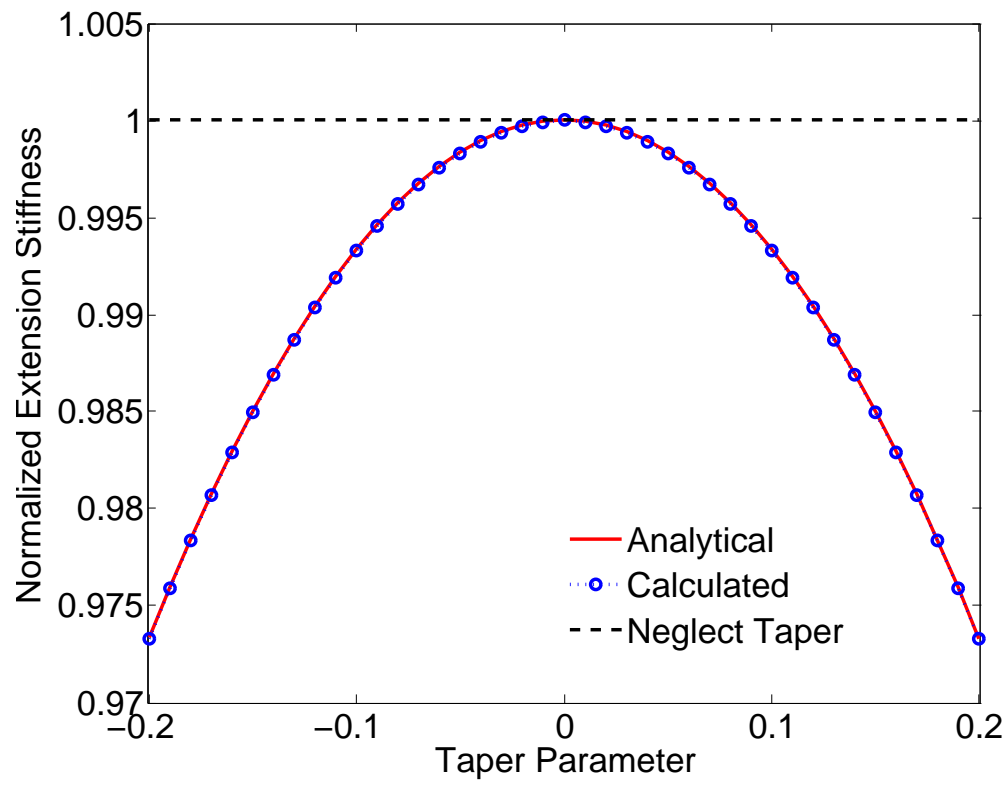


Figure 38: Generalized Timoshenko extension stiffness, isotropic tapered strip

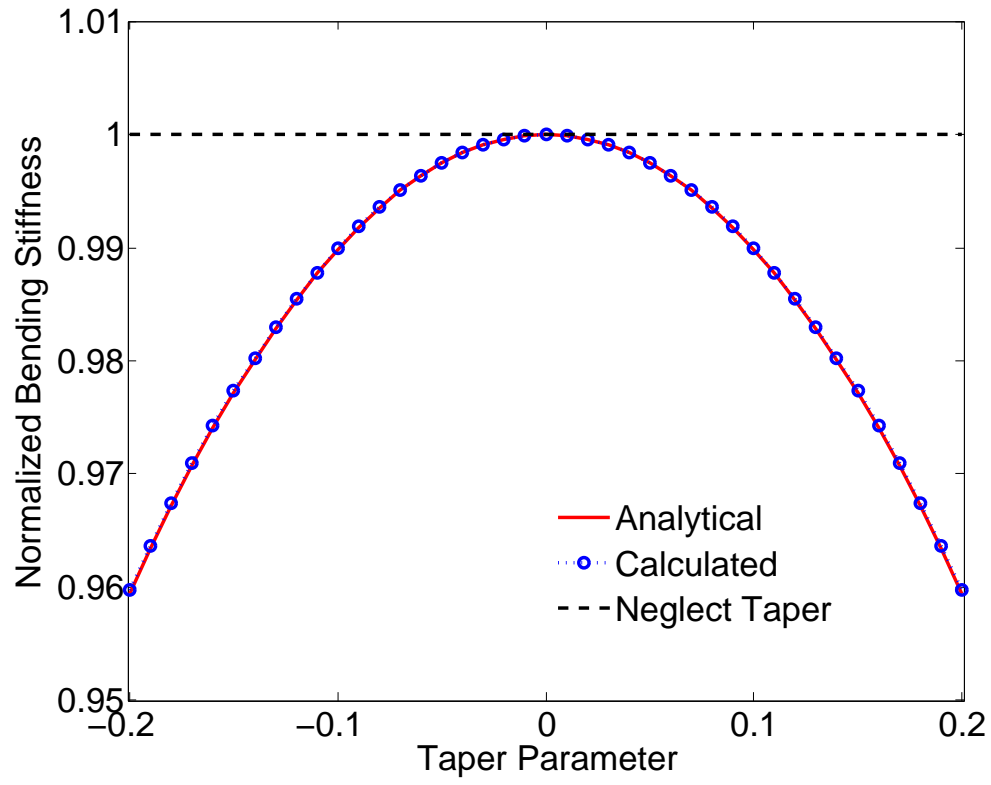


Figure 39: Generalized Timoshenko bending stiffness about the x_3 -axis, isotropic tapered strip, $\nu=0.3$

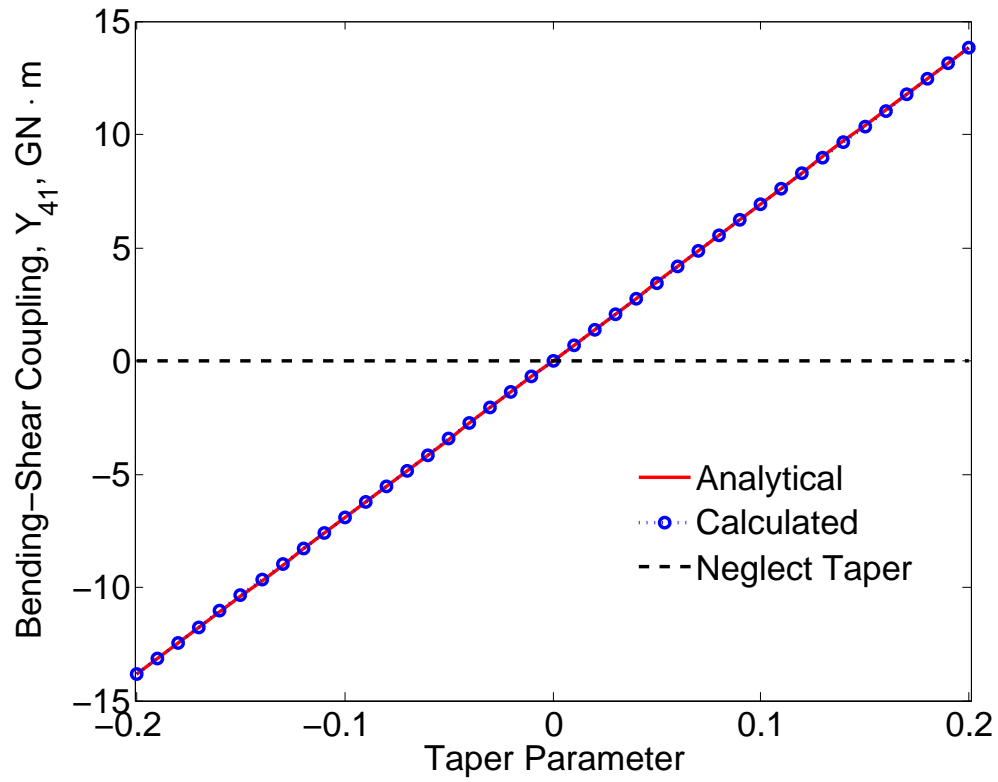


Figure 40: Generalized Timoshenko bending-shear coupling, Y_{41} , isotropic tapered strip, $\nu=0.3$

CHAPTER V

CONCLUSIONS AND RECOMMENDATIONS

The research presented in this thesis represents an attempt to extend the applicability, improve the accuracy, and further the understanding of beam theory. Its focus is on the 2D cross-sectional analysis aspect of beam theory. To be more specific, it focuses on the cross-sectional analysis of nonuniform beams and modeling of transverse shear deformations. This chapter reviews the main accomplishments, provides a reminder of issues that remain unresolved, and lists recommendations for future work.

5.1 Accomplishments

5.1.1 Nonuniform Beams of Arbitrary Cross-Sections

The theory for the cross-sectional analysis of beams, composed of arbitrary materials and geometries, is extended from all known previous works by inclusion of 3D effects due to spanwise nonuniformity. This extension from previous works is easily relevant. Rotor blades, for example, often feature regions of nonuniformity. Generality in allowance of arbitrary materials and geometries are due to usage of the finite element method. The variational-asymptotic method is applied to (1) rigorously decouple the original 3D elasticity problem into a global 1D analysis and the 2D cross-sectional analysis, (2) state the 2D cross-sectional analysis as a constrained minimization problem, and (3) solve the resulting constrained minimization problem. This results in finding an asymptotically-correct strain energy. For use with 1D analyses based on the generalized Timoshenko beam theory, the energy is transformed into the required form. Results from the 2D cross-sectional analysis include elastic stiffness constants and 3D displacement, stress, and strain fields. Unlike the case of a uniform beam, pointwise and sectionwise derivatives appear in the derivations. These derivatives are

suggested to be approximated by finite differences.

5.1.2 Modeling Transverse Shear

Approximations and one mistake in previous works (which are currently embedded in VABS), regarding the transformation of the asymptotically-correct strain energy into generalized Timoshenko form, are uncovered and corrected. One such approximation is the omission of certain terms. Results presented here for the prismatic composite box beam CUS shows that the omitted terms are not negligible. Another issue is that the solution involves an approximation (which was not previously realized to be an approximation) to solve its governing equations. Results presented here for the prismatic composite box beam CAS1 shows that the approximation is not the true solution to its equations. For uniform beams featuring initial twist and/or curvature, previous works incorrectly assume that the reduced classical stiffness matrix A_{cl} is merely the stiffness matrix A from the asymptotically-correct strain energy. It is explained that $A_{cl} \neq A$ unless the beam is prismatic. Unlike the solution from previous works, the present formulation advocates performing the transformation by iteratively solving a nonlinear system of equations. Differences in stiffness constants, between previous works and the present formulation, are shown as functions of the initial twist for the CUS section. For homogeneous sections composed of isotropic materials, differences in these results are seen as negligible for all cases examined.

Implications to the differences in stiffness calculations, between VABS prediction and the present formulation, are shown by results of the 1D global analysis. The results are the tip displacements and natural frequency calculations of a cantilevered beam, with the CUS cross-section, under uniformly distributed loading. These results are plotted as functions of the initial twist and differences in results are noted.

Calculations for initially twisted beams are shown (possibly for the first time) to be equivalent regardless if the calculations are performed with coordinate axes that

are initially twisted or not. Physically, the previous statement must be true. The demonstration here provides an indication that effects from initial twist embedded in the 2D cross-sectional analysis and 1D global analysis are correctly implemented. The beam analyzed is a cantilevered beam, with an isotropic rectangular cross-section, under uniformly distributed loading.

5.1.3 Linearly Tapered Isotropic Strip

A beam model is constructed using the variational-asymptotic method in analytical form. The beam model is capable of handling extension, in-plane bending, and in-plane shear for a homogeneous, isotropic strip beam. The width of the beam is linearly tapered along the length. The resulting beam model reveals that (1) stiffness constants are influenced by the local taper such that $b'(x) = -\tau$ appears explicitly; and (2) bending and shear deformations are coupled by τ in the resulting model. Solutions for three plane stress elasticity problems are presented and the corrections caused by $\tau \neq 0$ are found. The three plane stress elasticity problems are cases where the loading is applied such that the internal axial force, bending moment, or shear force is constant along the span. Excellent agreement, in predictions to the beam displacement and rotation variables, is demonstrated between the elasticity solutions and the beam solutions based on the constructed model. This excellent agreement validates the stiffness constants derived by the beam model.

Examples of the taper influence include a decrease in both extension and bending stiffnesses, the latter being large enough that its neglect cannot be justified for tapered beams. To avoid errors, the taper effect must be accounted for in the cross-sectional analysis prior to performing the beam analysis.

Correlations, between the elasticity solutions and beam solutions, in the recovery relations are also shown for the three loading cases. By comparison with the elasticity solutions, the recovered stress and strain fields from the beam theory solutions are

declared accurate up to the expected orders of accuracy (in terms of small parameters of the problem). As with the stiffness constants, the influence of taper appears explicitly. In addition, the recovered stress field from beam theory satisfies the traction boundary conditions up to 1st-order.

The nonlinear system of equations, for transforming the 2nd-order asymptotically-correct energy into generalized Timoshenko form from the numerical approach, is also validated for this tapered strip beam. Using the validated stiffness constants from the analytical beam theory solution as a benchmark, the calculated stiffness constants from iteratively solving the nonlinear system of equations are validated. Unlike previous cases of transforming to generalized Timoshenko form, this case is the first involving nonuniformity effects in its transformation.

5.2 Unresolved Issues

5.2.1 Nonuniform Beams of Arbitrary Cross-Sections

Two particular issues stand out in the modeling of spanwise nonuniformity effects for beams of arbitrary cross-sections. Both issues became evident in the case of the linearly tapered isotropic strip beam. The first issue is that components from the numerically calculated A and B , which are the stiffness matrices from the asymptotically-correct theory that exhibit nonuniformity effects, do not correlate well enough with those that are analytically derived. The influence of nonuniformity effects on A and B are correctly predicted by the numerical approach, but they are severely under-predicted in quantities A_{11} , A_{44} and B_{44} . The second issue is that the numerical procedure to attain generalized Timoshenko stiffness matrices did not yield satisfactory results. The nonlinear system of equations, for the transformation, itself is successfully validated; however, the validation involved using the analytically derived derivatives to stiffness matrices X , Y , and G . When the transformation is attempted without prior knowledge of these derivative matrices, i.e. calculating them

by finite difference approximations while neglecting nonuniformity effects, the calculated results show the correct trend from nonuniformity effects but are again severely underpredicted. Due to these two issues, this author sadly concludes that the ultimate goal of providing a cross-sectional analysis tool that correctly models spanwise nonuniformity effects is not achieved.

Aside from its lack of accuracy, the numerical procedure is impractical. The procedure shown in Fig. 6 involves numerous steps and is considerably more complicated than conventional cross-sectional analysis tools. Furthermore, decisions on how to apply the finite difference approximations to calculating pointwise derivatives are not trivial. The entire procedure is so cumbersome to apply that the original motivation for using beam theory is lost.

5.2.2 Modeling Transverse Shear

The system of equations for transformation to generalized Timoshenko form may be corrected, but difficulties remain in solving the system of equations. The transformation procedure does not guarantee the existence of a unique solution. For prismatic beams, the experience of this author is that a solution is always found for isotropic beams and it always agrees with the VABS solution. On the other hand, a solution is only found in roughly half of the cases (many of these attempts are not documented here) for prismatic beams composed of composite materials. For uniform beams having initial twist but no curvatures, a solution is always found in cases where the prismatic solution is found. For beams featuring initial curvature, no solution to the system of equations has been found. Cross-sectional analysis tools must be able to consistently find the generalized Timoshenko stiffness constants, so this is a serious matter. If it is allowed that the solution may be a mere approximation such as a least squares approximation, then it may be possible to find analytical formulae to the solution with help from the perturbation method.

5.3 *Recommendations for Future Work*

5.3.1 Nonuniform Beams of Arbitrary Cross-Sections

Results presented here for the linearly tapered isotropic strip beam demonstrate that nonuniformity effects are not negligible if the sections vary at a high enough rate along the span, so the need for a general cross-sectional analysis tool that properly models spanwise nonuniformity persists. If this author did not make any mistakes either in derivation or programming, then another approach to modeling spanwise nonuniformity is needed.

Without utterly abandoning the approach here, an alternative would be to reformulate the work shown here by using a curvilinear coordinate system that follows the varying nature of the cross-sections. Assuming that the cross-section is not at a location of spanwise discontinuity, e.g. ends of the beam or at a point of discontinuity in a step-beam, then each point in the structure (that follows such a coordinate system) must be varying smoothly along x_1 such that a corresponding point can be identified. For a point located on a type of physical boundary surface, e.g. the edge of the cross-section or the edge of a single ply, its corresponding point at a different x_1 location is found by following the direction of the instantaneous tangent vector to the surface until the desired x_1 is reached. For points located off the boundary, one may imagine interior surfaces and follow along the direction defined by instantaneous covariant base vectors until the desired x_1 is reached. This alternative approach has the advantage (over the approach from this thesis) that all finite element nodes have corresponding nodes at nearby sections. Therefore, the issue (from this thesis) that pointwise derivatives are undefined for nodes located on a spanwise boundary is eliminated. The disadvantage of this approach is that for beams composed of complicated geometries and multiple materials, such as realistic rotor blades, it may be difficult to determine the location of corresponding nodes from nearby sections.

Regardless of the approach, any cross-sectional analysis that models spanwise

nonuniformity must be validated against the results here for the linearly tapered isotropic strip. As stated already, stiffness constants from the analytical beam solution in this thesis represents a benchmark for validation. Stress, strain, and displacement fields should be validated against the elasticity solutions.

5.3.2 Solutions to Linearly Tapered Beams

In addition to having the analytical beam theory solution to the linearly tapered isotropic strip, it would also be useful to have solutions to other linearly tapered beams. Solutions to linearly tapered beams are suggested to be most useful among nonuniform beams, because their behaviors are likely governed by a finite set of taper parameters and thus can be interpreted more easily. For beams that are doubly-tapered so that the variation in the location of all sectional boundary points may be described by two taper parameters, it may even be possible to incorporate the higher-order corrections from these two parameters into VABS for sections of arbitrary materials and geometries in the same manner that corrections from k_1 , k_2 , and k_3 are implemented. This author still believes that it would be a daunting challenge to correctly solve the problem of doubly-tapered beams for arbitrary cross-sections, but it would not be so daunting for beams composed of simple cross-sections such as a beam with homogeneous elliptical sections. For a beam with such a simple geometry, the solution may be most easily derived analytically. It would also be of tremendous value to have an analytical solution to linearly tapered strip beams composed of composite materials.

5.3.3 Modeling Transverse Shear

To address the issue that the trust-region dogleg method from “fsolve” does not consistently find a solution, to the system of equations for transformation to generalized Timoshenko form, further work in this area is warranted. This author has tried the Newton-Raphson and Broyden methods as given in Ref. [37] and found both to be

far less effective than the trust-region dogleg method from “fsolve”. Other iterative methods should be considered in search of a more robust solver. Other available algorithms available in “fsolve” are the Gauss-Newton method [21], the Levenberg-Marquardt method (see Refs. [27] and [28]), and a “large-scale algorithm” that is “a subspace trust-region method and is based on the interior-reflective Newton method” (see Refs. [9] and [10]). Homotopy methods [22], which belong to the family of continuation methods, are known for being globally convergent and should also be tried. It may also be worthwhile to consider relaxing the requirements of finding a true solution and merely settle for an approximation, which would ideally be derived in analytical form and might also make use of the perturbation method.

The excellent correlation, between predictions by the Matlab solver and NABSA, from the prismatic CUS section is unexpected. The results are shown in Table (3). The theory on which NABSA is based upon is not from asymptotic considerations. There does not seem to be any reason why results based on an asymptotic methodology, which the theory presented in this thesis certainly falls under, should agree with NABSA. It would enhance the understanding of cross-sectional analysis in general to understand why the level of correlation is as good as shown.

A validation study of initially twisted beams with the CUS section should be conducted. Recall that predictions to the generalized Timoshenko stiffness constants differed significantly, between the Matlab solver and VABS solution, for the CUS section as initial twist is varied. A form of validation study by beam theory may be conducted by comparing calculations from a 1D global analysis between coordinate axes featuring initial twist and not featuring one (as is done in this thesis for initially twisted beams with an isotropic rectangular cross-section). If the stiffness constants used are correct, then results from the 1D global analysis should not depend on the choice of coordinate axes and the stiffness constants would be somewhat validated.

5.3.4 Transition Elements

An alternative to modeling spanwise nonuniform beam-like structures is by a combination of 3D finite elements, 1D beam elements, and transition elements. This hybrid approach is a tradeoff that ideally combines the efficiency of beam theory with the accuracy of 3D finite elements. This approach would model the nonuniform regions of the beam-like structure with 3D finite elements and uniform regions by 1D beam elements. Transition elements exist as a connection between the 3D elements and 1D elements to help preserve accuracy. Transition elements seem to hold great potential, but are still very much in development.

5.3.5 Recovery Relations

A conundrum exists regarding the need to incorporate the 1D distributed applied and inertial loading terms, ϕ , to recover the 3D displacement, stress, and strain fields. As explained in Sec. 2.5, these terms are needed for the recovery to be sufficiently accurate. The recovery relations also make use of the internal stress resultants, F_R , which are found by a balance of forces and moments at each section during the 1D global analysis. The effects of ϕ are embedded within the calculations of F_R , so it would seem that incorporating both ϕ and F_R in the recovery relations is redundant and possibly inconsistent. The puzzle that remains unanswered is then why ϕ is needed in the relations if it is already embedded within F_R ? The same conundrum also exists for plate theory [56] and shell theory [55].

5.3.6 Validation Needs

The ultimate form of validation on beam theory analysis is with solutions to the full 3D elasticity equations, which would most certainly come from 3D finite element analysis except for the simplest of cases. Quantities of comparison would be the stress, strain, and displacement fields. Beam theory seems to be well-validated for prismatic beams composed of isotropic materials, but it should be evident from the material

presented here that there still seems to be a lack of validation for composite beams. Even more limited are validations of beams featuring initial twist and/or curvature.

The state-of-the-art on 1D global beam analysis is a set of equations that is geometrically-exact with seemingly no flaws, which means that errors in predictions from the 1D global analysis likely originate from inaccurate stiffness constants. As seen in Fig. 24 for the cantilevered beam with CUS sections, frequency predictions for the third and fifth modes differ dramatically even in the prismatic case when using two different sets of stiffness constants. Due to this difference, it seems that beams with the CUS section are prime candidates for validation by 3D finite element analysis.

5.3.7 Nonuniform Plates and Shells

In an analogous manner to the present work on modeling spanwise nonuniformity in beam theory, one may attempt to model geometric nonuniformity in plate and shell theories. Plate and shell analyses involve a 2D global analysis. Elastic stiffness constants to the global analysis are found from a complementary 1D through-the-thickness analysis. As an example, a homogeneous plate-like or shell-like structure may have a varying thickness. Therefore, it is conceivable that geometric nonuniformity effects may alter the stiffness constants if the thickness is varying at a high enough rate along either of the two dominant dimensions.

APPENDIX A

3D STRAIN FIELD FORMULATION

The derivations to the 3D strain field are presented here. In the undeformed state, Wempner [51] defines the covariant base vectors as

$$\mathbf{g}_i(x_j) = \frac{\partial \hat{\mathbf{r}}}{\partial x_i} \quad (148)$$

Wempner also defines the contravariant base vectors as

$$\mathbf{g}^i(x_l) = \frac{e_{ijk} \mathbf{g}_j \times \mathbf{g}_k}{2\sqrt{g}} \quad (149)$$

where g is the determinant of the metric tensor and e_{ijk} are components of the permutation tensor in a Cartesian coordinate system. The metric tensor mentioned is taken in the undeformed state and its determinant is given by

$$g = \det(\mathbf{g}_i \cdot \mathbf{g}_j) \quad (150)$$

For the present problem, it is helpful to note that

$$\sqrt{g} = 1 - x_2 k_3 + x_3 k_2 \quad (151)$$

Any 3D continuum can be thought of as being composed of a network of smooth curves and surfaces. With our choice of coordinates, the vectors \mathbf{g}_i and \mathbf{g}^i are tangent to and normal to the undeformed coordinate curves, respectively. In the words of Yu [53], “When the structure is deformed due to loading, the material point which was previously specified by $\hat{\mathbf{r}}(x_i)$ has now the position vector $\hat{\mathbf{R}}(x_i)$ relative to the same fixed point. The covariant base vectors for the same coordinate system x_i in the deformed configuration are:

$$\mathbf{G}_i(x_j) = \frac{\partial \hat{\mathbf{R}}}{\partial x_i} \quad (152)$$

Now one should be able to obtain all the information of deformation by \mathbf{g}_i and \mathbf{G}_i .” Following a derivation that has been in use as early as 1992 [19] and involves using the polar decomposition theorem [12], the components of the deformation gradient in mixed-basis \mathbf{B}_i and \mathbf{b}_i , while assuming small local rotation, are given as

$$\chi_{ij} = (\mathbf{B}_i \cdot \mathbf{G}_k)(\mathbf{g}^k \cdot \mathbf{b}_j) \quad (153)$$

The Jauman-Biot-Cauchy strain components for small local rotation can now be calculated by

$$\Gamma_{ij} = \frac{\chi_{ij} + \chi_{ji}}{2} - \delta_{ij} \quad (154)$$

In order to form a connection between the 2D cross-sectional analysis and the 1D global analysis, 1D generalized strain measures are introduced. These 1D strain measures are the force strains, γ , and the moment strains, κ . They are defined as

$$\gamma = \underline{\mathbf{C}}^{bB} \cdot \mathbf{R}' - \mathbf{r}' \quad (155)$$

$$\kappa = \underline{\mathbf{C}}^{bB} \cdot \mathbf{K} - \mathbf{k} \quad (156)$$

where

$$\gamma = [\gamma_{11} \ 2\gamma_{12} \ 2\gamma_{13}]^T \quad (157)$$

$$\kappa = [\kappa_1 \ \kappa_2 \ \kappa_3]^T \quad (158)$$

and $\underline{\mathbf{C}}^{bB}$ and \mathbf{K} are defined so that

$$\mathbf{b}_i = \underline{\mathbf{C}}^{bB} \cdot \mathbf{B}_i \quad (159)$$

$$\mathbf{B}'_i = \mathbf{K} \times \mathbf{B}_i = e_{sij} K_s \mathbf{B}_j \quad (160)$$

Components of the force strains and moment strains are conjugates of the section forces and section moments, respectively. γ_{11} is the extensional strain measure, $2\gamma_{1\alpha}$ are shear strain measures, κ_1 is the torsional strain measure, and κ_α are bending strain measures. \mathbf{K} is the curvature vector of the deformed beam. Similar to \mathbf{K} ,

the kinematics dictate that beams featuring initial twist and curvatures form the relationship

$$\mathbf{b}'_i = \mathbf{k} \times \mathbf{b}_i = e_{sij} k_s \mathbf{b}_j \quad (161)$$

$\underline{\mathbf{C}}^{bB}$ is the inverse of the global rotation tensor $\underline{\mathbf{C}}^{Bb}$, which relates vectors \mathbf{B}_i and \mathbf{b}_i by

$$\underline{\mathbf{C}}^{Bb} = \mathbf{B}_i \mathbf{b}_i \quad (162)$$

The rotation tensor $\underline{\mathbf{C}}^{Bb}$ is chosen here so that \mathbf{B}_i coincides with \mathbf{b}_i in the case of zero deformation.

An approximation is now introduced to linearize the 2D cross-sectional analysis. Upon deriving the 3D strain field, products of warping and 1D strain measures are discarded. The justification is that both of these quantities are considered small in comparison with unity. Therefore, product terms are negligible.

At this point, the terms $2\gamma_{12}$ and $2\gamma_{13}$, which represent transverse shear strain measures, are dropped in the ensuing derivations. This simplification is made, because the goal of this appendix is to derive the 3D strain field for use with classical beam theory.

Upon following the steps outlined here, one may derive the linearized 3D strain field. The final form is given in Eq. (5).

APPENDIX B

CONSTRAINTS ON WARPING

Constraints on the warping field are explained here, so that the 2D cross-sectional analysis may be properly posed. A fundamental idea of the current procedure is that the 1D global and 2D cross-sectional analyses are decoupled from one another, so results from the 1D analysis are merely inputs into the 2D analysis. From the perspective of a single cross-section, the translations and rotations of the reference line are felt as rigid-body modes. Without considering transverse shear deformations, the reference line is only allowed to extend, twist, and bend in two directions; therefore each section has four rigid-body modes which cannot contribute to the sectional strain energy. Four constraints on the warping field are then required for a unique solution.

The four chosen constraints are given mathematically in Eq. (11). The first three rows mean that the average warping displacements over the cross-section are zero, which are explicitly given by

$$\langle w_i \rangle = 0 \quad (163)$$

The fourth row is a condition related to twisting and is explicitly written as

$$\left\langle \frac{\partial w_2}{\partial x_3} - \frac{\partial w_3}{\partial x_2} \right\rangle = 0 \quad (164)$$

APPENDIX C

SOLVING CLASSICAL BEAM THEORY

This section solves the 0th-order theory by finding the warping field, which minimizes the energy functional subject to the constraints from Eq. (17). The functional, from Eq. (18), is written once more as

$$2U_0 = V^T E V + 2V^T D_{a\epsilon} \bar{\epsilon} + \bar{\epsilon}^T D_{\epsilon\epsilon} \bar{\epsilon} \quad (165)$$

and the constraints, from Eq. (17), are also written again as

$$V^T D_c = 0 \quad (166)$$

Some properties are established before the 0th-order theory can be solved. First, the operator matrix Γ_a has a kernel, which implies that $\Gamma_a w = 0$ must be true for a nontrivial warping field. Now define ψ as the kernel matrix of Γ_a and it may be found as

$$\psi = \begin{bmatrix} 1 & 0 & 0 & 0 \\ 0 & 1 & 0 & -x_3 \\ 0 & 0 & 1 & x_2 \end{bmatrix} \quad (167)$$

Expressing the kernel matrix ψ in terms of its nodal value Ψ results in

$$\psi = S\Psi \quad (168)$$

It is now clear that $\Gamma_a \psi = \Gamma_a S\Psi = 0$, so that $E\Psi = 0$. Therefore, Ψ is the kernel matrix of E .

The derivation to the solution of 0th-order theory may now resume. Define Λ to be Lagrange multipliers corresponding to the constraints on the warping. $2U_0$ is minimized by setting its first variation, including the Lagrange multiplier terms, with

respect to the unknown warping functions to be zero. The resulting Euler-Lagrange equation is

$$EV + D_{a\epsilon}\bar{\epsilon} = D_c\Lambda \quad (169)$$

Solving this equation for Λ , while bearing in mind that $E\Psi = \Psi^T E = 0$, yields

$$\Lambda = (\Psi^T D_c)^{-1} \Psi^T D_{a\epsilon} \bar{\epsilon} \quad (170)$$

The result of substituting Eq. (170) into Eq. (169), while using the property $\Psi^T D_{a\epsilon} = \left\langle \left\langle [\Gamma_a S \Psi]^T D \Gamma_\epsilon \right\rangle \right\rangle = 0$, is that

$$EV = -D_{a\epsilon} \bar{\epsilon} \quad (171)$$

The right-hand side of the above equation is orthogonal to the null space, thus there is a unique solution that is linearly independent of the null space of E . By introducing the warping constraints, the singularities of the above coefficient matrix are eliminated and a solution V^* can be found. The complete solution is

$$V = V^* + \Psi\lambda \quad (172)$$

where λ is determined from Eq. (166) as

$$\lambda = -(\Psi^T D_c)^{-T} D_c^T V^* \quad (173)$$

The 0th-order warping field, which minimizes Eq. (165) subject to Eq. (166), is

$$V = [\Delta_3 - \Psi(\Psi^T D_c)^{-T} D_c^T] V^* = V_0 = \hat{V}_0 \epsilon \quad (174)$$

Warping is now in terms of the classical strain measures, which is the desired form. \hat{V}_0 is referred to as the 0th-order warping influence coefficient.

APPENDIX D

TRANSFORMATION TO FIND THE REDUCED CLASSICAL STIFFNESS MATRIX

The transformation, of the 2nd-order asymptotically-correct energy to classical beam theory form, is accomplished by the 1D constitutive law and the 1D static equilibrium equations. Using the reduced classical stiffness matrix in classical beam theory gives twice the sectional strain energy as

$$2U = \bar{\epsilon}^T A_{cl} \bar{\epsilon} \quad (175)$$

The 1D constitutive law is then

$$\begin{Bmatrix} \bar{F}_1 \\ \bar{M}_1 \\ \bar{M}_2 \\ \bar{M}_3 \end{Bmatrix} = [A_{cl}] \{\bar{\epsilon}\} \quad (176)$$

It is helpful to introduce matrix \bar{R}_{cl} as the flexibility matrix so that

$$[\bar{R}_{cl}][A_{cl}] = \Delta_4 \quad (177)$$

where Δ_4 is the identity matrix of order four. Substituting the 1D constitutive law into the linearized 1D static equilibrium equations, then the first four rows of the equilibrium equations from Eq. (40) become

$$[A_{cl}]' \{\bar{\epsilon}\} + [A_{cl}] \{\bar{\epsilon}\}' + [D_3][A_{cl}] \{\bar{\epsilon}\} + [D_4] \begin{Bmatrix} \bar{F}_2 \\ \bar{F}_3 \end{Bmatrix} = 0 \quad (178)$$

Rearranging the above equation, the first derivative of the classical strain measures may be written as

$$\{\bar{\epsilon}\}' = - \left[\bar{R}_{cl} \right] \left[\left[A_{cl} \right]' + \left[D_3 \right] \left[A_{cl} \right] \right] \{\bar{\epsilon}\} - \left[\bar{R}_{cl} \right] \left[D_4 \right] \begin{Bmatrix} \bar{F}_2 \\ \bar{F}_3 \end{Bmatrix} \quad (179)$$

Now taking the derivative of the 1D constitutive law yields

$$\begin{Bmatrix} \bar{F}_1 \\ \bar{M}_1 \\ \bar{M}_2 \\ \bar{M}_3 \end{Bmatrix}' = \left[A_{cl} \right]' \{\bar{\epsilon}\} + \left[A_{cl} \right] \{\bar{\epsilon}\}' \quad (180)$$

The last two rows from the above equation may be written as

$$\begin{Bmatrix} \bar{M}_2 \\ \bar{M}_3 \end{Bmatrix}' = \begin{bmatrix} A_{cl3:} \\ A_{cl4:} \end{bmatrix}' \{\bar{\epsilon}\} + \begin{bmatrix} A_{cl3:} \\ A_{cl4:} \end{bmatrix} \{\bar{\epsilon}\}' \quad (181)$$

where

$$\begin{aligned} \begin{bmatrix} A_{cl3:} \end{bmatrix} &= [A_{cl}(3, 1) \quad A_{cl}(3, 2) \quad A_{cl}(3, 3) \quad A_{cl}(3, 4)] \\ \begin{bmatrix} A_{cl4:} \end{bmatrix} &= [A_{cl}(4, 1) \quad A_{cl}(4, 2) \quad A_{cl}(4, 3) \quad A_{cl}(4, 4)] \end{aligned} \quad (182)$$

The last two rows from the 1D equilibrium equations, again from Eq. (40), may be written as

$$\begin{Bmatrix} \bar{M}_2 \\ \bar{M}_3 \end{Bmatrix}' + \begin{Bmatrix} k_3 \bar{M}_1 - k_1 \bar{M}_3 - \bar{F}_3 \\ -k_2 \bar{M}_1 + k_1 \bar{M}_2 + \bar{F}_2 \end{Bmatrix} = 0 \quad (183)$$

The above equation may be rewritten as

$$\begin{Bmatrix} \bar{F}_2 \\ \bar{F}_3 \end{Bmatrix} = \left[D_{3L} \right] \{\bar{\epsilon}\} + \begin{Bmatrix} -\bar{M}_3' \\ \bar{M}_2' \end{Bmatrix} \quad (184)$$

where

$$\left[D_{3L} \right] = \begin{bmatrix} 0 & k_2 & -k_1 & 0 \\ 0 & k_3 & 0 & -k_1 \end{bmatrix} \quad (185)$$

Now substituting Eqs. (181) and (184) into Eq. (179), the first derivative of the classical strain measures may be written in terms of the classical strain measures as

$$\{\bar{\epsilon}\}' = -[Z] \{\bar{\epsilon}\} \quad (186)$$

where

$$[Z] = \left[\begin{bmatrix} \Delta_4 \end{bmatrix} + \begin{bmatrix} \bar{R}_{cl} \end{bmatrix} \begin{bmatrix} D_4 \end{bmatrix} \begin{bmatrix} -A_{cl4:} \\ A_{cl3:} \end{bmatrix} \right]^{-1} \begin{bmatrix} \bar{R}_{cl} \end{bmatrix} \begin{bmatrix} Z_{post} \end{bmatrix} \quad (187)$$

and

$$\begin{bmatrix} Z_{post} \end{bmatrix} = \left[\begin{bmatrix} A_{cl} \end{bmatrix}' + \begin{bmatrix} D_3 \end{bmatrix} \begin{bmatrix} A_{cl} \end{bmatrix} + \begin{bmatrix} D_4 \end{bmatrix} \left[\begin{bmatrix} D_{3L} \end{bmatrix} + \begin{bmatrix} -A_{cl4:} \\ A_{cl3:} \end{bmatrix}' \right] \right] \quad (188)$$

Taking the derivative results in

$$\{\bar{\epsilon}\}'' = [Z_2] \{\bar{\epsilon}\} \quad (189)$$

where

$$[Z_2] = [Z]^2 - [Z]' \quad (190)$$

and

$$\begin{aligned} [Z]' &= \left[\begin{bmatrix} \Delta_4 \end{bmatrix} + \begin{bmatrix} \bar{R}_{cl} \end{bmatrix} \begin{bmatrix} D_4 \end{bmatrix} \begin{bmatrix} -A_{cl4:} \\ A_{cl3:} \end{bmatrix} \right]^{-1} \begin{bmatrix} \bar{R}_{cl} \end{bmatrix} \begin{bmatrix} Z_{post} \end{bmatrix} \\ &+ \left[\begin{bmatrix} \Delta_4 \end{bmatrix} + \begin{bmatrix} \bar{R}_{cl} \end{bmatrix} \begin{bmatrix} D_4 \end{bmatrix} \begin{bmatrix} -A_{cl4:} \\ A_{cl3:} \end{bmatrix} \right]^{-1} \begin{bmatrix} \bar{R}_{cl} \end{bmatrix}' \begin{bmatrix} Z_{post} \end{bmatrix} \\ &+ \left[\begin{bmatrix} \Delta_4 \end{bmatrix} + \begin{bmatrix} \bar{R}_{cl} \end{bmatrix} \begin{bmatrix} D_4 \end{bmatrix} \begin{bmatrix} -A_{cl4:} \\ A_{cl3:} \end{bmatrix} \right]^{-1} \begin{bmatrix} \bar{R}_{cl} \end{bmatrix} \begin{bmatrix} Z_{post} \end{bmatrix}' \end{aligned} \quad (191)$$

The first and second derivatives of the classical strain measures are now in terms of the classical strain measures, so an expression for A_{cl} may be found. This is done by equating Eq. (28) with Eq. (175). In general, the result is a system of nonlinear 2nd-order ODEs in terms of the unknown reduced classical stiffness matrix A_{cl} .

The resulting system of equations may be written as

$$A_{c\ell} = A_{c\ell}^A + A_{c\ell}^B + A_{c\ell}^C + A_{c\ell}^D \quad (192)$$

where the superscript indicates the source of the contribution. For example, $A_{c\ell}^A$ represents the contribution to $A_{c\ell}$ from stiffness matrix A . These individual contributions may be written as

$$A_{c\ell}^A = A; \quad A_{c\ell}^B = -2B[Z]; \quad A_{c\ell}^C = [Z]^T C[Z]; \quad A_{c\ell}^D = 2D[Z_2] \quad (193)$$

What is presented here may seem like a plausible way to find the reduced classical stiffness matrix from having knowledge of the 2nd-order asymptotically-correct stiffness matrices, but it does not work in practice. The cause of the issue is slightly different between prismatic beams and beams that are not prismatic.

The transformation procedure shown here is not valid for prismatic beams. A key to the transformation is establishing a relationship between the classical strain measures and its own derivative. If one follows the derivation while ignoring geometric correction terms from spanwise nonuniformity, initial twist, and initial curvatures, then it would be clear that such a relationship cannot be established and the transformation procedure breaks down. Not that its derivation is valid, but using the results from Eqs. (186) and (187) lead to $\bar{\epsilon}' = 0$ and $[Z] = 0$. It is not surprising that $\bar{\epsilon}' = 0$, because this relationship is established from the 1D static equilibrium equations with applied loads set to zero. Having $\bar{\epsilon}' = 0$, Eqs. (189) and (190) then naturally lead to $[Z_2] = 0$ and $\bar{\epsilon}'' = 0$. Note that the final result of this invalid transformation is that $A_{c\ell} = A$, which is actually a correct statement that is shown to be true from the “condensation” of shear strain measures. If this transformation is valid (which it is not), then it would serve as a confirmation that the relationship $A_{c\ell} = A$ is indeed true.

For beams that are not prismatic, the $[Z]$ matrix involves an inverse of a matrix. This matrix, whose inverse is needed, is actually singular if $k_2 = k_3 = 0$ and it is

nearly singular even with nonzero values of k_2 and k_3 . For cases examined by this author, even increasing the values of k_2 and k_3 does not help resolve this issue. This issue could be a sign that there is a fundamental problem with the transformation procedure shown.

REFERENCES

- [1] ANDRADE, A. and CAMOTIM, D., “Lateral-torsional buckling of singly symmetric tapered beams: Theory and applications,” *Journal of Engineering Mechanics*, vol. 131, no. 6, pp. 586–597, 2005.
- [2] BANERJEE, J. R. and WILLIAMS, F. W., “Exact Bernoulli-Euler static stiffness matrix for a range of tapered beam columns,” *International Journal for Numerical Methods in Engineering*, vol. 23, no. 9, pp. 1615–1628, 1986.
- [3] BERDICHEVSKY, V. L., “Variational-asymptotic method of constructing a theory of shells,” *Prikladnaya Matematika i Mekhanika*, vol. 43, no. 4, pp. 664–687, 1979.
- [4] BOLEY, B. A., “On the accuracy of the Bernoulli-Euler theory for beams of variable section,” *Journal of Applied Mechanics*, vol. 30, pp. 373–378, 1963.
- [5] CESNIK, C. E. S., *Cross-Sectional Analysis of Initially Twisted and Curved Composite Beams*. PhD thesis, Aerospace Engineering, Georgia Institute of Technology, Atlanta, Georgia, 1994.
- [6] CESNIK, C. E. S. and HODGES, D. H., “VABS: A new concept for composite rotor blade cross-sectional modeling,” *Journal of the American Helicopter Society*, vol. 42, no. 1, pp. 27–38, 1997.
- [7] CHANDRA, R., STEMPLE, A. D., and CHOPRA, I., “Thin-walled composite beams under bending, torsional, and extensional loads,” *Journal of Aircraft*, vol. 27, no. 7, pp. 619–626, 1990.
- [8] CLEGHORN, W. L. and TABARROK, B., “Finite element formulation of a tapered Timoshenko beam for free lateral vibration analysis,” *Journal of Sound and Vibration*, vol. 152, no. 3, pp. 461–470, 1992.
- [9] COLEMAN, T. F. and LI, Y., “On the convergence of reflective newton methods for large-scale nonlinear minimization subject to bounds,” *Mathematical Programming*, vol. 67, no. 2, pp. 189–224, 1994.
- [10] COLEMAN, T. F. and LI, Y., “An interior, trust region approach for nonlinear minimization subject to bounds,” *SIAM Journal on Optimization*, vol. 6, pp. 418–445, 1996.
- [11] COSSERAT, B. and COSSERAT, F., *Théorie des Corps Deformables*. Paris, France: Hermann, 1909.

- [12] DANIELSON, D. A. and HODGES, D. H., “Nonlinear beam kinematics by decomposition of the rotation tensor,” *Journal of Applied Mechanics*, vol. 54, no. 2, pp. 258–262, 1987.
- [13] DE SAINT-VENANT, A. J. C. B., “Mémoire sur la torsion des prismes,” *Mémoire des Savants Étrangers*, vol. 14, pp. 233–560, 1856.
- [14] FLANDERS, H., “Differentiation under the integral sign,” *The American Mathematical Monthly*, vol. 80, no. 6, pp. 615–627, 1973.
- [15] GIAVOTTO, V., BORRI, M., MANTEGAZZA, P., GHIRINGHELLI, G., CARMASCHI, V., MAFFIOLI, G. C., and MUSSI, F., “Anisotropic beam theory and applications,” *Computers and Structures*, vol. 16, no. 1–4, pp. 403–413, 1983.
- [16] HIBBELER, R. C., *Statics and Mechanics of Materials*. New York, New York: Macmillan, 1993.
- [17] HODGES, D. H., “Geometrically-exact, intrinsic theory for dynamics of curved and twisted anisotropic beams,” *AIAA Journal*, vol. 41, no. 6, pp. 1131–1137, 2003.
- [18] HODGES, D. H., *Nonlinear Composite Beam Theory*, vol. 213 of *Progress in Astronautics and Aeronautics*. Reston, Virginia: AIAA, 2006.
- [19] HODGES, D. H., ATILGAN, A. R., CESNIK, C. E. S., and FULTON, M. V., “On a simplified strain energy function for geometrically nonlinear behaviour of anisotropic beams,” *Composites Engineering*, vol. 2, no. 5–7, pp. 513–526, 1992.
- [20] HOPKINS, A. S. and ORMISTON, R. A., “An examination of selected problems in rotor blade structural mechanics and dynamics,” *Journal of the American Helicopter Society*, vol. 51, no. 1, pp. 104–119, 2006.
- [21] J E DENNIS, J., “Nonlinear least-squares,” *State of the Art in Numerical Analysis*, pp. 269–312, 1977. D. A. E. Jacobs, ed., Academic Press.
- [22] JUDD, K. L., *Numerical Methods in Economics*. Cambridge, Massachusetts: MIT Press, 1998.
- [23] JUNG, S. N., NAGARAJ, V. T., and CHOPRA, I., “Refined structural model for thin- and thick-walled composite rotor blades,” *AIAA Journal*, vol. 40, no. 1, pp. 105–116, 2002.
- [24] KARABALIS, D. L. and BESKOS, D. E., “Static, dynamic and stability analysis of structures composed of tapered beams,” *Computers and Structures*, vol. 16, no. 6, pp. 731–748, 1983.
- [25] KITIPORNCHAI, S. and TRAHAIR, N. S., “Elastic behaviour of tapered monosymmetric I-beams,” *Journal of the Structural Division, ASCE*, vol. 101, no. ST8, pp. 1661–1678, 1975.

- [26] KRAHULA, J. L., “Shear formula for beams of variable cross section,” *AIAA Journal*, vol. 13, no. 10, pp. 1390–1391, 1975.
- [27] LEVENBERG, K., “A method for the solution of certain problems in least-squares,” *Quarterly Applied Mathematics*, vol. 2, pp. 164–168, 1944.
- [28] MARQUARDT, D., “An algorithm for least-squares estimation of nonlinear parameters,” *SIAM Journal on Applied Mathematics*, vol. 11, pp. 431–441, 1963.
- [29] MORÉ, J. J., GARBOW, B. S., and HILLSTROM, K. E., “User guide for MINPACK-1,” Tech. Rep. ANL-80-74, Argonne National Laboratory, Argonne, Illinois, August 1980.
- [30] OZGUMUS, O. O. and KAYA, M. O., “Energy expressions and free vibration analysis of a rotating double tapered Timoshenko beam featuring bending-torsion coupling,” *International Journal of Engineering Science*, vol. 45, no. 2–8, pp. 562–586, 2007.
- [31] PALACIOS, R., *Asymptotic Models of Integrally-Strained Slender Structures for High-Fidelity Nonlinear Aeroelastic Analysis*. PhD thesis, Aerospace Engineering, University of Michigan, Ann Arbor, Michigan, 2005.
- [32] PATIL, M. J. and HODGES, D. H., “Flight dynamics of highly flexible flying wings,” *Journal of Aircraft*, vol. 43, no. 6, pp. 1790–1799, 2006.
- [33] PIOVAN, M. T., FILIPICH, C. P., and CORTINEZ, V. H., “Exact solutions for coupled free vibrations of tapered shear-flexible thin-walled composite beams,” *Journal of Sound and Vibration*, vol. 316, no. 1–5, pp. 298–316, 2008.
- [34] POPESCU, B. and HODGES, D. H., “Asymptotic treatment of the trapeze effect in finite element cross-sectional analysis of composite beams,” *International Journal of Non-Linear Mechanics*, vol. 34, pp. 709–721, 1999.
- [35] POPESCU, B. and HODGES, D. H., “On asymptotically correct Timoshenko-like anisotropic beam theory,” *International Journal of Solids and Structures*, vol. 37, no. 3, pp. 535–558, 2000.
- [36] POWELL, M. J. D., “A Fortran subroutine for solving systems of nonlinear algebraic equations,” *Numerical Methods for Nonlinear Algebraic Equations*, 1970. P. Rabinowitz, ed., Chapter 7.
- [37] PRESS, W. H., TEUKOLSKY, S. A., VETTERLING, W. T., and FLANNERY, B. P., *Numerical Recipes in Fortran 90*, vol. 2 of *Fortran Numerical Recipes*. New York, New York: Cambridge University Press, 1996.
- [38] PRICE, M. A., KOFFI, K., and RAGHUNATHAN, S. R., “Static aeroelastic effect of local skin deformations on a NACA 0012 airfoil,” in *Proceedings of the 43rd AIAA/ASME/ASCE/AHS/ASC Structures, Structural Dynamics, and Materials Conference*, (Denver, Colorado), AIAA, April 2002.

- [39] RAJASEKARAN, S., "Equations for tapered thin-walled beams of generic open section," *Journal of Engineering Mechanics*, vol. 120, no. 8, pp. 1607–1629, 1994.
- [40] RENTON, J. D., "Generalized beam theory applied to shear stiffness," *International Journal of Solids and Structures*, vol. 27, no. 15, pp. 1955–1967, 1991.
- [41] STAROSEL'SKII, L. A., "On equations describing the vibrations of curvilinear elastic rods," *Prikladnaya Matematika i Mekhanika*, vol. 24, no. 7, pp. 584–585, 1979.
- [42] TENA-COLUNGA, A., "Stiffness formulation for nonprismatic beam elements," *Journal of Structural Engineering*, vol. 122, no. 12, pp. 1484–1489, 1996.
- [43] TIMOSHENKO, S. P., "On the correction for shear of the differential equation for the transverse vibrations of prismatic bars," *Philosophical Magazine*, vol. 41, pp. 744–746, 1921.
- [44] TIMOSHENKO, S. P., "On the transverse vibrations of bars of uniform cross-section," *Philosophical Magazine*, vol. 43, pp. 125–131, 1922.
- [45] TIMOSHENKO, S. P. and GOODIER, J. N., *Theory of Elasticity*. Maidenhead, United Kingdom: McGraw-Hill, 1970.
- [46] TO, C. W. S., "A linearly tapered beam finite element incorporating shear deformation and rotary inertia for vibration analysis," *Journal of Sound and Vibration*, vol. 78, no. 4, pp. 475–484, 1981.
- [47] VLASOV, V. Z., *Thin-Walled Elastic Beams*. Washington, District of Columbia: National Science Foundation and Department of Commerce, 1961.
- [48] VOLOVOI, V. V. and HODGES, D. H., "Theory of anisotropic thin-walled beams," *Journal of Applied Mechanics*, vol. 67, no. 3, pp. 453–459, 2000.
- [49] VU-QUOC, L. and LÉGER, P., "Efficient evaluation of the flexibility of tapered I-beams accounting for shear deformations," *International Journal for Numerical Methods in Engineering*, vol. 33, no. 3, pp. 553–566, 1992.
- [50] WASHIZU, K., *Variational Methods in Elasticity and Plasticity*. Oxford, UK: Pergamon Press, 1968.
- [51] WEMPNER, G., *Mechanics of Solids with Applications to Thin Bodies*. Sijthoff & Noordhoff, 1981.
- [52] YOUNG, W. C., *Roark's Formulas for Stress and Strain*. New York, New York: McGraw-Hill, 1989.
- [53] YU, W., *Variational Asymptotic Modeling of Composite Dimensionally Reducible Structures*. PhD thesis, Aerospace Engineering, Georgia Institute of Technology, Atlanta, Georgia, 2002.

- [54] YU, W. and HODGES, D. H., “Elasticity solutions versus asymptotic sectional analysis of homogeneous, isotropic, prismatic beams,” *Journal of Applied Mechanics*, vol. 71, no. 1, pp. 15–23, 2004.
- [55] YU, W., HODGES, D. H., and VOLOVOI, V. V., “Asymptotic generalization of Reissner-Mindlin theory: Accurate three-dimensional recovery for composite shells,” *Computer Methods in Applied Mechanics and Engineering*, vol. 191, no. 44, pp. 5087–5109, 2002.
- [56] YU, W., HODGES, D. H., and VOLOVOI, V. V., “Asymptotically accurate 3-D recovery from Reissner-like composite plate finite elements,” *Computers and Structures*, vol. 81, no. 7, pp. 439–454, 2003.
- [57] YU, W., HODGES, D. H., VOLOVOI, V. V., and CESNIK, C. E. S., “On Timoshenko-like modeling of initially curved and twisted composite beams,” *International Journal of Solids and Structures*, vol. 39, no. 19, pp. 5101–5121, 2002.

VITA

How does one summarize one's own life by a short account to properly describe its essence? By the person's educational background? By the person's proudest accomplishments or some way that the person would like to be known by? I will attempt to describe my life thus far by some of its ever shifting outside influences with its one definite constant presence.

I was born in Taiwan during the year 1977. While still an infant, my family and I moved to Connecticut. I learned English as my first language. We then moved to Indiana and I vividly remember being fascinated with cartoons and being confused at life in general. We then moved back to Taiwan, where I learned Chinese and started attending school. I recall that I liked fighting other kids, liked watching cartoons and movies, liked reading fictional stories and collecting comic books, and missed American comic books and candies. We then lived for a couple of years each in Kansas and then New York. My grasp of English improved as my grasp of Chinese worsened. I focused on collecting comic books and video games. We moved to Michigan. During my high school and undergraduate years, I often played basketball and became a basketball junkie. I continued collecting comic books until I felt that its quality became unacceptably low. I increased my time spent on coursework. Video games were fun until the gaming industry ruined it by shifting its focus from 2D games to 3D games and started emphasizing reality. As I begin graduate school, I became addicted to running. As I ran more and improved my ability to repeatedly place one leg ahead of the other, I played less basketball and my ability to jump vertically decreased. I moved to California and started working. I hurt my knee, which forced me to stop running. I moved to Georgia and focused on learning like

I have never done before. For my next phase in life, I will return to California and resume working. What worldly pursuit will preoccupy me next?

The one constant in my life has been that God loves me. I have believed in God as far as I remember. While the idols of my heart continue to evolve as I struggle to find my place in this world, I constantly look forward to that day when I may finally enter the kingdom of heaven.